Advanced Propulsion Systems for Linear Motion with High Performance Requirements

by

Xiaolin Zhou

A DISSERTATION

submitted to

Oregon State University

in partial fulfillment of
the requirements for the
degree of

Doctor of Philosophy

Presented January 6, 2006

Commencement June 2006

AN ABSTRACT OF THE DISSERTATION OF

Xiaolin Zhou for the degree of
Doctor of Philosophy in
Electrical and Computer Engineering presented
on January 6, 2006
Title: Advanced Propulsion Systems for Linear Motion with High Performance Requirements

Abstract approved:

_____

Annette von Jouanne

Traditionally linear actuator applications are addressed by the use of hydraulic systems. The high maintenance cost and poor reliability will always be the most critical problem in the real applications. Benefited from both the high mechanical advantage of the roll screw and the simple structure of the switched reluctance motor, a new SRM driven linear actuator is proposed as a replacement for the traditional hydraulic system. The key factor is to improve drive system reliability without losing the high thrust/ high power density characteristic of the original system. Through the Landing Craft Air Cushion (LCAC) project example, the detail of the magnetic design is done step-by-step to maximize the SRM power density. The technique credibility is crosschecked by both the SRDaS software and the finite element method. For further improvement of system reliability, converter structure, sensorless control and fault tolerance ability are also investigated. Both the computer simulation and the experimental results verified the validity of the high thrust linear actuator design.

The Linear Induction Motor (LIM) is another type of low cost, low maintenance linear

actuator for medium/high speed application. There are several constraints which should be considered during the LIM design procedure. The motor manufacturer needs to minimize the motor weight to save material and also limit the total supply current for thermal consideration. The drive designers are always looking for the maximum thrust with less supplied voltage. The wide operating speed requirement also makes the design decision more complex. In the research new asymmetric structure is proposed in the design, which can ideally double the design option from just even coil numbers per slot to the full integer range. The asymmetric structure has the potential to introduce a new balance point between the low-speed and high-speed performance of the LIM. Experimental results demonstrate the significant gain of the asymmetric motor compared with its symmetric counterpart. The airgap length is also found to be a key factor for the application in the experiments.

Advanced Propulsion Systems for Linear Motion with High Performance Requirements

by

Xiaolin Zhou

A DISSERTATION

submitted to

Oregon State University

in partial fulfillment of
the requirements for the
degree of

Doctor of Philosophy

Presented January 6, 2006

Commencement June 2006

Doctor of Philosophy dissertation of Xiaolin Zhou

presented on January 6, 2006

APPROVED:

Major Professor, representing Electrical and Computer Engineering

---

Director of the School of Electrical Engineering and Computer Science

---

Dean of the Graduate School

I understand that my dissertation will become part of the permanent collection of Oregon State University libraries. My signature below authorizes release of my dissertation to any reader upon request.

Xiaolin Zhou, Author

To my family

ACKNOWLEDGEMENTS

I would like to thank my major professors, Dr. Annette von Jouanne and Dr. Alan Wallace, for their advice and great support during the years of my study at Oregon State University. I am so grateful being able to work with Drs. Annette von Jouanne and Alan Wallace.

Many thanks and appreciation to the members of my graduate committee: Dr. Huaping Liu, Dr Larry Marple, Dr. James Coakley, Professor Mei-Ching Lien and Dr. Jimmy Eggerton for their guidance and advice in the completion of this dissertation. And special thank to Manfred Dittrich for all the great help on the test platforms.

I also want to show my thanks to my colleagues at Oregon State University for their valuable input and assistance, comments and help.

Special thanks to my wife, Bo Hong and my daughter, Michelle Zhou, I really appreciate their support and encouragement for each step of my study.

TABLE OF CONTENTS

Page

TABLE OF CONTENTS (Continued)

Page

LIST OF FIGURES

Figure Page

TABLE OF FIGURES (Continued)

Figure Page

TABLE OF FIGURES (Continued)

Figure Page

TABLE OF FIGURES (Continued)

Figure Page

LIST OF TABLES

Table Page

1 CHAPTER THE INTRODUCTION OF LINEAR ACTUATOR

1.1 Introduction

In modern industrial and commercial applications there is a great need for high thrust linear actuators with medium speed or short stroke. The focus for these kinds of applications is high thrust or high power density. Traditionally this market is well covered by the hydraulic systems which can provide sufficient thrust within an acceptably sized package. Unfortunately a variety of problems associated with all hydraulic systems become more and more severe with the long-term consideration. OSU conducted a Landing Craft Air Cushion (LCAC) project with the U.S Navy shown in Figure 1.1. As shown in Figure 1.2, there is a hydraulic linear actuator at the end of LCAC acting as the rudder controller. But based on the historical records of 10 units in services, the maintenance cost just for this small part can be as high as 4 million US dollars per year. There is an urgent need for a new generation of linear actuator with high performance and especially low maintenance requirement.

Figure 1.1 LCAC (Landing Craft Air Cushion)

Figure 1.2 Existing Hydraulic Linear Actuator

The US Navy is making considerable effort to replace nearly all hydraulic systems with power electronics and motors. This effort is not only consistent with the long-term strategy to develop an all-electric ship, but it will also eliminate or minimize a variety of problems currently being encountered. The ongoing problems associated with all hydraulic systems include the following:

- **Common mode failures.** A breach in the pressure boundary anywhere in a centralized hydraulic system, or the failure of any central component, will cause the failure of the entire system and all hydraulic cylinders. A responsive solution would use self-contained units that will not impact any other unit.

- **Complicated.** Hydraulic systems are complex; they have pumps, valves, pipes, surge tanks, pressure gages and so on. These components are typically spread out and require considerable room.

- **Susceptible to damage.** Due to being spread out, the components of a hydraulic system are exposed to damage from combat or accidents.

- **Frequent and difficult maintenance.** Seals around moving parts are fundamentally imperfect. Some of the moving parts in a hydraulic system must be frequently inspected and replaced. Hydraulic systems are also messy! Produce leaks or spill of hydraulic fluid. In addition, simple repairs are often difficult in that an entire hydraulic system might have to be drained, thus causing other power equipment to be taken out of operation. The system must then be recharged, followed by the inspection or replacement of components that might have "dried" out.

- **Risk to Humans.** Mil-standard hydraulic fluid can be harmful to humans. In addition, high pressure in a hydraulic system can lead to high velocity leaks, a further danger to humans. The best type of replacement actuator would simply have no hydraulic fluid nor use high pressure.

- **Redundancy is difficult.** Redundancy and modularization is difficult with mechanical parts, as opposed to electrical and electronic systems. A wire for conducting electrical power is physically flexible and can be readily duplicated.

- **Lack of controllability.** Hydraulics are fundamentally inaccurate; it is difficult to control fluid flow on a minute scale in order to position a piston accurately. Power electronics systems are orders of magnitude more accurate and can be programmed with varying ramp rates and other features which optimize operation and minimize stresses.

1.2 Past work on the high performance Linear Actuator

In order to solve these problems, a significant amount of research and design have been invested on the linear systems with high performance. There are three kind replacements existing in the public domain, which are the electro-mechanical actuators ("EMAs"), electro-hydrostatic actuators ("EHAs"), and integrated actuator packages ("IAPs") shown in Figure 1.3. All three technologies have previously been investigated in NASA, military, and commercial aerospace research programs as potential alternatives to traditional hydraulic flight control actuators.

Among many previous studies, of particular interest is the Electrically Powered Actuation Design ("EPAD") study conducted as a joint effort by the Air Force, Navy, and NASA. This study comparatively evaluated EMA and EHA approaches for use in aircraft flight control applications.

While an EMA replaces hydraulics entirely, an EHA is essentially a "half measure." The EHA still uses pressurized hydraulic fluid to transfer power, but the hydraulic fluid is kept local to the actuator, rather than being distributed by a centralized system.

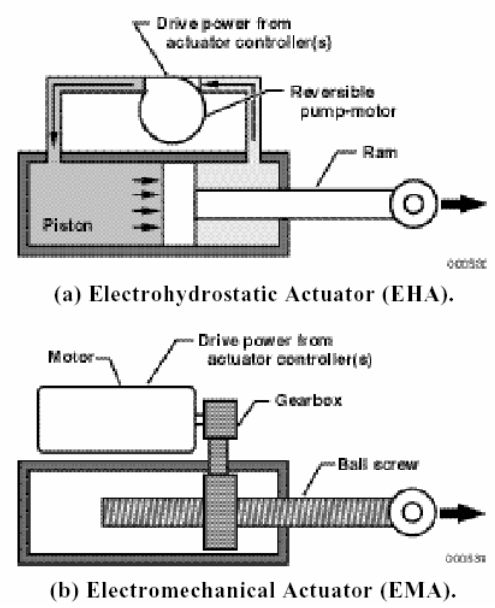

Figure 1.3 Power-by-Wire Actuators, EHA and EMA

As part of the EPAD program in Figure 1.4, working prototype EMAs and EHAs were built, ground-tested, and then flown on NASA's F-18 research aircraft. The conclusions, documented in "Flight Test Experience with an Electromechanical Actuator on the F-18 Systems Research Aircraft", included the following:

- "Compared to an EHA, the EMA has certain advantages. It is lighter, smaller, and less complex than an equivalent EHA because of the absence of an internal hydraulic system."
- "Since there is no hydraulic fluid in the load path, the EMA tends to be stiffer than an equivalent EHA."
- "The EMA tends to be more efficient because there are no windage losses or pump inefficiencies."
- "Finally, since there is no leak potential with an EMA, it is better suited to long-term storage…"

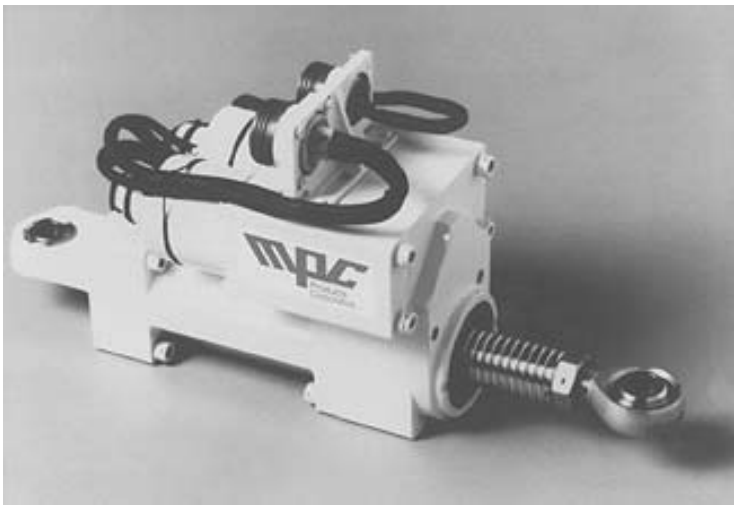

Figure 1.4 EMA Developed for EPAD Program

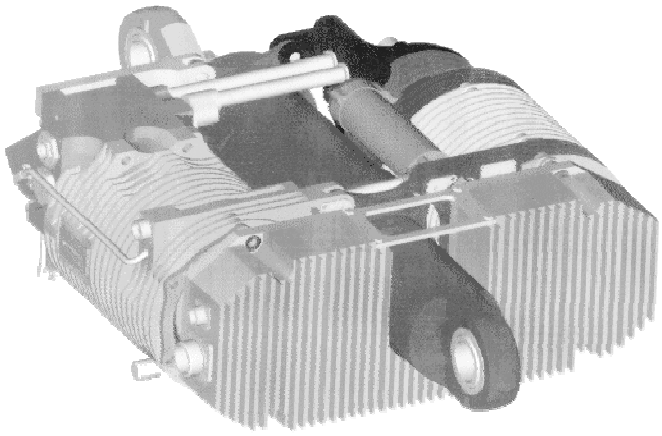

Figure 1.5 EHA Developed for EPAD Program

The EMA developed for the EPAD program uses a laterally offset permanent magnet DC motor to drive a ball screw via a gearbox. The assembled unit apparently weighs around 17 pounds and delivers over 13,000 pounds of thrust.

In general, the aircraft industry is currently implementing EHA technology. A paper titled "Electric Innovative Surface Actuation (ELISA)" puts the rationale this way:

"…currently the airframers appear to favor electro-hydraulic actuators (EHAs) since they retain many of the characteristics and advantages of conventional hydraulic actuators, and require minimal change in system definition."

EHAs are being designed into the new F-35 Joint Strike Fighter's flight control system, and have been in use by Airbus as back-up systems for several years.Boeing is also considering the use of power-by-wire actuators in flight control applications. Of particular interest in their projects are integrated actuator packages (IAPs), which combine motors, gears, electronics, and distributed intelligence within the actuator housing.

An IAP-type device would be an objective for which to strive for LCAC, that is, a system which is as integrated and as self-contained as possible. However, the vibratory environment in this application would tend to argue against the relatively high localized and suspended mass that an IAP concept would involve. Even in the NASA F-18 test bed, the power, control, and monitor electronics ("PCME") were located separately within the wing from the EMA itself, in that case, because of space constraints.

Again, because of the vibratory environment and the desire to minimize suspended mass on the LCAC rudder actuator, an EHA for this application would probably involve a separately mounted (although dedicated) pump with associated hydraulic supply lines. Since this would eliminate some of the advantages of the EHA approach over centralized hydraulics, and since the EMA already has inherent advantages, an EHA for this application would not appear to be an attractive option.

EHA technology appears to retain the preference of the aircraft industry due primarily to two things: conservative design philosophies and concerns related to the durability and failure modes of a screw-based actuator. Time and accumulated experience with EMAs should relieve the former; efforts put into material selection and lube-free performance could do much to relieve the latter.

Table 1.1 provides a brief comparison of the power-by-wire alternatives versus traditional centralized hydraulics[38].

Criterion	Central Hydraulics	EHA	EMA / IAP
Load Rating	Very High	Very High	Very High
Speed & Acceleration	Moderate	Moderate	Very High
Efficiency	< 50%	50 - 70%	> 90%
Stiffness & Shock Tolerance	Very High	Very High	Very High
Positioning & Control	Difficult	Difficult	Easy
Maintenance	Very High	High	Very Low
Relative Space Requirements	High	Moderate	Low
Environmental Concerns	Fluid leaks and disposal	Fluid leaks and disposal	Negligible
Lifetime	Proportional to maintenance effort	Proportional to maintenance effort	Very Long
Single Mode Failure Vulnerability	High	Low	Low

Table 1.1 Power-by-wire Actuator Versus Traditional Technology Comparison

1.3 Switched Reluctance Motor driven Linear Actuator

A comparison of available motor alternatives was conducted as the first step in the motor development process. The versatility of the leadscrew actuator concept lends itself well to the incorporation of a wide range of torque producing machines.presents the simplified cross sections of nine rotary electric motors, demonstrating the variety of designs available to match different application requirements.[22,24] In addition to the linear motor mentioned previously, consideration was given to the following candidates:

- AC induction motors (Figure1.6 b)
- Brushed DC motors (Figure1.6 j)
- Permanent magnet DC motors (Figure1.6 a)
- Reluctance motors (Figure 1.6 e)

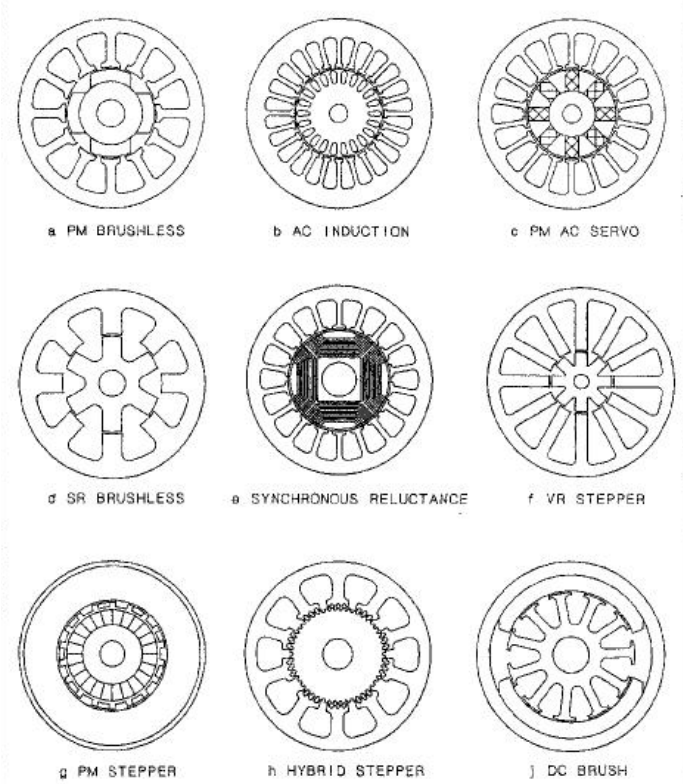

Figure 1.6 Simplified Cross Sections of Various Rotary Electric Motors

The following table shows a summary of the results of the comparative analysis[20,21,23,29]:

FEATURE	LINEAR MOTORS	INDUCTION MOTORS	DC MOTORS	PERMANENT MAGNET MOTORS	RELUCTANCE MOTORS
Power Density		A	A	A	A
Robustness	A	A			A
Damage Tolerance					A
Controllability			A	A	A

A - Acceptable

Table 1.2 Acceptability of Motor Technologies for LCAC Rudder Application

As shown in table 1.2, for this particular application reluctance motor technology stands out as the most promising choice, due primarily to the inherent robustness of its materials and construction, and fault tolerance. Recent efforts have been devoted to overcoming the shortcomings of other motor technologies (particularly permanent magnet) in this regard. However, to-date those efforts have only narrowed rather than eliminated the gap, and the complexity added to the construction, fabrication, and control of the other motor types does not appear to be balanced by any compelling advantages in this application.

Given the preference for a reluctance motor, further research indicated that there is a subset of technologies to choose from within this technology. Variable reluctance stepper motors and switched reluctance motors are perhaps the best known, but advances in semiconductor technology has also led to the potential viability of cage-less synchronous reluctance motors.[9,10,17,18,19] Table 1.3 outlines the qualitative differences between these reluctance motor technologies that would be relevant to this application.

	SYNCHRONOUS RELUCTANCE	FLUX-SWITCHING	STEPPER	SWITCHED RELUCTANCE
MAINTENANCE	EXCELLENT	EXCELLENT	GOOD	EXCELLENT
POWER DENSITY	FAIR	GOOD?	EXCELLENT	EXCELLENT
POSITION HOLDING	GOOD	FAIR ?	FAIR	EXCELLENT
POSITION CONTROL	GOOD	GOOD	GOOD	EXCELLENT
TORQUE RIPPLE	EXCELLENT	POOR	POOR	POOR
CONTROLS	COMPLEX	COMPLEX	SIMPLE	COMPLEX
TEMPERATURE TOLERANCE	EXCELLENT	EXCELLENT	FAIR	EXCELLENT
SHOCK TOLERANCE	EXCELLENT	EXCELLENT	GOOD	EXCELLENT
DAMAGE TOLERANCE	FAIR	FAIR	FAIR	EXCELLENT
COST	FAIR	GOOD	GOOD	FAIR

Table 1.3 Reluctance Motor Comparison

As shown, on balance the SR motor receives the highest score. The three areas where it compares less favorably would not seem to be the highest priority criteria for the LCAC application. Torque ripple should not be a significant factor, given the expected insensitivity of the mechanical system to variations at the expected frequencies and magnitudes produced in this system. The control complexity is greater than that of a stepper system, but is by no means unacceptable. And the magnitude of the cost difference between the motor types should be small relative to the overall cost of the system.

1.4 Advanced Leadscrew Technologies

Besides the electric design partial, there is a need to give some brief introduction for other key factors of the LCAC project, like the leadscrew technologies. The lead screw transfers the rotation into linear motion. Three general types of leadscrews exist which could function in this application. The two most commonly known are power (or ACME) screws and ball screws. These two types of screws have been used in industry motion and load control applications for many years. A third type of screw, called a roller screw, has begun in recent years to see use in place of ball screws in demanding applications. See Figure1.7.

In a power screw, a female-threaded nut, usually of either bronze or polymer, rides along a male-threaded steel shaft. At high speeds (above about 300 to 400 RPM), frictional heating and excessive wear become significant concerns, even in a pristine operating environment. Power screws are relatively cheap and quite good for high load, low speed applications where precision is not a concern.

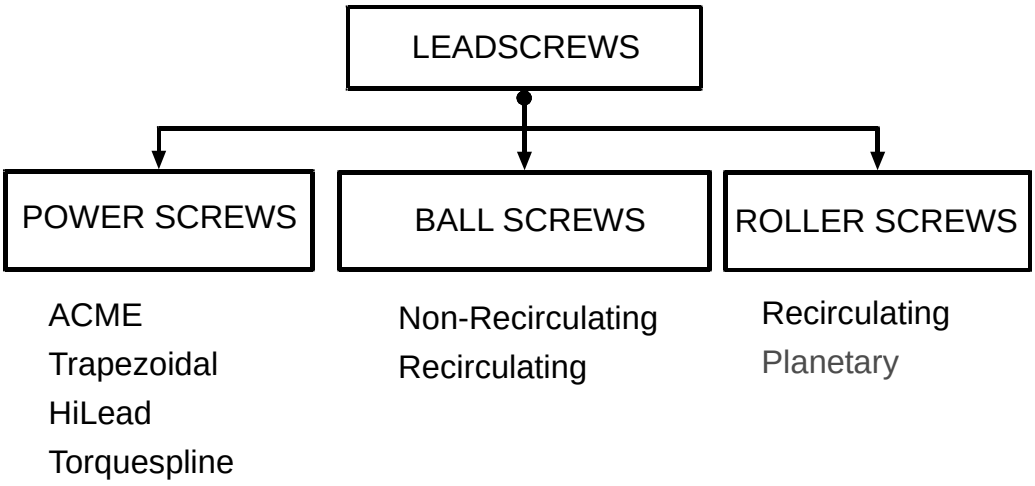

Figure 1.7 Various Types of Leadscrews Considered

In a ball screw, a nut with an internal bearing race travels along a steel shaft with ground helical splines. Steel or ceramic ball bearings roll within the nut's bearing race, greatly reducing friction when compared with a power screw. In a recirculating ball screw (one in which the balls travel continuously in a loop through the nut by means of a return channel), there is theoretically no surface-to-surface skidding. Efficiencies of greater than 90% are common in practice, allowing for speeds of 2,000 to 3,000 RPM.

Consequently, ball screws are very good for higher speed applications and also offer advantages in precision and control. In a roller screw, the threaded shaft is similar to that of a power screw, but the nut is a radical departure. Within the nut, a set of smaller threaded shafts surrounds the screw shaft. Threads on these "satellite" rollers mesh with the threads of the screw shaft, but are opposite threaded so that they will counter-rotate. Gear teeth at the ends of the rollers mesh with a planetary gear in the nut to keep the action of all the rollers synchronized.

Roller screws fill much the same general niche as ball screws with respect to speed and precision, but are actually capable of significantly higher speeds (4,000 to 5,000 RPM). They are also capable of carrying higher loads than ball screws and are much more durable and tolerant of damage and contamination. A projected service life advantage for roller screws of over fifteen times compared to ball screws is advertised by manufacturers who supply both technologies.

1.5 The objective of this research

The main challenge of the linear actuator design will be how to improve drive system reliability without losing the high thrust/ high power density characteristic of the original hydraulic system.

The following are the design specification for the mechanical side based on the original hydraulic actuator:

- Stroke: 2.55 inches forward and 2.55 inches backward
- Bearing-axis-to-bearing-axis length: 23.8 inches at mid-stroke
- Diameter: approximately 3.5 inches
- Operating thrust: up to 1100 pounds
- Speed: 5.5 inch per second
- Weight: <30 lbs totally

The new linear actuator could be completely self-contained with the lead screw, motor and power electronics integrated into a single package, but in the LCAC application it is more prudent to put the power electronics unit on the inside of the robust metal support for the nacelle which surrounds the propulsion propellers shown in Figure 1.8. This location provides protection from damage and direct sun, and will also minimize the weight of the components subject to vibration.

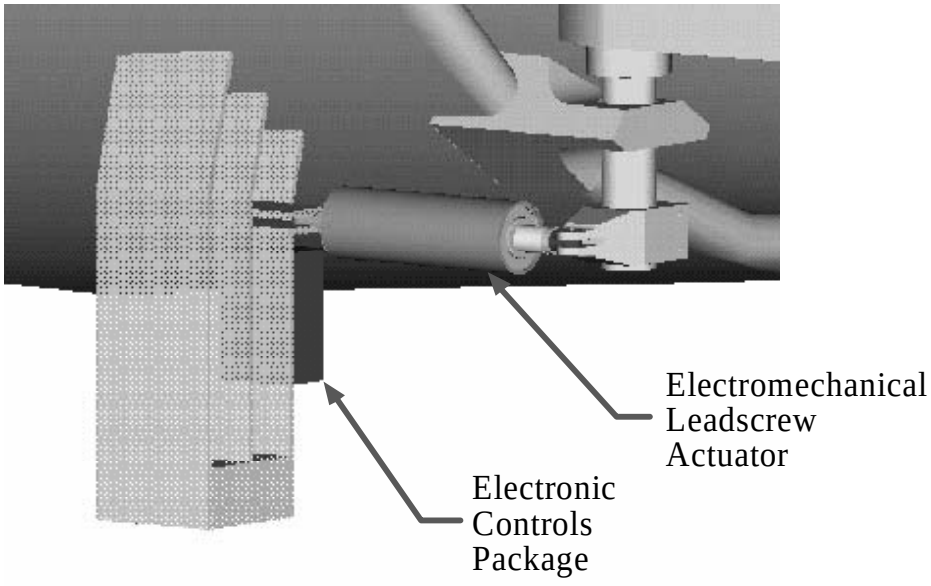

Figure 1.8 Proposed Actuator and Electronics Shown "Installed"

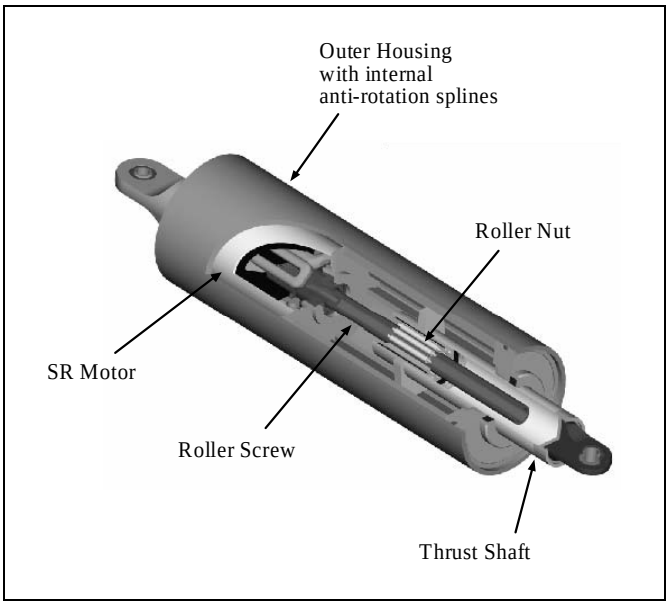

Figure 1.9 Proposed Actuator Configuration

The proposed actuator configuration will be the one to one replacement of the hydraulic actuator shown in Figure 1.9. Through the roller screw the linear motion will finally be transferred into the rotation of the Switched Reluctance Motor. The focus of this research will be torque /power density maximization within the weight and size limitation based on the magnetic design. System reliability is another main concern of the design. The key parameters of the SRM design are summarized in table 1.4.

Parameter	Formula	Value	Unit
Stroke	s	5.6	inch
Operating thrust	F	1,100	Lb
Speed	v	5.5	in / sec
Thread lead	l	0.25	in / rev
Rotational speed of screw	$n_r = v / l$	22	rev / sec
Rotational speed of screw in RPM	n_r'	1320	RPM
Assumed screw efficiency	η	80%	%
Screw outer diameter in inches	d	0.79	inches
Mechanical advantage of the screw	$MA_s = \frac{\pi d}{l}\eta$	25.1	NA
Force applied to the screw	$F_{screw} = F / MA_s$	44	lbf
Motor output torque	$T = F_{screw} * d / 2$	17	in*lbf
Output torque in Newton meters	T'	6.18	N*m
Angular speed of screw	$\omega = 2\pi n_r'$	138	Rad/sec
Min. output power of the motor,W	$P_{OutMin} = T'\varpi$	854	Watts

Table 1.4 Key Design Parameters and Calculations

2 CHAPTER SWITCHED RELUCTANCE MOTOR DESIGN

The Switched Reluctance Motor is a doubly-salient singly-excited reluctance motor [1]. Figure 2.1 show the cross section of an 8 stator poles/6 rotor poles Switched Reluctance Motor (SRM). The rotor structure is simply a stack of salient-pole laminations with no windings or permanent magnets. The electromagnetic field is generated only from the stator side. When a stator pole-pair is energized, it has the tendency to attract the most adjacent rotor pole-pair to minimize the reluctance or maximize the inductance of the magnetic path. Due the different numbers of poles between stator and rotor side, there will always be one or more rotor pole-pairs in the no alignment position refereed to the stator poles. Then either direction of rotation can be realized by turning on the appropriate stator phase in succession. The torque generation of the SRM is a result of the variation of the phase reluctance, which is highly position dependent. And the magnetic saturation effect makes the problem more complex.

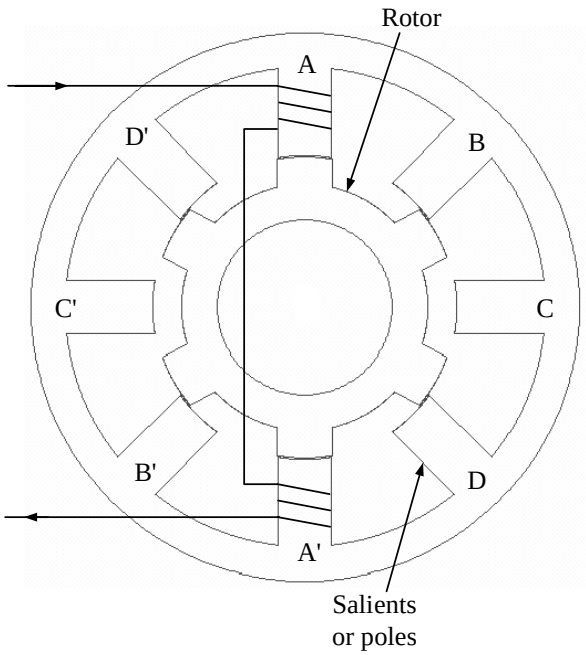

Figure 2.1 An 8/6 switched reluctance motor

2.1 Basic magnetic principle of SRM

Like all the other motor types, the general voltage equation in one phase of SRM is

$$V_{ph} = iR + \frac{d\lambda}{dt} \qquad \text{(Equation 2.1)}$$

V_{ph} is the phase voltage, i is the instantaneous phase current, R is the stator winding resistance and λ is the flux-linkage of the stator winding. The flux-linkage will be a function of both phase current and rotor position as $\lambda = \lambda(i,\theta)$, which is shown in Figure 2.2 .Now the phase voltage equation will be

$$V_{ph} = iR + \frac{d\lambda(i,\theta)}{dt} = iR + \frac{\partial\lambda}{\partial i}\frac{di}{dt} + \frac{\partial\lambda}{\partial\theta}\frac{d\theta}{dt} \qquad \text{(Equation 2.2)}$$

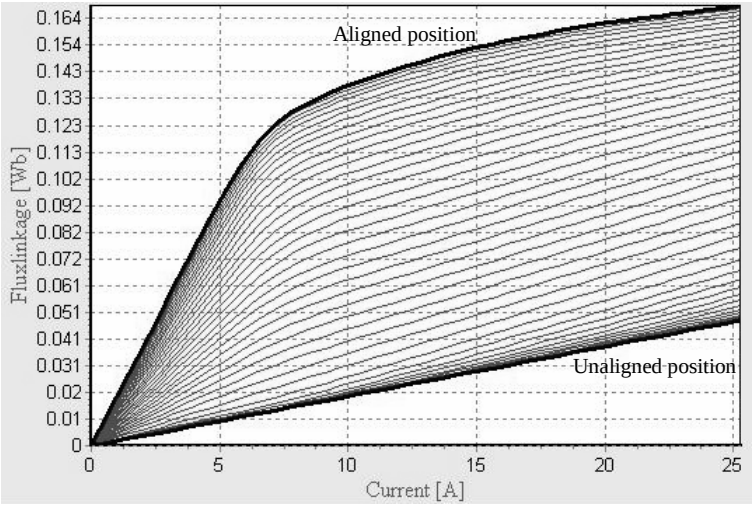

Figure 2.2 Flux-linkage of the SRM

When the magnetic saturation effect is negligible, the flux linkage is only position dependent. $\lambda = L(\theta)\cdot i$ The above equation can be simplified as

$$V_{ph} = iR + \frac{d\lambda(i,\theta)}{dt} = iR + L(\theta)\frac{di}{dt} + i\cdot\frac{dL(\theta)}{dt}\omega \qquad \text{(Equation 2.3)}$$

The last term is the back-emf which is proportional to both the speed and the instantaneous changing ratio of the phase inductance. With a limited DC voltage supply, there is a speed upper limitation caused by this factor.

The torque equation of SRM can be developed from the energy conversion equation. By multiplying phase current i on both side of the voltage equation, the instantaneous power can be developed as

$$P = V_{ph} \cdot i = i^2 R + \frac{d}{dt}\left[L(\theta) \cdot i^2\right] + \frac{1}{2} i^2 \cdot \frac{dL(\theta)}{dt} \omega \qquad \text{(Equation 2.4)}$$

The first term is the copper loss in the stator winding. The second component is related to the magnetic energy stored in the core. The third item is the output mechanical power. So the electromagnetic torque is

$$T = \frac{1}{2} i^2 \cdot \frac{dL(\theta)}{dt} \qquad \text{(Equation 2.5)}$$

Since there is no real separation between the ‘field ‘ current or ‘armature’ current in SRM, the output torque is proportional to the square of the phase current. So any improvement in the phase current will generate more gain in the output torque. Another way to develop higher torque is to increase the changing ratio of the phase inductance as in Figure 2.3.

The torque can also be defined by the rate of change coenergy to the rotating angle

$$T = \left.\frac{\partial W'(\theta, i)}{\partial \theta}\right|_{i=cons\tan t} \qquad \text{(Equation 2.6)}$$

$W' = \int_o^i \lambda \cdot di$ is the coenergy

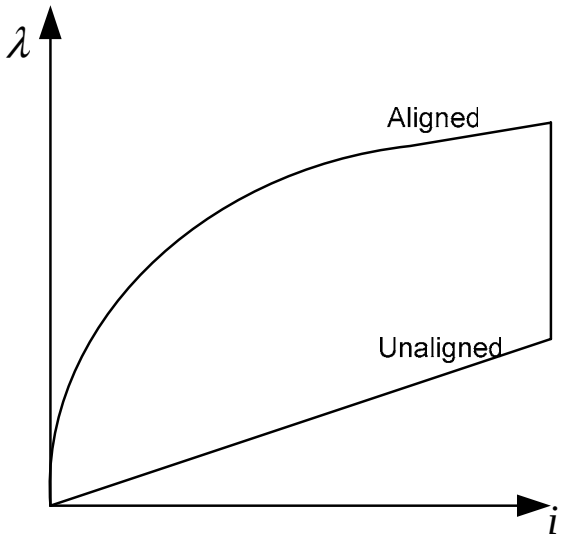

Figure 2.3 The principle of torque production

As shown in Figure 2.3, the total output torque for the whole cycle will be the area between the unaligned magnetic line and the aligned line. The main purpose of the switched reluctance motor design will either maximize the phase inductance at aligned position or minimize the inductance at unaligned position.

2.2 Preliminary SRM design

Due to the limitation of both the dimension and the total weight, maximizing the output torque at rated speed is the key factor in the design[27]. Three methods are used to cross check the technique credibility as shown in Figure 2.4.

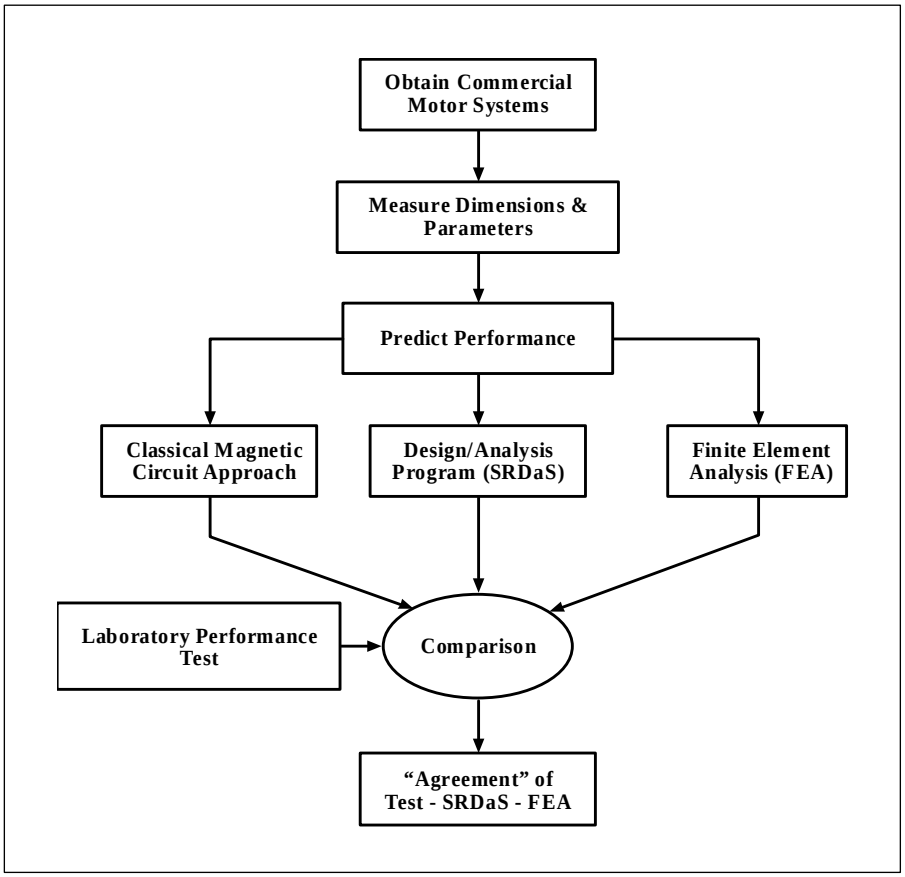

Figure 2.4 Establishing design technique credibility

An Emerson Switched Reluctance Drive is used to establishing the design technique credibility. Through the classical magnetic circuit approach the rotor and stator dimensions are measured step by step. Once the airgap flux density is estimated from the B-H characteristics of the material, the motor operation point can be predicted. Then a analysis program (SRDaS) and a Finite Element Analysis (FEA) are used to check the agreement with each method.

2.2.1 SRM analytical method

A step-by-step analytical procedure is used following the method mentioned in paper [41]. The operating peak flux density in the stator pole is set at $B_s = 1.95T$. Then the flux density of the stator pole, stator yoke, rotor pole and the rotor core can be calculated based on the flux continuity. The magnetic equation of the total ampere-turns in either the aligned position or the unaligned position is expressed as

$$\Im = \sum H_x l_x = 2(H_s l_s + H_r l_r) + H_g l_g + H_{rc} l_{rc} + H_y l_y$$

Since $\Im = T_{ph} \cdot i$ The phase inductance is calculated as $L = \frac{T_{ph}\phi}{i} = \frac{\Im B_s A_s}{i^2}$

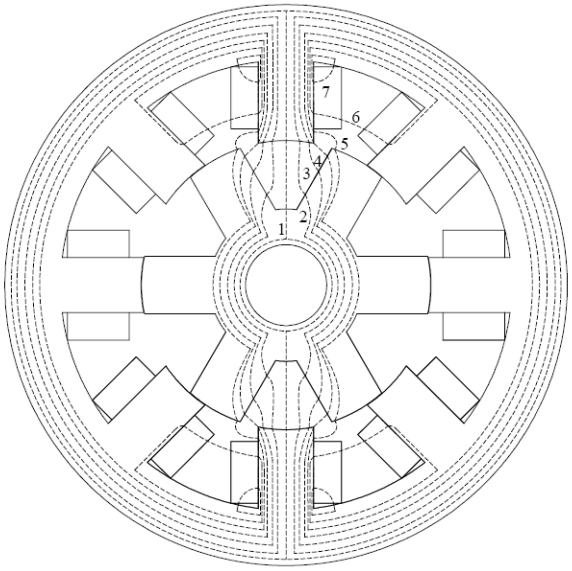

Figure 2.5 The flux tubes in the analytical calculation of the phase inductance(Praveen)

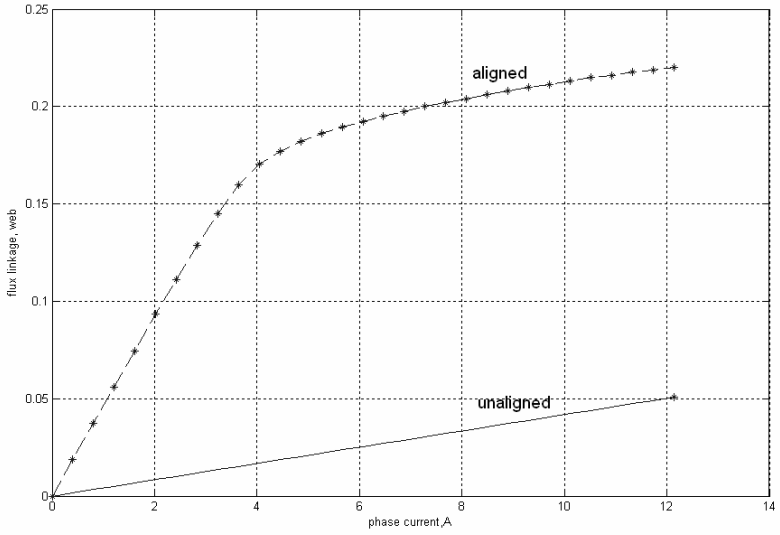

Figure 2.6 The flux linkage vs. phase current for unaligned and aligned position

Figure 2.6 is the flux linkage vs. phase current for both aligned and unaligned positions. The calculation detail can be found in Appendix 1. Table 2.1 is the design summary of this analytical method.

Parameter	Value
Rated torque	6.2 Nm
Rated speed	1320 rpm
Stator outer radius	71 mm
Rotor outer radius	33.5 mm
Shaft length	181 mm
Stack length	55 mm
Air gap	0.25 mm
Number of windings	166
Aligned inductance	18.2 mH
Unaligned inductance	4.2 mH
Total weight of the motor	11 lbs

Table 2.1 The main parameters of the preliminary design

2.2.2 Verification of the SRM design with SRDaS and Finite Element method

SRDaS is a SRM design software developed by Dr. Rasmussen[40], which can estimate the SRM performance based on motor dimension and the power rating. All the parameters of the SRM are directly taken from the preliminary design developed through the analytical method.

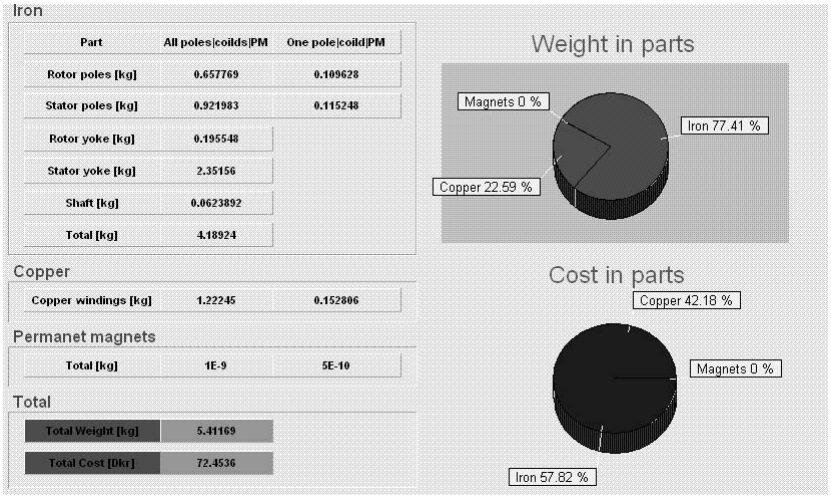

Figure 2.7 The weight of the SR motor

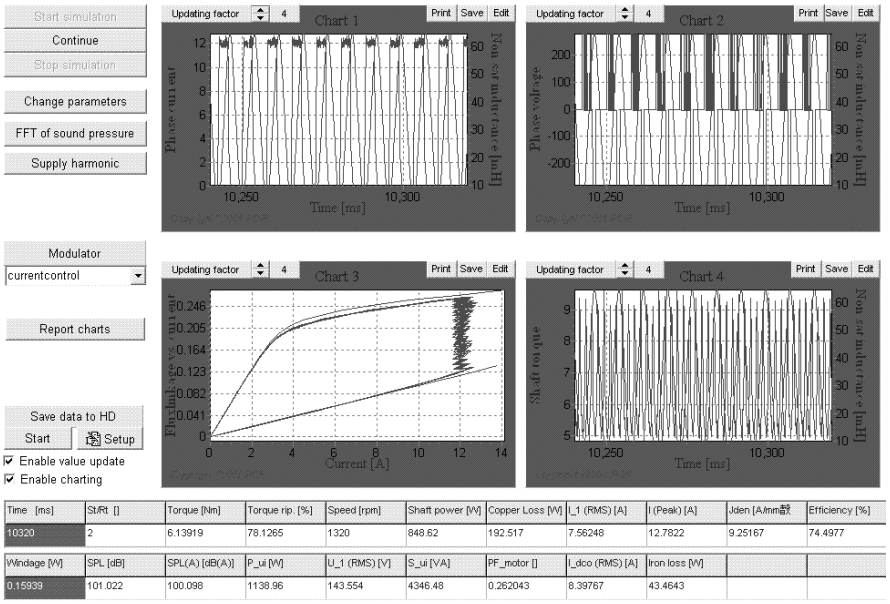

Figure 2.8 The performance estimation of the SR motor

The calculated total weight of the motor is about 11.8 lbs, which is very close to 11 lbs calculated through the analytical method. The output torque is 6.14Nm when the phase current peak value is about 12.78A. It is a good fit to the preliminary design. The efficiency of the SRM is 74.5% and it has been found that 82% of the power loss is due to copper loss. In the future, high-flux density materials such as permendur can be investigated to improve the SRM efficiency and optimize the SRM design.

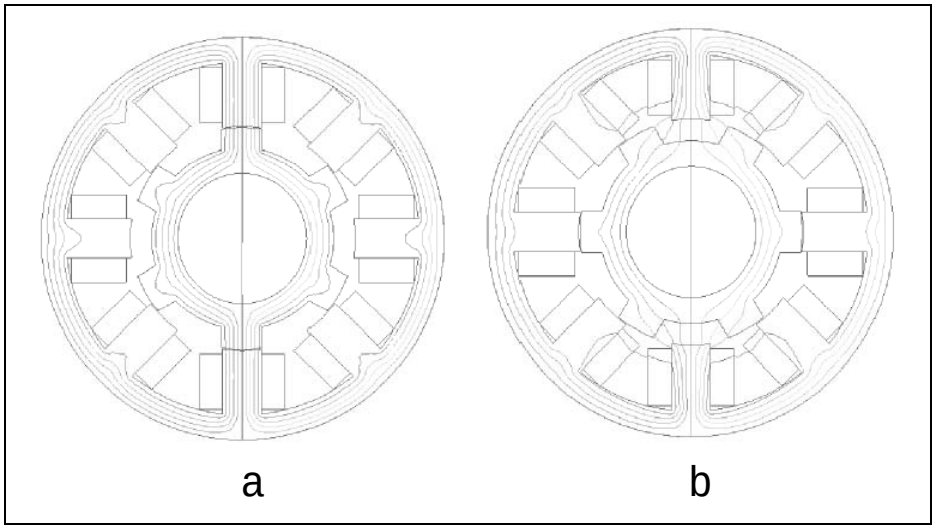

Figure 2.9 FEA Model of Magnetic Flux in (a) Aligned and (b) Unaligned position

Finite element method is also used to check the validity of the preliminary design. The calculated torque referred back to the stack length=55mm in FEM is also around 6 Nm.

2.3 Conclusion

The magnetic motor design using analytical method is checked step-by-step. By the careful selection of the motor dimension, the total motor weight is kept within 12 lbs, while the average output torque is still about 6 Nm, which will guarantees the 1,100 lbs output thrust through roll screw with high mechanical advantage. The validity of the design data is crosschecked with both SRDaS and FEA method.

3 CHAPTER THE CONTROL OF SRM

In order to fully valuate the system reliability, there is a need also to investigate the SRM controller[39,40]. The SRM performance will depend on its power supply—the switched reluctance converter. Fig 3.1 is the asymmetric bridge converter for SRM control. For each phase, the winding is energized when both transistors are turned on. If the phase current rises above the current reference, one or both transistors are turned off, the phase current will be discharged through the diodes and the stored energy is returned back to the power supply[30]. The characteristics of SR converter include:

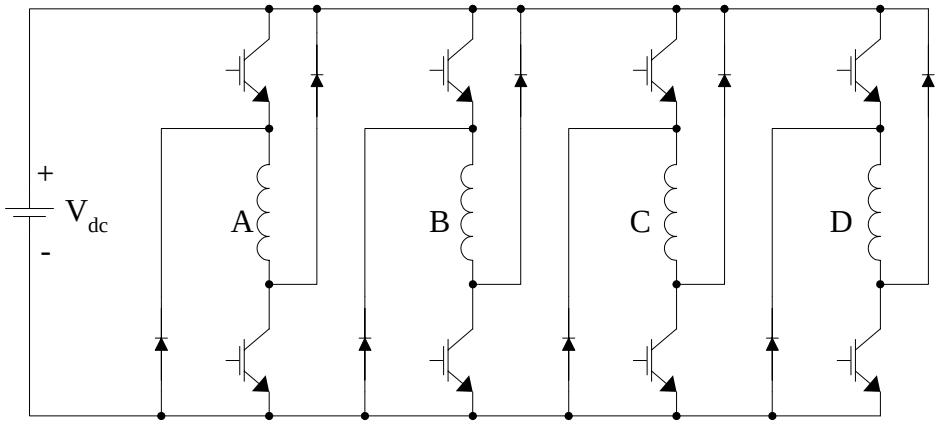

Figure 3.1 The converter of an 8/6 SRM

1. These two power transistors is connected through the phase winding, which will automatically limit the instantaneous changing ratio of the phase current. As a result, no dead time is needed in the control. Over current protection is greatly simplified.

2. There is no commutation between each phase coil. Phase control can be totally independent from each other. This redundancy leads to the unique ability of SRM—the fault tolerance.

3. A partial of the total energy is stored in the winding. Extra capacity is needed for the energy charging and discharging conversion. The over voltage problem could be more severe for the SR converter.

3.1 Fundamental Control strategies

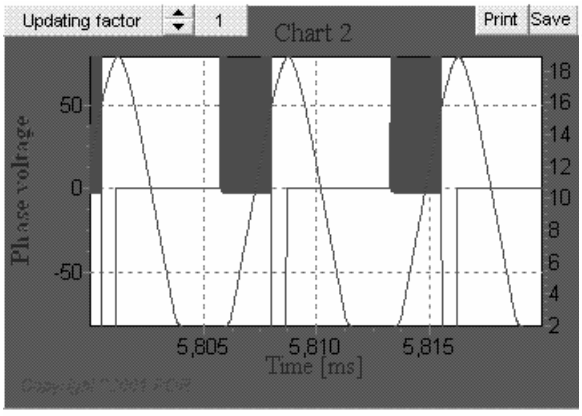

Figure 3.2 The phase voltage of the voltage controlled SRM drive

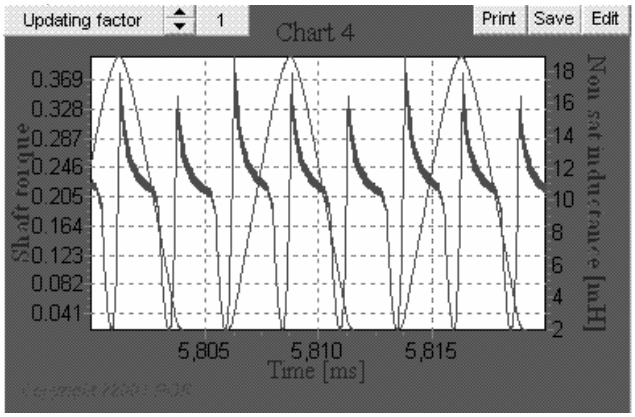

Figure 3.3 The output torque of the voltage controlled SRM drive

Generally there are two types of SR converters, voltage controlled converter and the current controlled one[1]. Traditionally the voltage control is used in low-performance SR drives, where precise torque control is not critical. The control signals are mainly the turn-on and turn-off angles shown in Figure 3.2. The total conduction period is controlled by the phase voltage command. Voltage control only controls the average output torque of the cycle. The torque profile can hardly be predicted. As shown in Figure 3.3 there is not only a high peak but also a very low notch in the torque profile. The torque ripple is high.

\

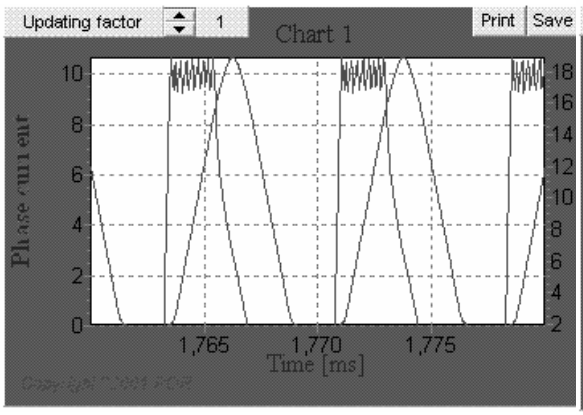

Figure 3.4 The phase current of the current controlled SRM drive

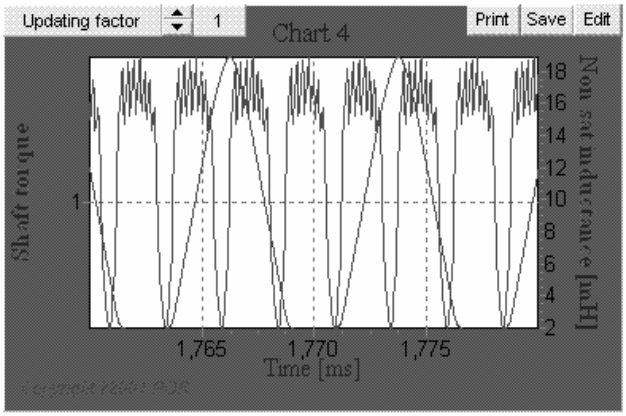

Figure 3.5 The output torque of the current controlled SRM drive

For high performance application, the torque is indirectly controlled by direct phase current regulation. Based on the torque equations in chapter 2, the phase torque will be nearly a constant by regulating phase current to a fixed value shown in Figure 3.4 and Figure 3.5 if the inductance increment from the unaligned position to the aligned position is a constant. Unfortunately the torque ripple caused by phase commutation and the magnetic saturation is still a problem[25,26,34,35].

More complex control strategies can be introduce into switched reluctance drive control to realize higher performance index. For instance torque ripple minimization can be achieved by precise control of the phase current profile during the commutation stage[35].

3.2 Sensorless control

Any advanced motion control will need the feedback signals including speed or position as the next step's reference. Even though the position/ speed encoder is always the preferred component for the control system, the position/ speed sensor is also the most vulnerable part in the severe environment. By indirectly estimating the position information from either phase voltage or phase current, the sensorless control can greatly

improve the system reliability.[5-8] There are five fundamental classes of sensorless control[1]:

1) Open-loop control with additional stabilization.
2) Passive waveform dictation.
3) Active probing.
4) State observers.
5) Flux-linkage control.

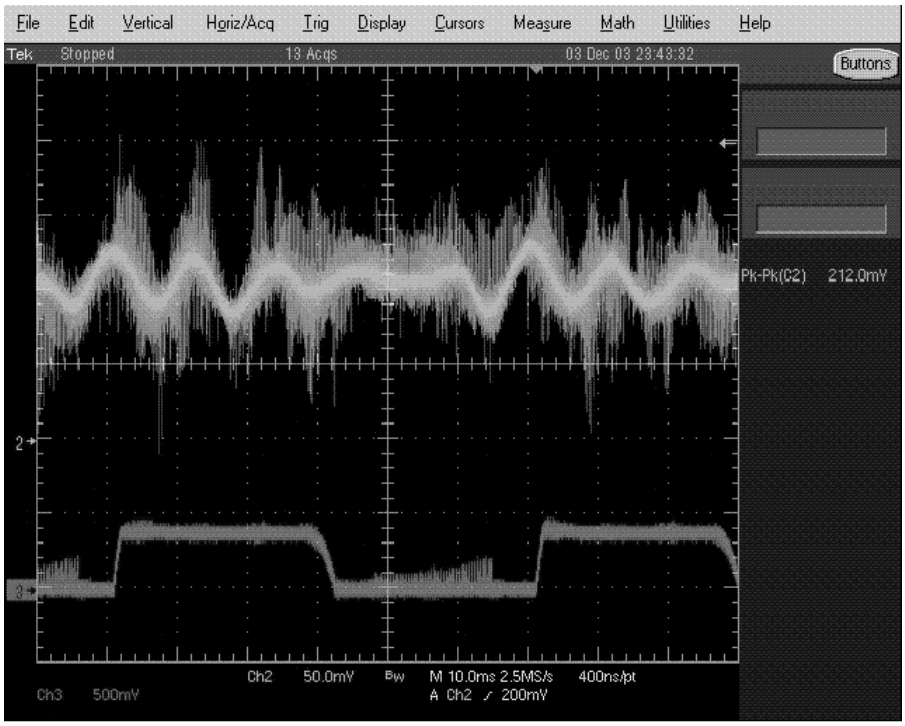

Figure 3.6 The pulse injection in active probing

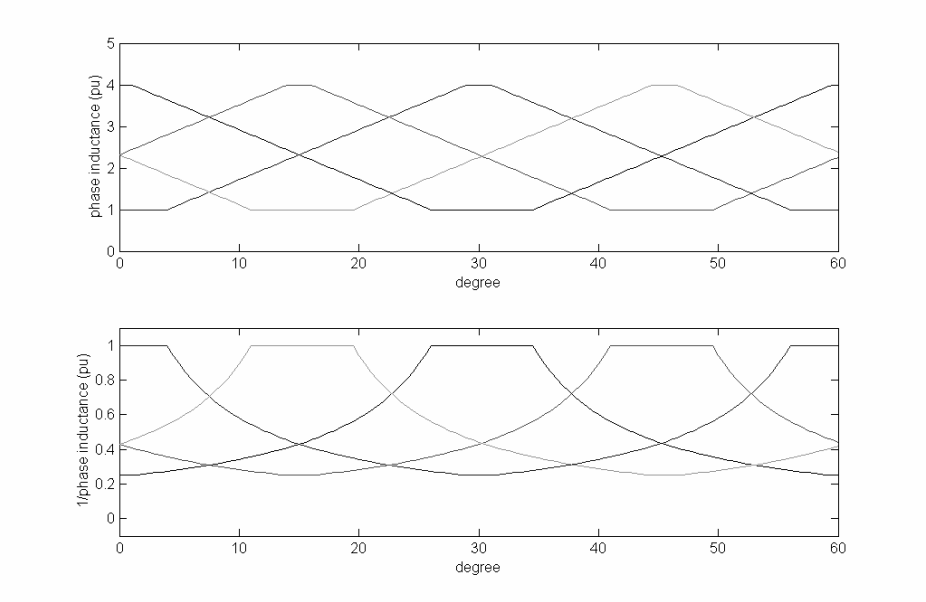

Figure 3.7 Active probing strategy

The active probing strategy is chosen for its simplicity and wide operation range. The basic idea is shown in the following equation;

$$i_{peak} = \frac{V_{dc} \cdot T_{on}}{L(\theta)} \qquad \text{(Equation 3.1)}$$

When constant width voltage pulse is applied, the peak current is proportional to the inverse of the phase inductance. Then the unaligned position can be easily found when the maximum current is reached. The main shortcoming of this method is additional current may cause negative torque, which decrease total efficient output torque. The 8/6 structure has 2 or 3 unexcited phases to choose for the sensorless control, the unwanted negative torque can be avoided with careful control strategy. Each unaligned position invokes a pulse in the controller. The stable speed control is obtained by filtering the digital time sequence with a digital phase-lock-loop.

3.3 Motor Start-up

The rotor position needs to be known before the motor starting. There is a very simply position estimation algorithm for SRM at standstill[2-4], which has the following features[13,15]:

a). No computation is required.

b). No pre-stored magnetic characteristic of the SRM is needed.

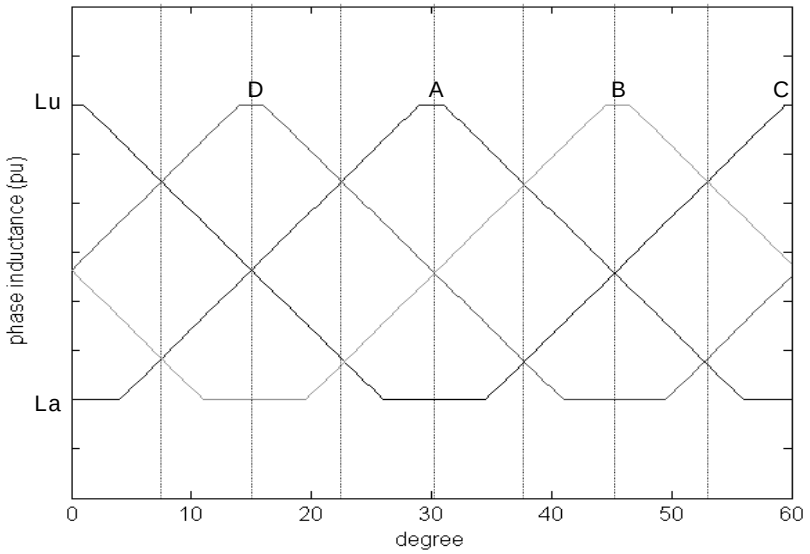

Figure 3.8 The phase inductance profile of a 8/6 SRM

Applying active voltage pulse to all phases A ~D. The peak current value in each phase is measured. The rotor position can be obtained from the relation of the phase currents; the proper phase can be selected. All the logics are in the following table for A-B-C-D sequence. The shape of phase inductance will repeat every 60°, only $0^\circ \sim 60^\circ$ is included.

Phase current order	Rotor position	Chosen Phase
$i_C < i_D < i_B < i_A$	$0^\circ \sim 7.5^\circ$	(1) D, (2) A
$i_D < i_C < i_A < i_B$	$7.5^\circ \sim 15^\circ$	(1) A, (2) D
$i_D < i_A < i_C < i_B$	$15^\circ \sim 22.5^\circ$	(1) A, (2) B
$i_A < i_D < i_B < i_C$	$22.5^\circ \sim 30^\circ$	(1) B, (2) A
$i_A < i_B < i_D < i_C$	$30^\circ \sim 37.5^\circ$	(1) B, (2) C
$i_B < i_A < i_C < i_D$	$37.5^\circ \sim 45^\circ$	(1) C, (2) B
$i_B < i_C < i_A < i_D$	$45^\circ \sim 52.5^\circ$	(1) C, (2) D
$i_C < i_B < i_D < i_A$	$52.5^\circ \sim 60^\circ$	(1) D, (2) C

Table 3.1 The check table of the starting up

The scenario when two detected phase currents are equal isn't included because this will not change the chosen phase. Considering the limited precise current measurement and the always-existing system noise, this sensorless start-up strategy is very reliable.

3.5 Fault tolerance ability

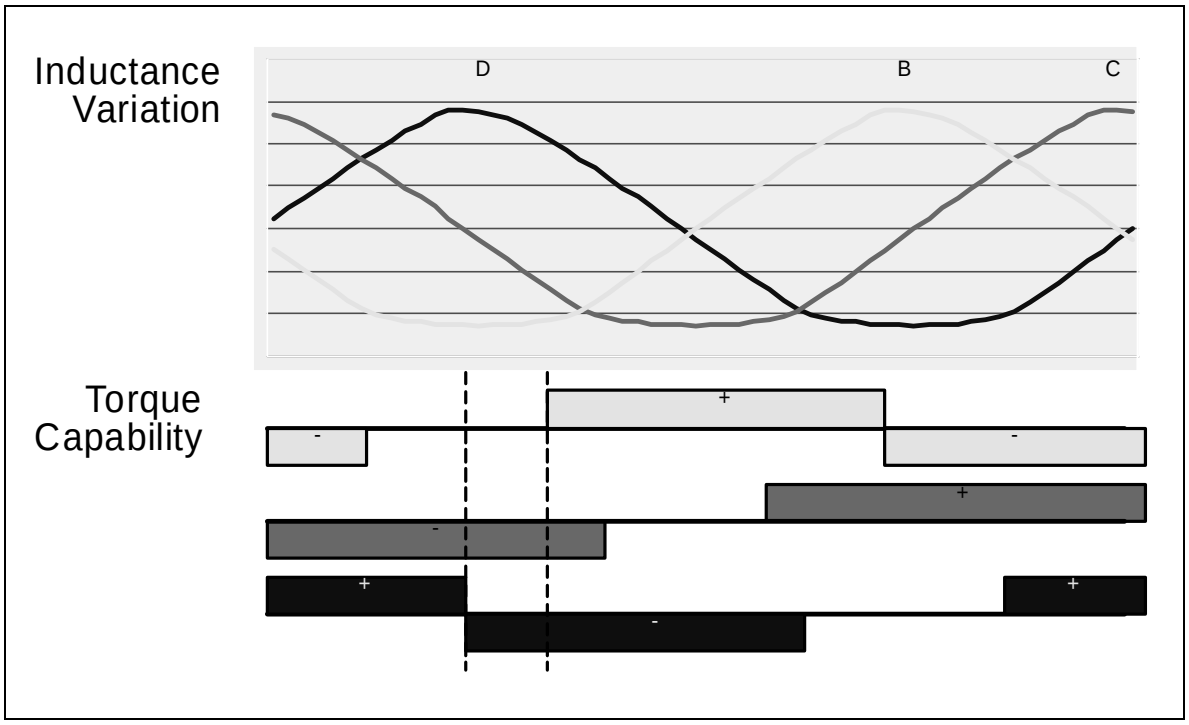

Figure 3.9 Torque Capability With One Phase Inoperative in a 8/6 SRM

Due to related independence of each phase, the SRM can still operate without one phase[32-33] Figure 3.9 simulates the scenario that phase A is lost due to some damage. The bottom torque capability plot clearly demonstrates that the SR motor is still able to generate positive torque, except in a small rotor angle range. Losing any phase will cause total system failure for other types of motors; for the SR motor, however, it will only slightly decrease the average torque. This can be compensated for when some redundancy is left at the design stage. Fault-tolerance is a unique characteristic of the SR motor.

3.6 Design summary

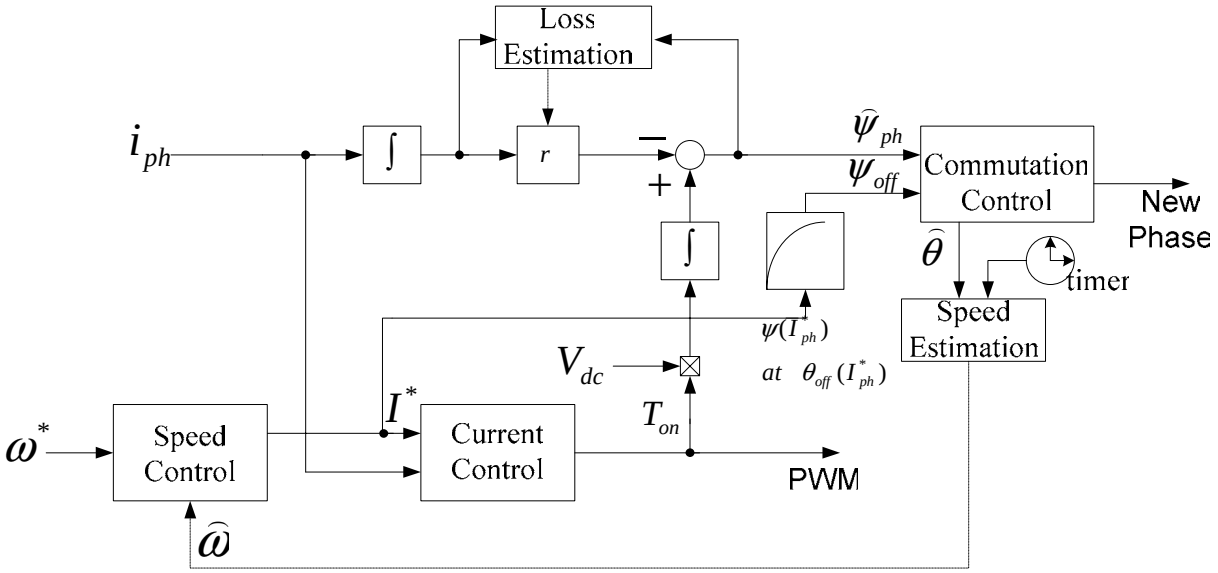

Figure 3.10 The control diagram

A sensorless control strategy based on flux-current-angle 3-D look-up table method is proposed. The phase current, DC voltage and the turn-on time are used to estimate the transient flux linkage. The rotor point can be located from the flux-current-angle look-up table. A more accurate prediction will be possible by including the loss estimation[36].

As an adjustable speed equipment, the future actuator operates either around 1200 rpm or as high as 4000 rpm. And the actuator needs to be turned on and turn off frequently. The active probing method works very well in the low speed range. The high speed will increase the back EMF, which causes a long tail phase current with the large aligned phase inductance. The long tail current occupying the rather limited zone may cause sensorless . The 8/6 structure gives the design some space to make a wider unaligned range, which benefits both the sensorless control and high initial current for the high-speed operation[37].

If the final motor design finds the target 4,200 rpm to be in the high-speed range, flux-linkage control will be added. Because the current-flux-angle have a fixed relationship, whenever two parameters, such as the current and flux, are known, the third parameter can be determined. The main shortcomings are that tedious measurement or FEA calculation is needed to obtain the motor parameters, and a large amount of controller memory will be used to store the current-flux-angle look-up table. However this should not be a problem for LCAC applications where the motor parameters will be well known.

4 CHAPTER THE EXPERIMENT VERIFICATIONS

In order to verify the design procedure, An experimental linear actuator is built using an Emerson SR drive system with a linear screw as in Figure4.1. The primary consideration is the relation between the output mechanical torque and the electromagnetic characteristics.

Figure 4.1 the test platform of the Linear Actuator

4.1 Torque estimation

Figure 4.2 is the phase inductance profiles vs. the rotor angle energized by phase current with different amplitude. There is almost no different between the inductance profiles when the phase current is less than 4 A. The magnetic core is in the linear range. As a result, the phase inductance is only position dependent. There is a significant variation only when the phase current arises above 4A. The original phase inductance at the aligned position is about 115 mH, which drops to 77mH when the phase current is 8A.

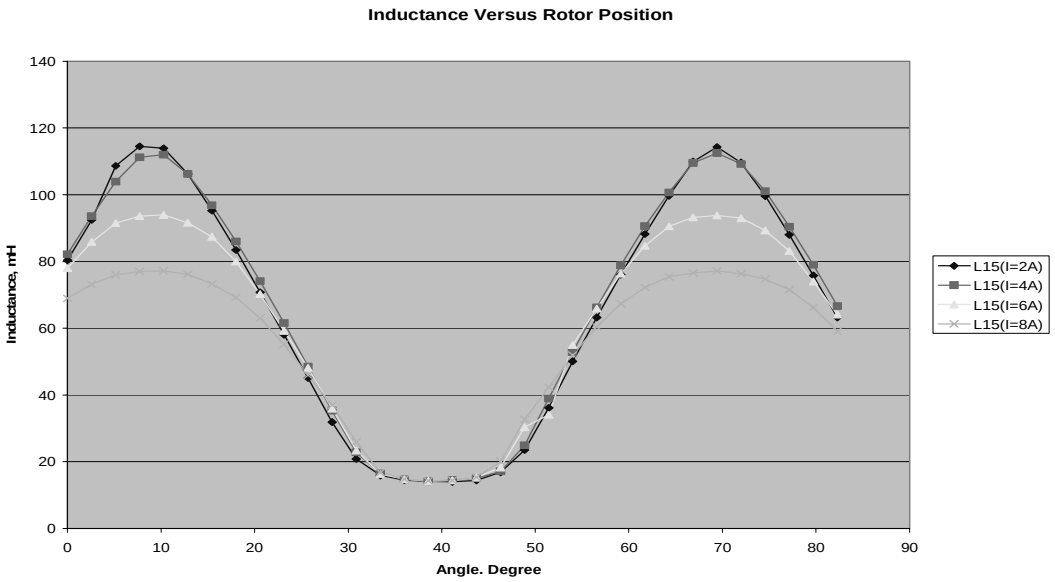

Figure 4.2 The experimental phase inductance profile

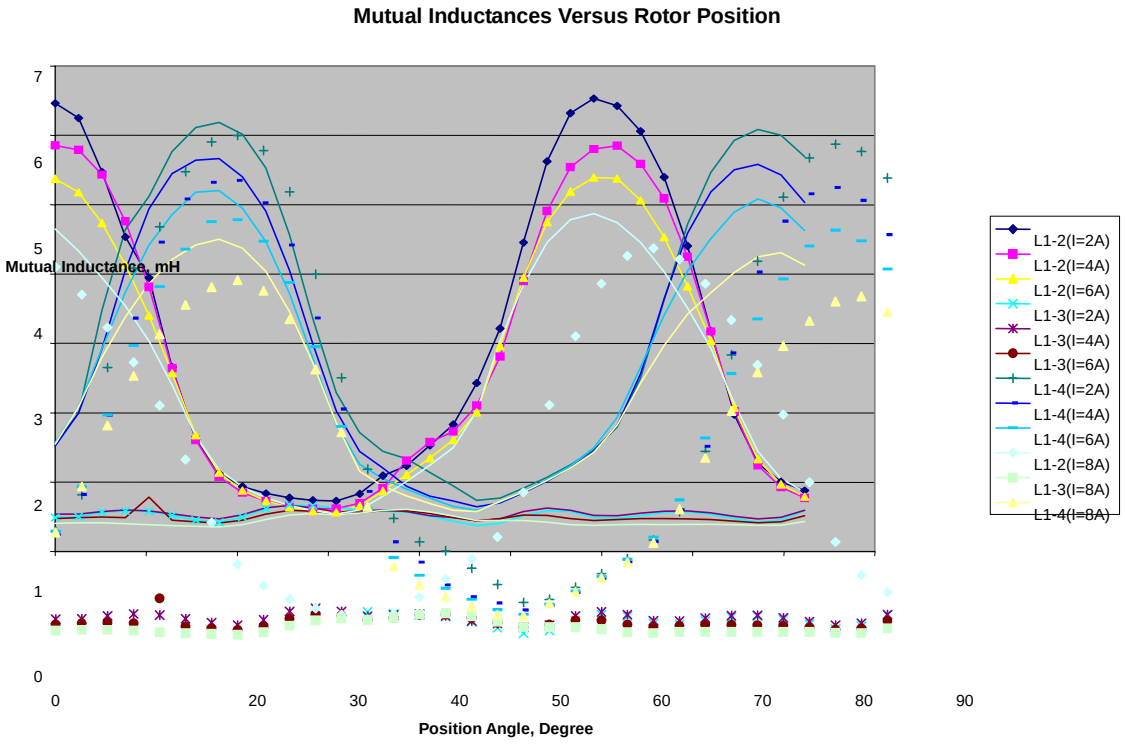

Figure 4.3 Mutual inductances of Phase reference to the other 3 phases

Fig 4.3 is the mutual inductance of one phase to the other 3 phases. Like the phase inductance, the mutual inductance between adjacent phases is also a function of both

position and phase current. The mutual inductance is always less than 10% of the self phase inductance, whose effect is negligible in the preliminary design.

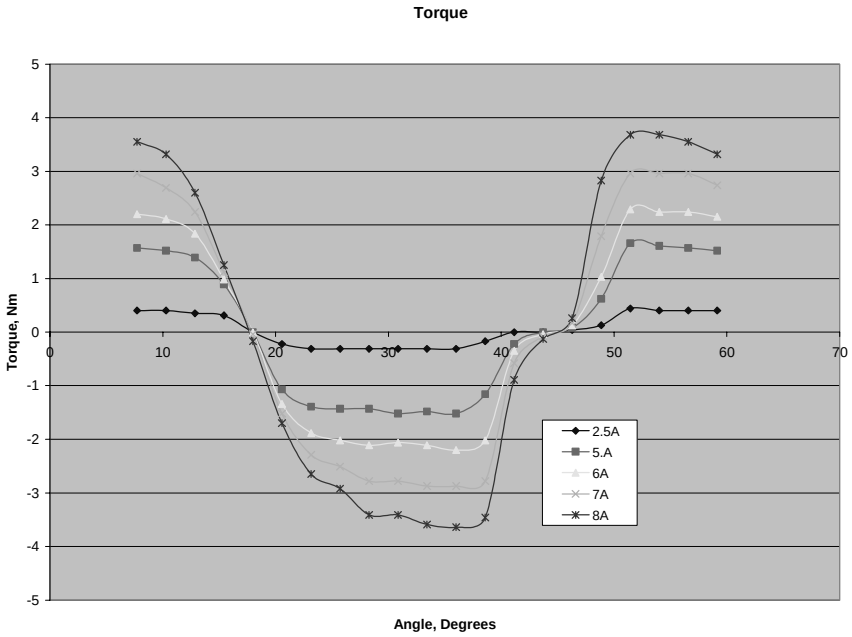

Figure 4.4 Experimental results of output torque vs. rotor angle

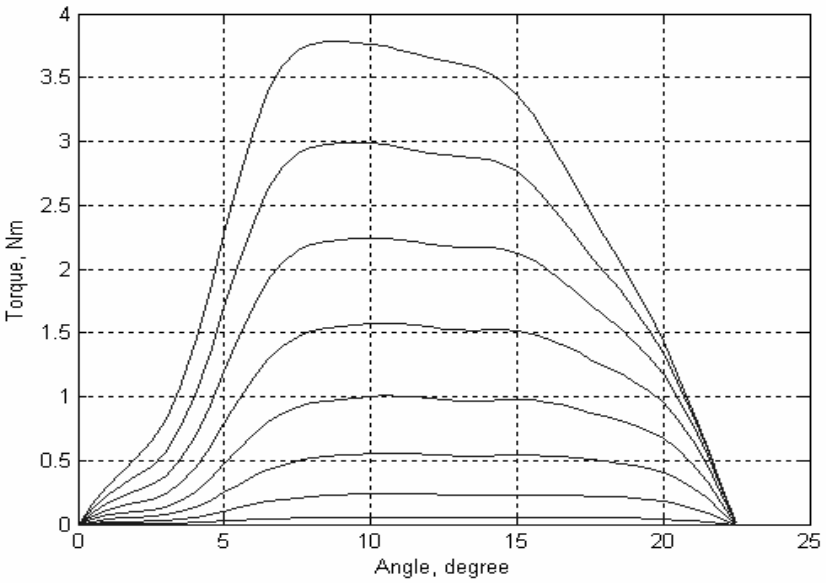

Figure 4.5 The calculated results of output torque vs. rotor angle

The experimental phase inductances data in Figure 4.4 is directly transferred into the magnetic estimation program. The flux-current-angle characteristic of this motor is estimated through curving fitting and is shown in Figure 4.6. Figure 4.5 is the calculated torque using the torque equations in chapter 2. Except some small notches on the experimental output torque, there is an excellent fit between the simulation results and the experimental results in both torque amplitude and the torque profile vs. position. Such as the calculated torque at the aligned position is 3.8 Nm when I=8A , while the experimental result is just around 3.7 Nm. The error is less than 5%..

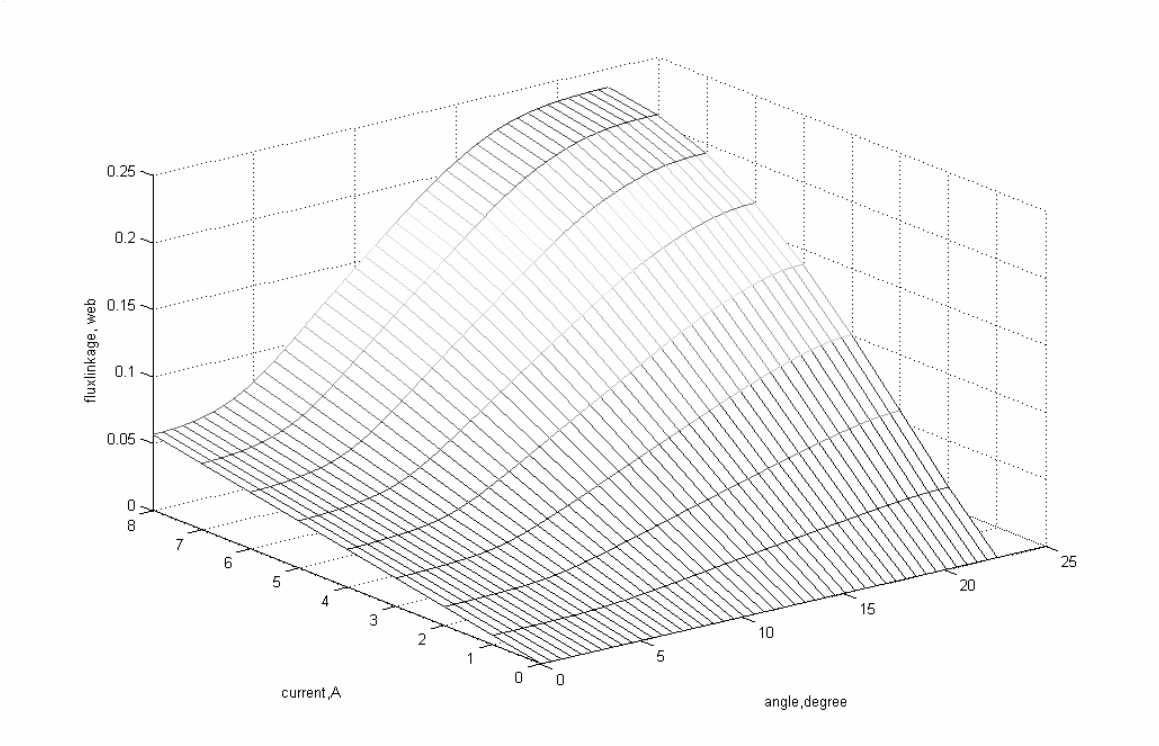

Figure 4.6 The calculated flux-current-angle data based on the experimental results

4.2 Lifting test for the Linear actuator

The ability of the prototype Linear Actuator is tested by a series lifting test shown in table 4.1 and figure 4.7

Weight		duty cycle	Iin (A)	Iphase (A)	Pin (W)	p.f.
kg	lbs					
9.5	21.1	0.1	1.10166	2.9	59.1	0.45908
11.5	25.6	0.204	1.17924	3.4	64.76	0.4716
15.5	34.4	0.262	1.444	3.8	62.06	0.48728
17.5	38.0	0.303	1.7199	4	101.47	0.5088
21.5	47.8	0.345	1.7836	4.4	105.68	0.51084
25.5	56.7	0.388	1.9107	4.8	114.16	0.51479
29.5	65.6	0.44	2.0998	5	127.15	0.52206
33.5	74.4	0.505	2.4209	5.8	150.26	0.53594

Table 4.1 Lifting test data

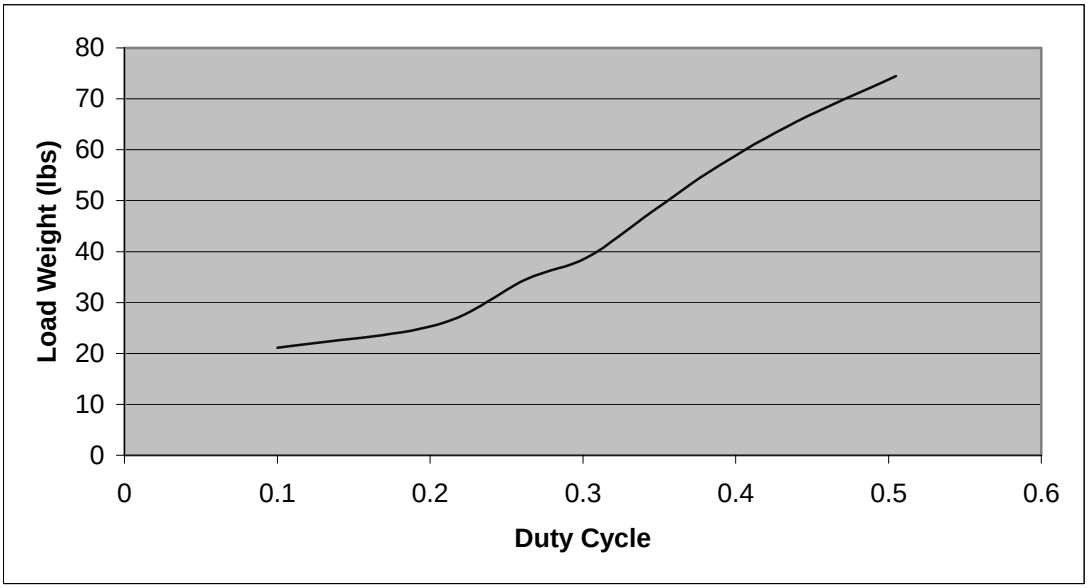

Figure 4.7 Load weight vs. duty cycle

The maximum lifting weight used is almost 75 lbs. The screw pitch used in the test is about 5 inch. 20 times thrust will be developed when the designed 0.25 inch pitch screw is used. There output thrust of the final design should easily reach 1100 lbs within the weight limitation.

5 CHAPTER LINEAR INDUCTION MOTOR BASICS

5.1 How Does A LIM Work

1. Take a squirrel cage induction motor

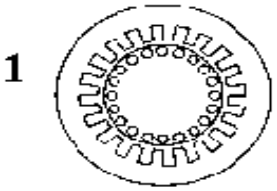

2. Open it out flat

3. Smooth the rotor bars into a conductor sheet

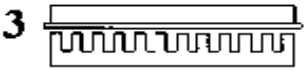

4. Apply AC power and you have a LIM

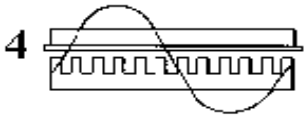

5. With two stators you can remove the reaction plate iron

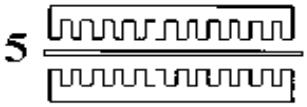

Figure 5.1 LIM diagram

As the diagrams show, the LIM is essentially a circular motor opened out flat. The magnetic field, instead of rotating, now sweeps across the flat motor face. The stator, usually known as the LIM, consists of a 3-phase winding in a laminated iron core. When energized from an AC supply a traveling wave magnetic field is produced. Swapping any two of the phases can reverse travel. The reaction plate is the equivalent of the rotor. This is usually a conductor sheet of aluminum or copper backed by steel, but any of these may be used alone. Currents induced in the reaction plate by the stator-traveling field create a secondary field. LIM is not a new technology but can be treated as a different form of the squirrel cage motor. Along with this change and orientation come some distinct advantages[54].

1. Power supply is only needed for primary side. The secondary is simply an induction plate made from aluminum, copper and steel metal layers. The manufacturing cost will be very low compared with other types of linear motors, such as the linear synchronous motor in the long distance public transportation application proposed in Germany

2. There is no physical coupling between the stator and the reaction plate, which means silent operation and reduced maintenance

3. The linear induction motor can be easily controlled as the normal rotating counterpart. The installation and assembly process is also relatively simple[53].

Linear motor thrusts vary from just a few to thousands of Newtons, depending mainly on the size and rating of the LIM. Speeds can vary from zero to many meters per second and are determined by pole pitch design and supply frequency. The speed can be controlled by either the simple or complex systems, stopping, starting, reversing, are all easily accomplished.

The horizontal travel is only limited by the length of the reaction plate or motor, many long conveyors use multi-motor systems. If the reaction plate is a flat disc then rotary motion is produced. The motion is not dependant on friction between wheels and rails so LIMs driven vehicles can be used in adverse weather conditions. It is possible by the design of the LIM that either the LIM itself or the reaction plate can move while the other is fixed[51,52].

A LIM can be used in most all conditions where straight-line motion or reciprocating forces are needed, or where unusual rotary drives are a disadvantage. By implementing a

LIM mechanical transmissions can often be eliminated, increasing reliability, and in some cases cost. The LIM is ideal for applications where space is at a premium.

A LIM makes an ideal variable speed drive, its behavior works much like a magnetic clutch and gives a very steady and controllable soft-start action. Maximum speed is fixed by design and frequency but load speed can be controlled in several ways: From on / off switching to phase control with tachometer type feedback.

Applications are many and varied, ranging from simple sliding doors to full control of vehicles weighing many tons, however it is more typical that certain applications have stood out as the ideal place that the LIM technology has been used. Applications such as sliding doors, robotic systems, conveying systems, steel tube movement, linear accelerators, theme park rides, and rapid transport systems have all lent their need for linear motion to the obvious choice of a LIM for main propulsion. All these and many others justify the use of a LIM because the LIM has many characteristics that help to make it very attractive. Size, shape, ease of control and overall ease of maintenance have all had large impacts on the demand for the LIM technology[47,46].

5.2 The general theory—equivalent circuit method

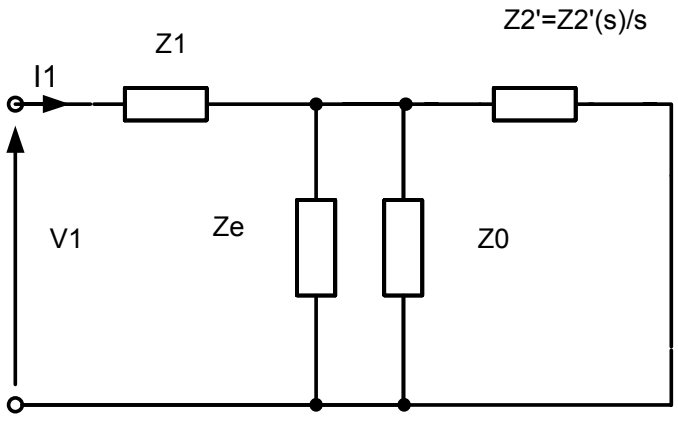

Figure 5.2 The T-type equivalent circuit with the longitudal end effects (J.F. Gieras)

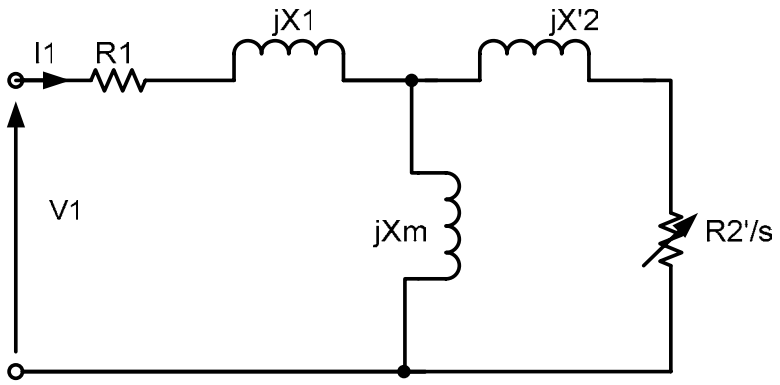

Figure 5.3 Equivalent circuit diagram that neglecting end effect

(S. A. Nasar and I Boldea)

One of the simplest approaches to calculate LIM parameters is to use equivalent circuit diagram. There are several types of equivalent circuit diagrams used in LIM theory. The most common and simplest ones are the T-type equivalent circuit with the longitudinal end effects [55], and the T-type equivalent circuit diagram that neglects the end effect. The first equivalent circuit (Figure 5.2) accounts for the transverse edge and the longitudinal end effects. The transverse edge effect can be included by correcting the secondary impedance. The longitudinal end effect can be included by connecting a slip-depended impedance in parallel with the vertical branch (the so called end-effect impedance) because longitudinal end effects are only significant at high speed. Another approach that was used in our project is an equivalent circuit that neglects the end-effect (Figure 5.3). This equivalent circuit includes the primary branch R_1, jX_1, magnetizing branch jXm and secondary branch R'_2/s.

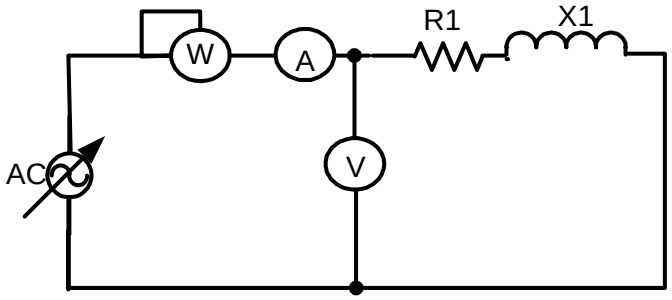

Figure 5.4 The circuit configuration of the secondary removed test

The parameters of the existing primary were determined by performing the secondary removed test (Figure 5.4). During this test the delta-connection was disconnected and each phase of the motor was supplied by ac voltage. The main electrical parameters like voltage, current active power and power factor were recorded during the test. Then the parameters of primary branches can be easily found by using well-known formulas

$$Z_1 = V_{ph} / I_{ph} \quad , \qquad R_1 = Z_1 \cos\phi \, , \quad X_1 = \sqrt{Z_1^2 - R^2{}_1}$$

In the same time, the primary resistance is:

$$R_1 = \rho \frac{l}{A} \qquad \text{(equation 5.1)}$$

Where ρ is a primary winding material resistivity;

l is a phase wire length;

A is an effective cross sectional area of a phase wire. Theoretically, an effective wire can consist of several wires or have several parallel branches. It is known that $l = l_{av} N_1$, where l_{av} is an average of a single turn, N_1 is a number of turns. The primary reactance $X_1 = X_{1s} + X_{1e} + X_{1d}$, where X_{1s}, X_{1e} and X_{1d} are respectively slot leakage reactance end connection leakage reactance and differential leakage reactance.

$$X_1 = 4\pi f \mu_0 L_1 N_1^2 (\lambda_{1s} k_x + \lambda_{1e} + \lambda_{1d}) / pq \qquad \text{(equation 5.2)}$$

where f is a frequency; L_1 is an equivalent primary core width; λ_{1s}, λ_{1e}, λ_{1d} are respectively slot, end connections and differential specific leakage permeances; p is a number of pole pairs; q is a number of slots per pole and phase.

Thus, by knowing R_1 and X_1 and all primary geometry dimensions, we can determine A and N_1 for the further calculations. By omitting here the detailed description of the calculations of different correction factors mostly correlated with the skin effect, we can

determine the magnetizing reactance

$$X_m = 12\mu_0 \varpi_1 L_1 k_{w1} N_1^2 \tau / \pi^2 p g_{ei} \qquad \text{(equation 5.3)}$$

where τ is a pole pitch; g_{ei} - corrected air gap; k_{w1} - primary winding factor; ϖ_1 - angular frequency. After that, the secondary resistance could be found

$$R_2' = X_m / G_{ei} \qquad \text{(equation 5.4)}$$

where G_{ei} is the so-called "goodness factor" that is inversely proportional to the air gap. Now, we have all of the equivalent circuit parameters, and, thus, the LIM output characteristics can be easily determined. The equation for thrust is

$$F_x = \frac{3I_2'^2 R_2'}{2s\tau f} \qquad \text{(equation 5.5)}$$

The input power is $P = F_x^2 \tau f + 3I_1^2 R_1$.

The efficiency is $\eta = F_x 2\tau f (1-s)/(F_x \tau 2f + 3I_1^2 R_1)$.

The power factor is $\cos\phi_1 = (F_x 2\tau f + 3R_1 I_1^2)/3V_1 I_1$.

5.3 Russell and Norsworthy method

The structure of the LIM results a very complex electromagnetic coupling. The two open ends generate undesirable waves beside the normal traveling wave.

$$b = B_s \exp[\ j(\omega t - \frac{\pi}{\tau} x)] \qquad \text{the normal wave}$$

$$+ B_1 \exp(-\frac{x}{\alpha_1}) \exp[\, j(\omega t - \frac{\pi}{\tau_e} x)] \qquad \text{the entry-end effect wave}$$

$$+ B_2 \exp(\frac{x}{\alpha_2}) \exp[\, j(\omega t + \frac{\pi}{\tau_e} x)] \qquad \text{the exit-end effect wave}$$

Since $\alpha_1 >> \alpha_2$, the exit-end wave will attenuate very quickly, the entry-end wave has the main effect. A very important factor is the wavelengths of the end effect waves are not only related to the pole pitch, but the motor speed.

A general electrical equivalent circuit as the rotating motor may cause unacceptable error for high speed operation. As the result, all parameters are developed from the magnetic field; then with the distribution of the magnetic flux density B and magnetic field density H, the power and the loss in each layer can be obtained; in the end the familiar electrical equivalent circuit is developed and can be easily compared with the cylinder motor. The layer theory and the equivalent circuit model are the two basic theories for this LIM magnetic calculation.

First, two different kinds of power supplies are considered. In the simplified one-dimension model of LIM, the practical discrete currents in the stator windings are usually presented by a current sheet. When the constant current source is used, it is quite simple to analysis the distribution of the current on the sheet. But in real world a constant voltage is more likely to be used, which means the current through each winding will also be influenced by the impedance of LIM, It will be extremely difficult to guarantee the accuracy of the current distribution. Fortunately Russell and Norsworthy's classic paper solved the current distribution for a finite width current sheet[42] There is another pole-by-pole model used by T.A Lipo [44,45].

The next step is to simplify the complexity of the multi-layer structure of LIM. Basing on the magnetic "T" equivalent circuit. Each layer of the LIM is presented by a very simple T-equivalent circuit. The whole structure of the LIM is simplified as a cascade network of T circuits. The resulting parameters are determined by the characteristics of the layer, i.e. the material's resistivity, the layer's thickness and the relative permeability, etc.The equivalent circuit used in the program can be found in Figure 5.5.

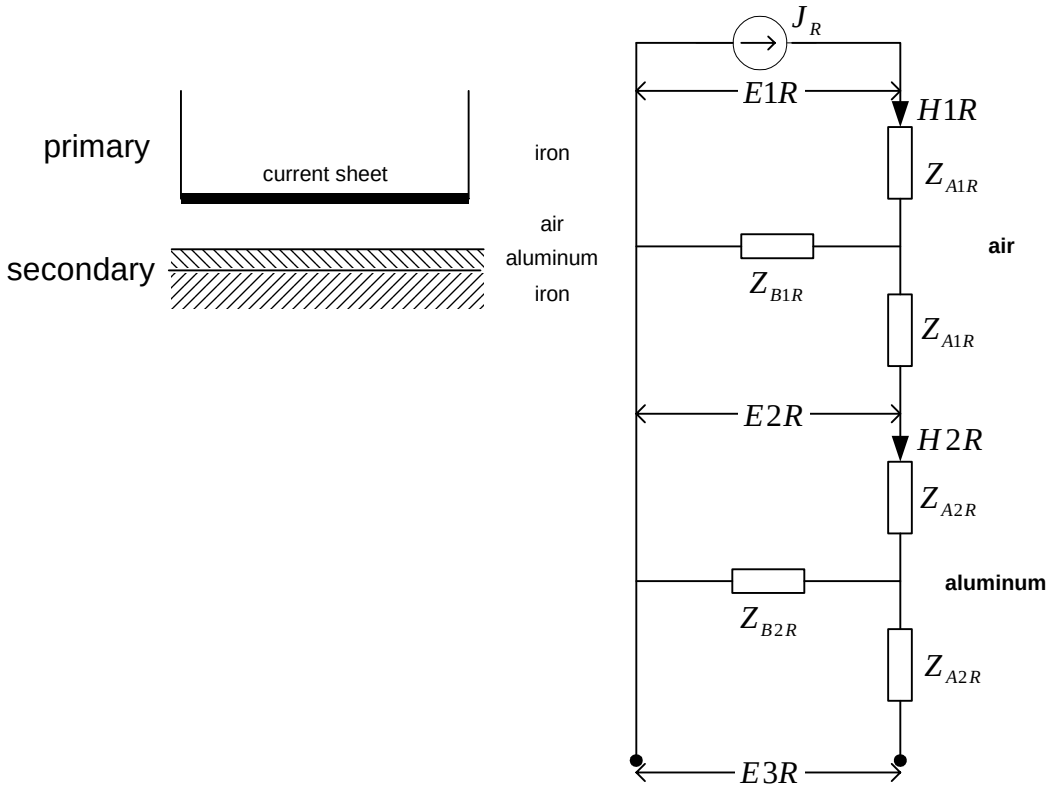

Figure 5.5 The equivalent circuit of Russell and Norsworthy method

All the analysis is based on the steady state. The LIM is separated into several tens small sections in the space position. Each small part will have different flux density. The program is also able to take into account of the effects of the harmonics. One interesting part is the negative frequencies will be considered since the moving direction has to be used as the positive reference. The negative frequency will generate flux wave with opposite moving direction.

Shown in Figure 5.6, the brief structure of the program is as following:

1. Break in motor along its moving direction y into 48 grids;
2. Calculate the current density for each section;
3. Calculate the effect of harmonics;

4. Calculate the characteristic parameters for each layer;
5. Build the T equivalent circuit.
6. Compute the magnetic field density for each layer;
7. Calculate the magnetic flux density;
8. Develop the equivalent electric parameters.

The detail is in Appendix 3.

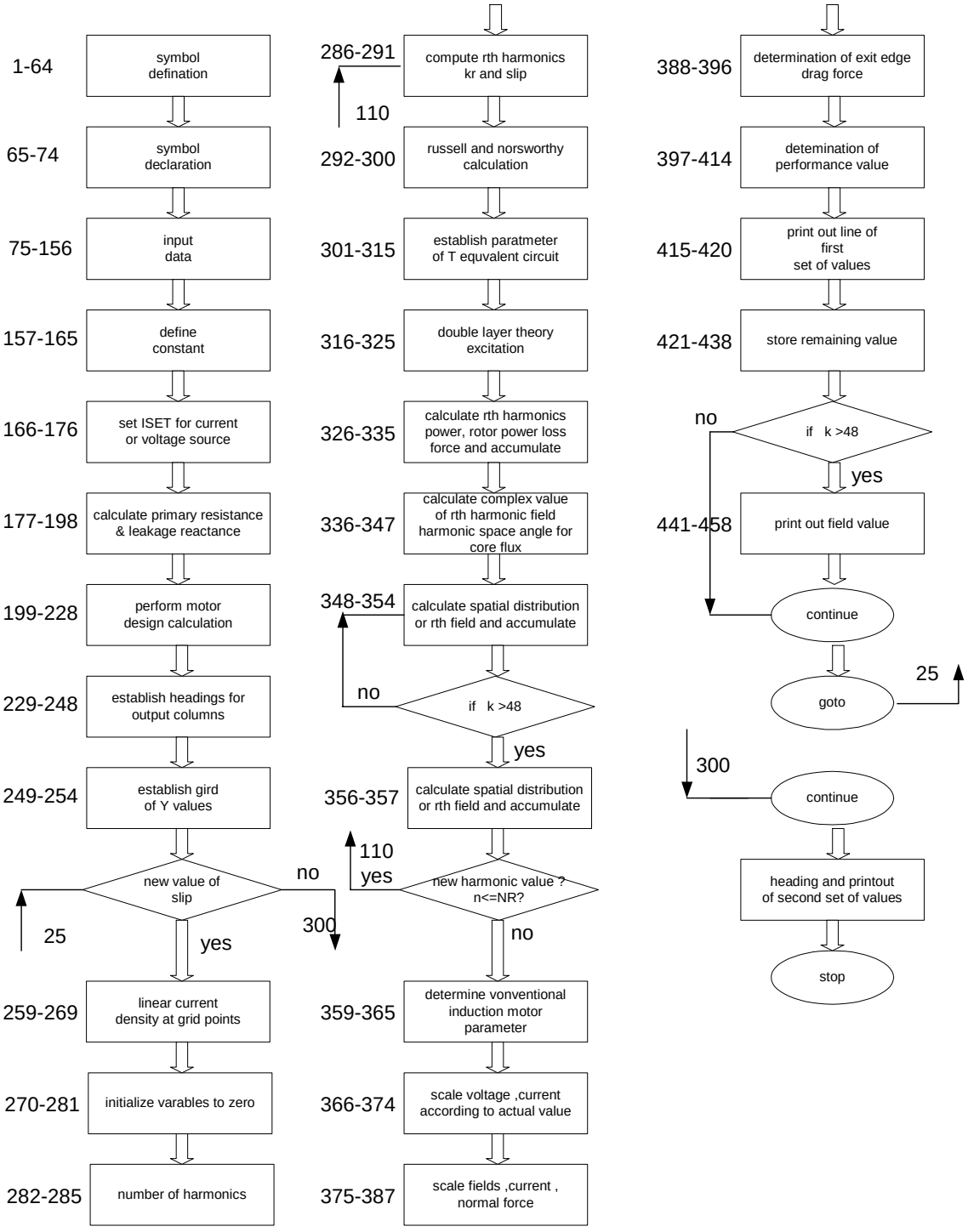

Figure 5.6 The flowchart of the Russell and Norsworthy method

6 CHAPTER LINEAR INDUCTION MOTOR (LIM) DESIGN

6.1 LIM control mode

There are several constraints which should be considered during the LIM design procedure. The motor manufacturer needs to minimize the motor weight to save material and also limit the total supply current for thermal consideration. While the drive designers are always looking for the maximum thrust with less supplied voltage. The wide operating speed requirement for the application point of view makes the design decision more complex.[53] Figure 6.1(a) demonstrates the output thrust vs. speed performance when I1rms=constant.

For each supplied frequency there is a thrust vs. velocity curve. By changing motor frequency the motor can shift between different operating curves The Constant Current Mode (CCM) control is highly preferred since the output thrust is nearly proportional to the amplitude of the primary current. The output thrust control can be easily realized be just measuring the primary current, supply frequency and the speed. One of the LIM characteristics should be emphasized. The same thrust vs. velocity operation point can be achieved by as many as different frequencies and voltages combination. The LIM operating zone is rather arbitrary if there is no any consideration from the input side. The efficiency and power factor are two good indicators for the system consideration. From figure 6.1(c) and Figure 6.1(d) there is some difference between the operating point selected either by maximum efficiency or the maximum power factor. Their product is used as a trade-off. A good result of this method is that the operating zone is also very close to the peak value of the output thrust.

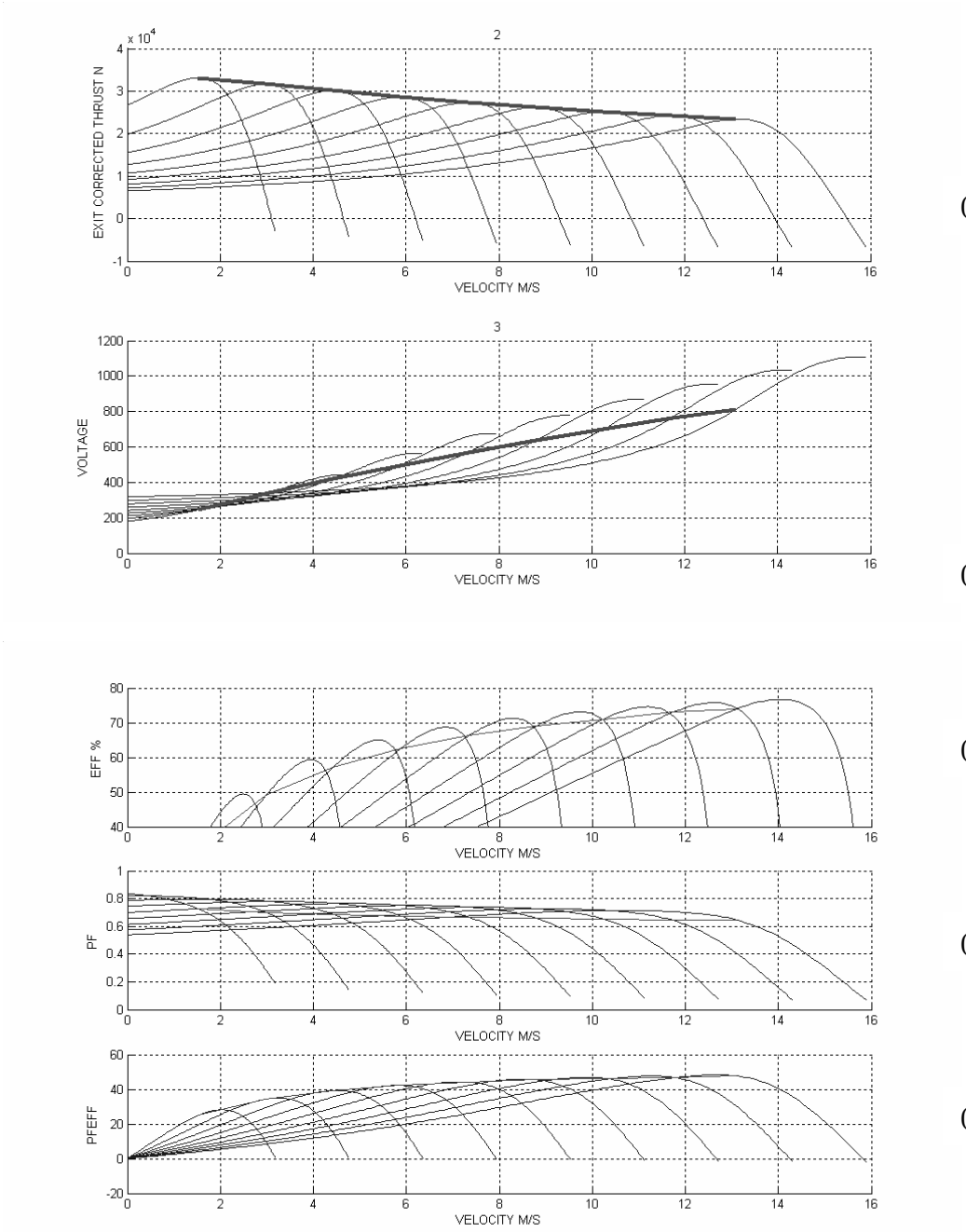

Figure 6.1 The characteristic curves of the LIM in Constant Current Mode

however CCM has a significant limitation shown in the related voltage vs. velocity plot. In order to keep the constant supplied current, the primary voltage keeps on increasing when operating speed is high. When the voltage meets the upper voltage limitation from

the drive side, the control has to be changed into the Constant Voltage Mode (CVM). The voltage drop across the motor impedance is almost proportional to the frequency, or the speed. The output thrust will dramatically decrease as a result of significant drop of the primary current. In real application of the LIM driven high-speed train, when Lim is in its high speed operation zone, the train is also in the middle of each station, where the supplied DC voltage from the power station is the weakest. The voltage constraint is the most severe bottleneck in motor design.[48,49]

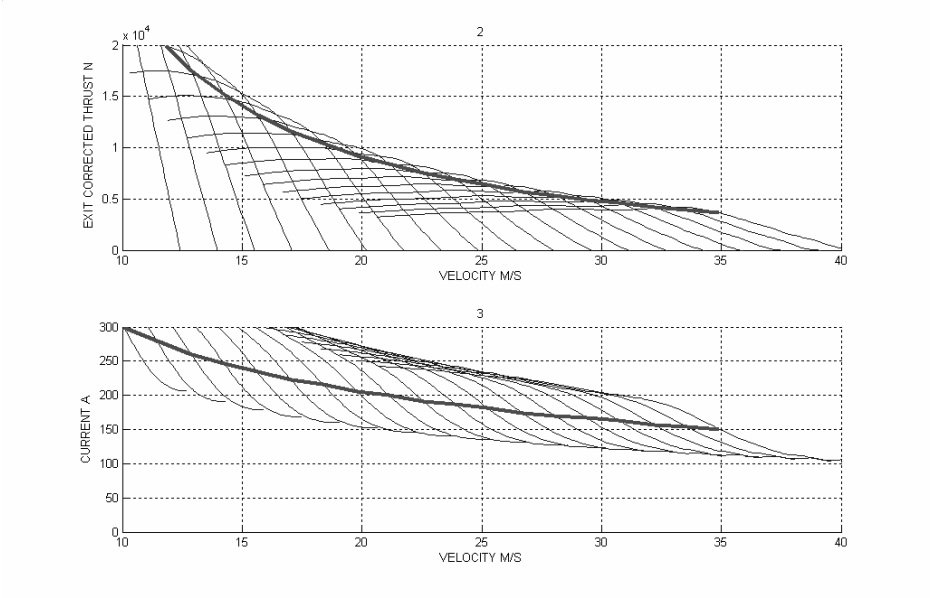

Figure 6.2 The characteristic curves of the LIM in Constant Voltage Mode

6.2 Asymmetric structure

One of the most efficient ways to decrease phase impedance is to use less number of conductors in series. Figure 6.1 and Figure6.2.are based on design 1, whose number of conductor is 16 (8 per slot). While Fig 6.3 is the results of design 2, whose number of conductor is 12 (6 per slot). The details for each design can be found in Appendix 2.

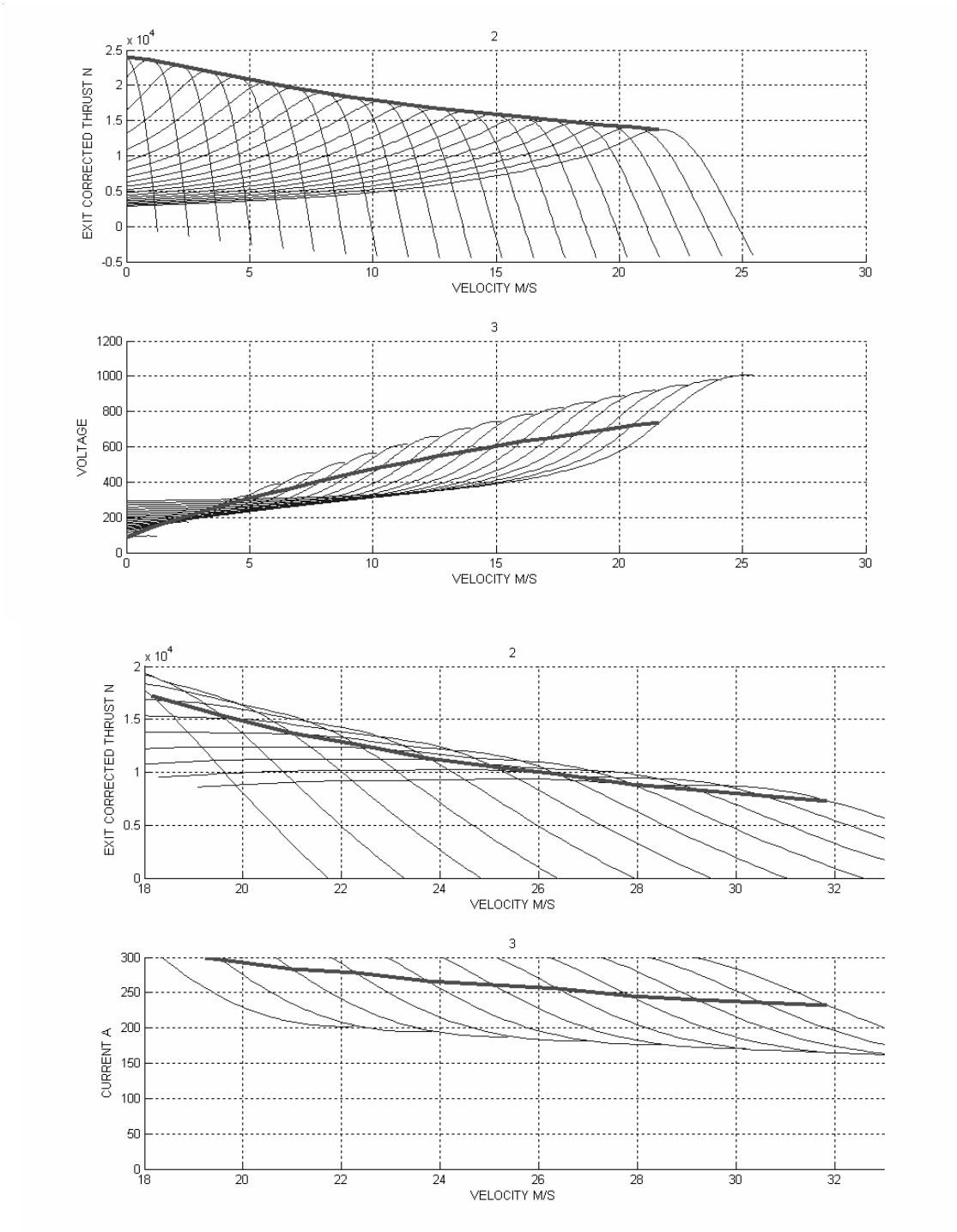

Figure 6.3 The characteristic curves of Design 2 in both CCM and CVM

Based on the technical description of the project,

the maximum mass /LIM AW3=49,820/2=24910 kg;

the preferred starting acceleration a>=1m/s

As a result the starting thrust should be greater than 25 kN.

The maximum gradient on the whole line is 3% when velocity=25m/s, still using AW3

The target thrust at 25m/s should be no less than 7.5 kN.

Design 1 the starting thrust can easily be more than 33 kN but drops to less than 7 kN. By deceasing the number of conductors per slot from 8 to 6, the output thrust at high speed is met but unfortunately the starting thrust drops to less than 30kN. The original design rule from the motor manufacturer limits the number of conductors per slot to be an even number considering the structure long reliability in such an severe environment full of vibration. While from our design point of point, 7 conductors per slot will be an optimal solution for both starting and the high-speed operation. The gain in the primary core size, conductor size and total material usage will be very significant.

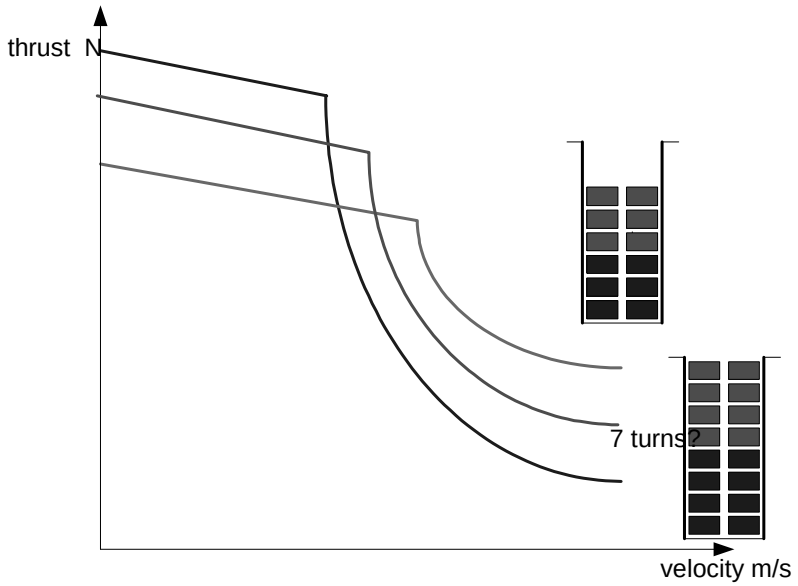

Figure 6.4 The thrust vs. velocity diagram

Fortunately there are totally 4 poles per phase in this LIM design. Instead of using 8 conductors in each slot building a 8,8,8,8 structure for 4 pairs of 6 conductors in each slot

building a 6,6,6,6 structure, an asymmetric structure 8,6,6,8 is used as shown in Figure 6.5. The average number of conductors for each phase will equal to 7. An additional 1 turn will build a 0.5 order harmonic MMF, which could be the only potential drawback. A new design 3 is investigated using asymmetric winding structure.

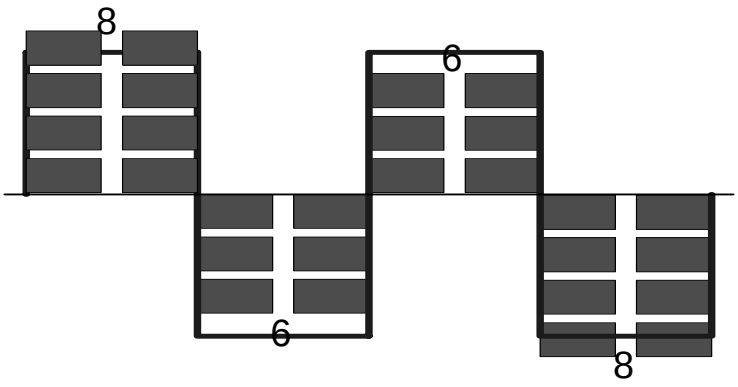

Figure 6.5 The 8,6,6, 8 asymmetric structure

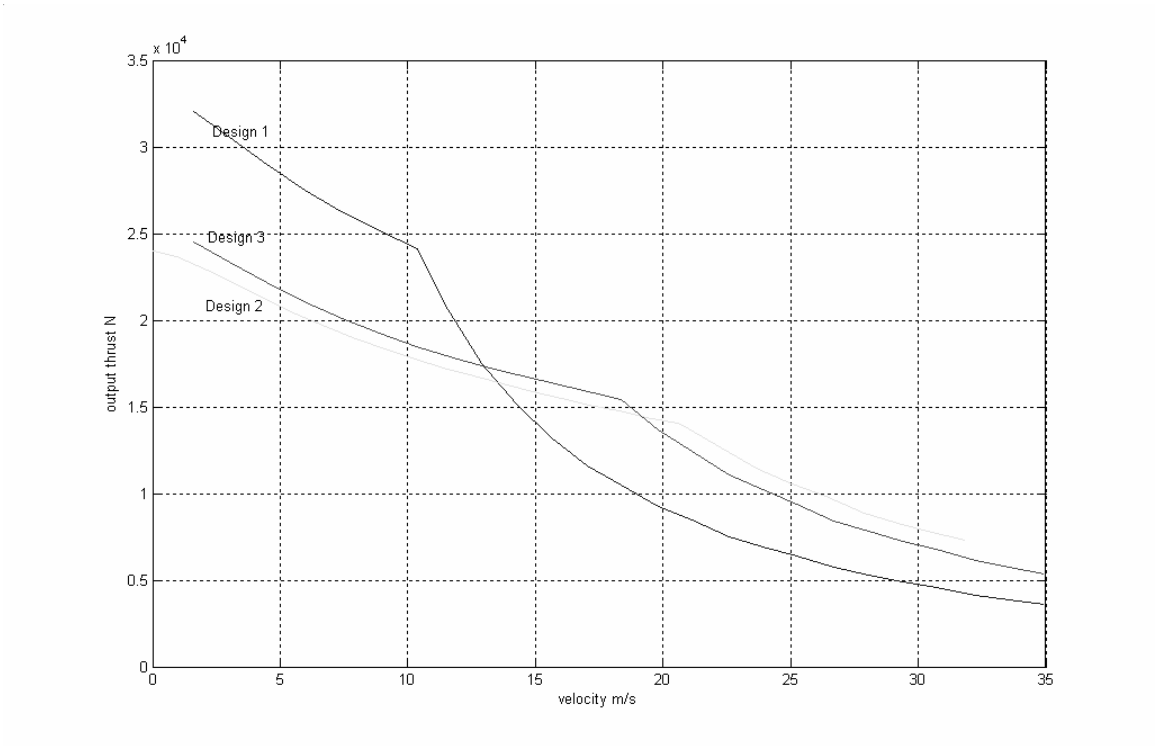

Figure 6.6 Comparison of the three LIM design solutions

By using the asymmetric structure, the high-speed output thrust increases from a little less than 7 kN to more than 9 kN when motor velocity is 25 m/s. Even though there is some loss at the low speed range. The starting thrust can still more than 25 kN. The asymmetric structure idea is like to double the total design solution by increasing the number of conductors from just even number to the whole integer range. Further experimental verification will be explained in the next chapter.

6.3 LIM system evaluation

In this design practice, the LIM design and the drive design are processed in two different manufacturers to minimize the design cycle. Beside the detail of the magnetic design and the operating point selection, the motor designer needs to always prove accurate but simple information to the drive designer.

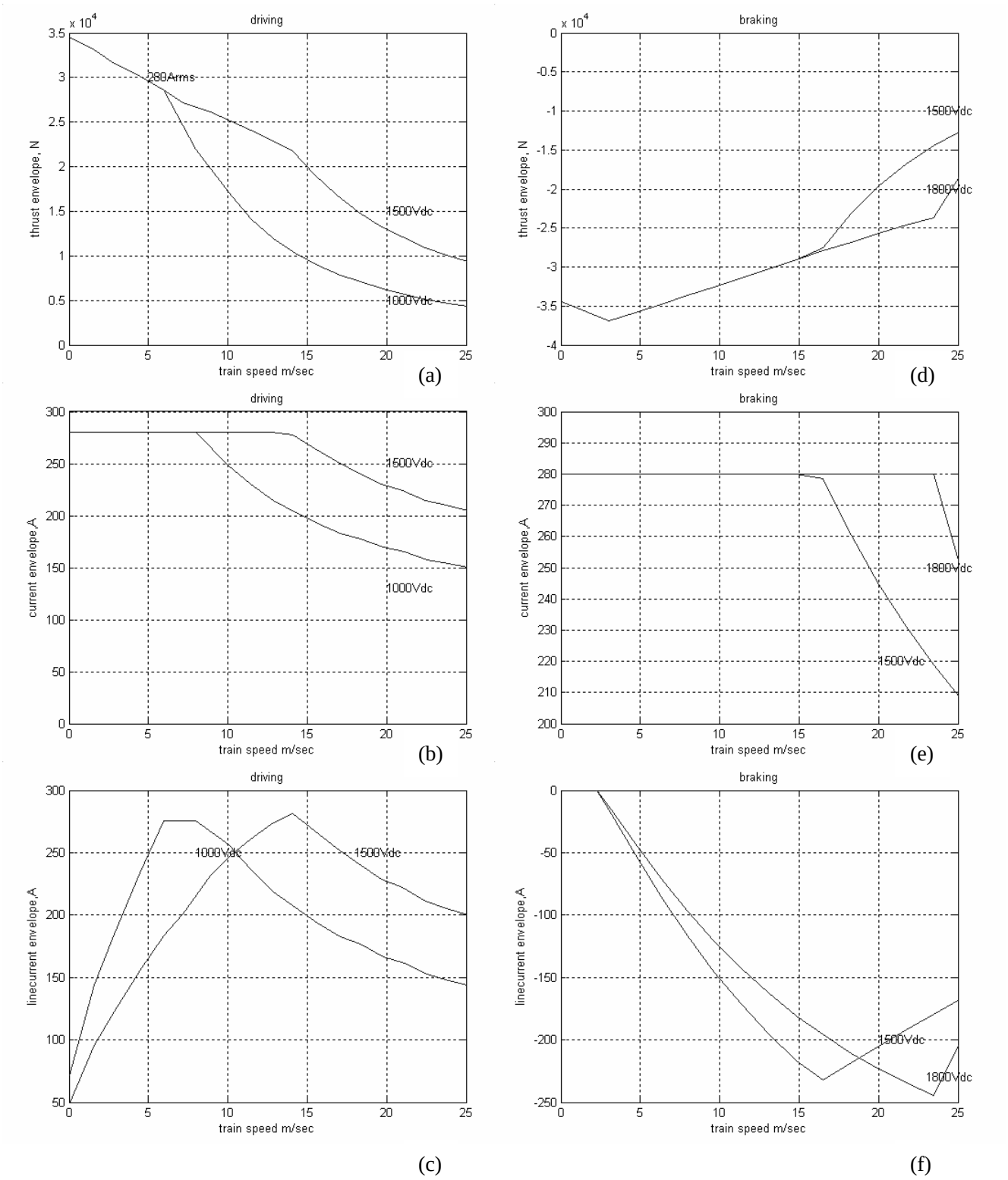

Figure 6.7 Motor performance envelopes for both driving(a-c) and braking mode(d-f)

As shown in Figure 6.7(a-f), The LIM drive system can be evaluated with these 6 performance envelopes. Giving the absolute position of the each station and the gradient information, the system model (Figure 6.8) can simulate all stages of the LIM drive system including starting, constant speed operation and braking. Figure 6.9 is an example for starting stage. The RMS current of each station interval is calculated in table 6.1. The RMS current for the total route is the key factor for motor thermal evaluation.

STATION	Iup(A)	uptime(s)	I^2*T		Idown(A)	downtime(s)	I^2*T
						25/2	
1		16/2			171	129	3768509
2	177	120	3768509		195	134	5106727
3	193	121	4487750		180	103	3342067
4	187	97	3388053		162	119	3133302
5	170	112	3239397		157	143	3501327
6	169	138	3940765		194	84	3166434
7	197	82	3156416		184	102	3447866
8	194	99	3725339		184	105	3524182
9	174	98	2965426		192	92	3399473
10	200	89	3568682		192	81	3008475
11	201	74	3007159		179	101	3237025
12	194	96	3599423		179	95	3040294
13	188	93	3307714		165	114	3111244
14	180	113	3629817		195	90	3452234
15	193	85	3190668		175	117	3596515
16	185	113	3864155		167	139	3860440
17	164	133	3563381		212	84	3786094
18	212	84	3782357		169	136	3907023
19	173	133	3961103		176	113	3507042
20	189	111	3973621		179	100	3184463
21	186	98	3375494		177	127	3982572
22	190	130	4691492		168	131	3679922
23	170	128	3679554		181	124	4043524
24	176	122	3788138		161	154	3999299
25	158	152	3788199		190	96	3475808
26	198	91	3558614			16/2	
27		13/2					
				LINE(Arms)			LINE(Arms)
		2712	91001226	183		2814	89261862 178

Table 6.1The summary of RMS current for each station interval

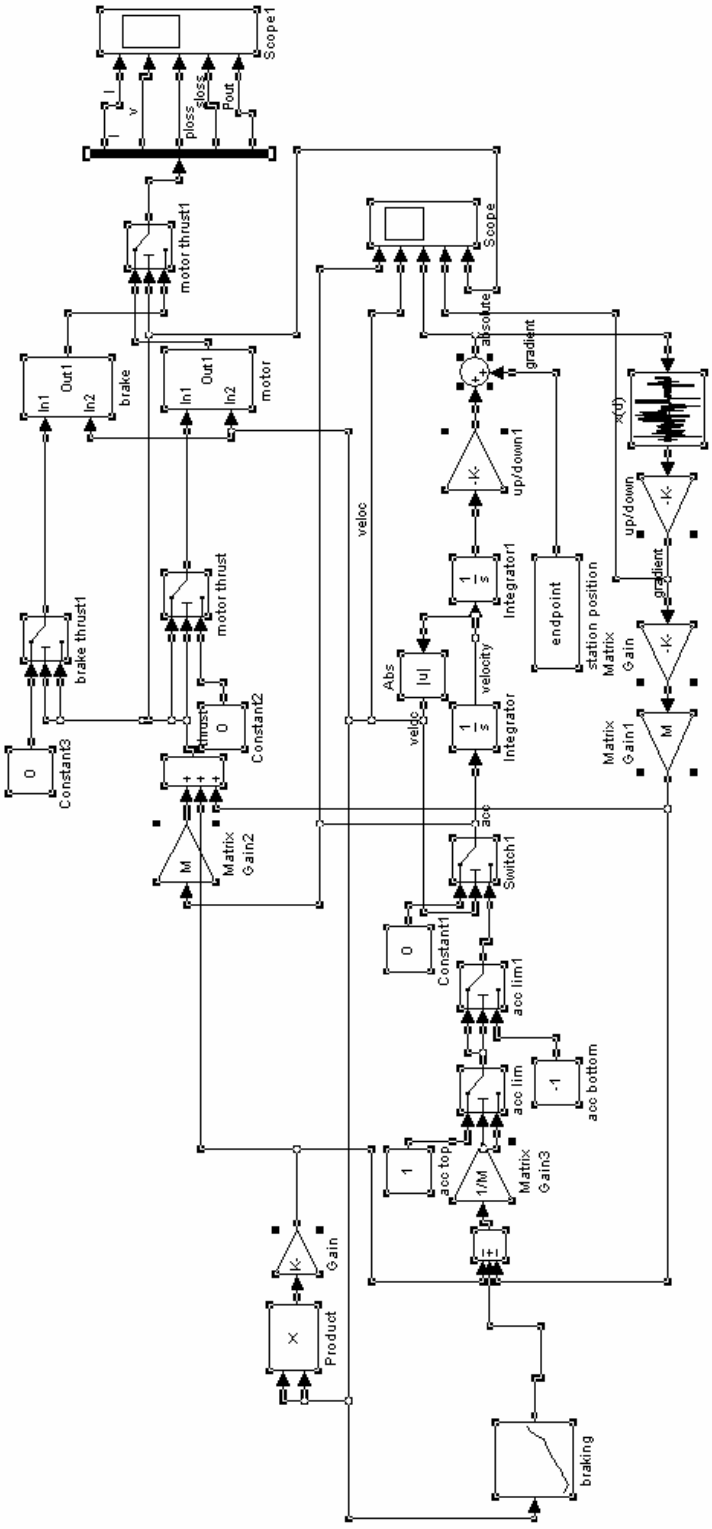

Figure 6.8 The LIM system simulation model

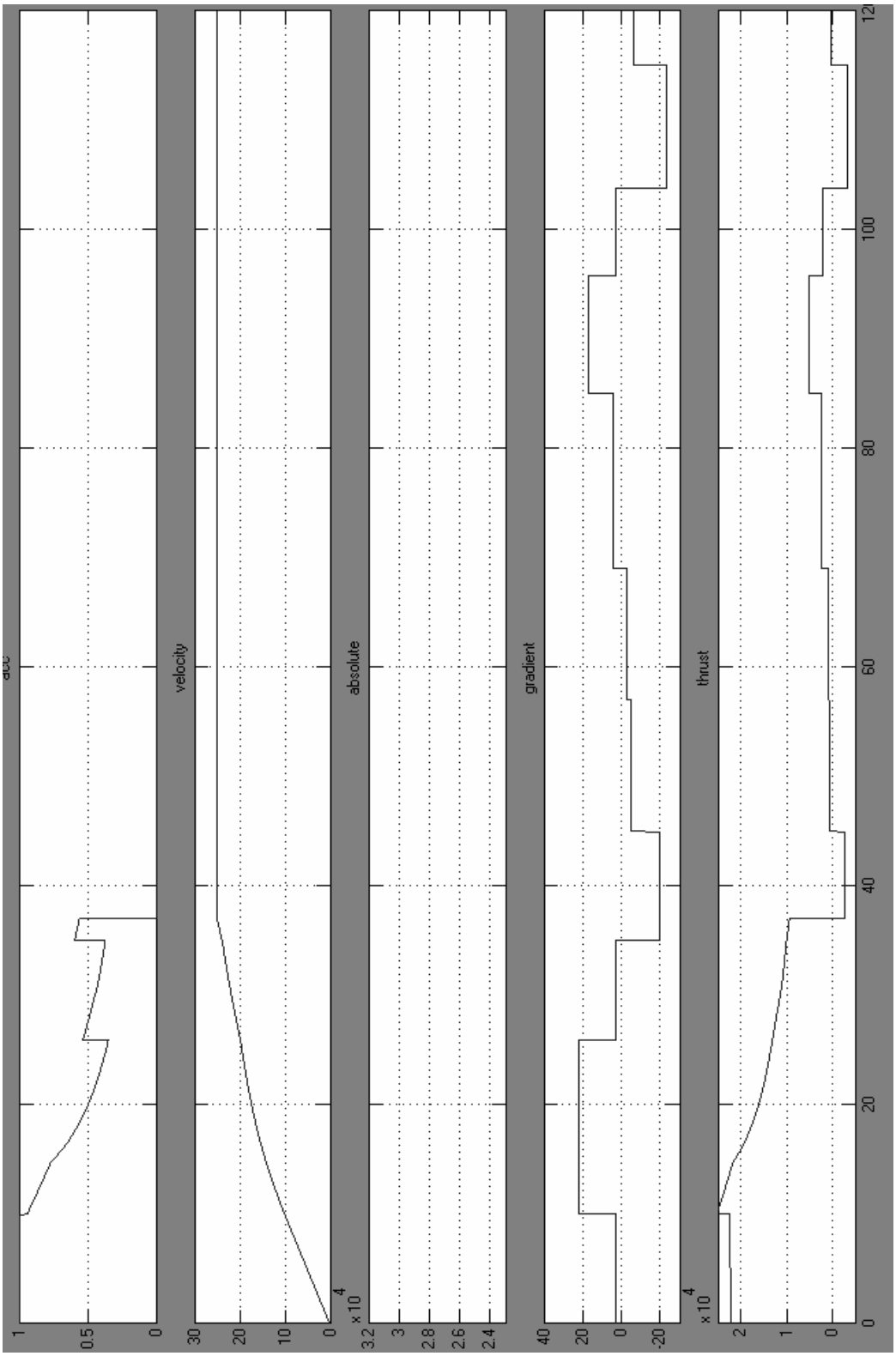

Figure 6.9 An example of the system simulation at starting stage

7 CHAPTER LIM EXPERIMENTS

7.1 The test platform

Two linear induction motors with symmetric and asymmetric windings are built respectively in MSRF. The primary core is shown in Figure 7.1. The symmetric motor has a constant 78 turns per slot per phase.While the asymmetric motor is built with 2 large coils contained 88 turns at both end. And there is a small coil contained 68 turns in the middle. The objective of the motor comparison is to evaluate the performance of the asymmetric motor to normal symmetric motor, especially in the high-speed range. even though there are only 3 poles for each phase instead of 4 as originally proposed. The testbed is shown is in Figure 7.2.

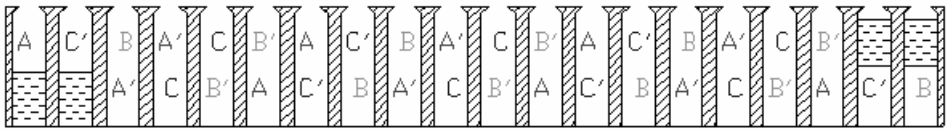

Figure 7.1 The primary core windings of LIM

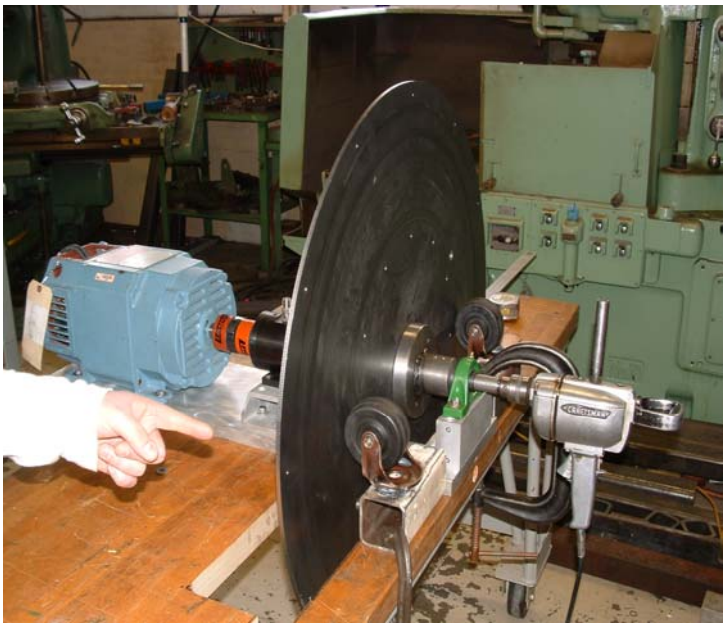

Figure 7.2 LIM test bed

The ideal induction plate is replaced by an Aluminum and steel disk with a diameter of 1m. The motor is controlled by a common Baldor 5hp induction drive. The drive will be in the Constant Voltage mode when the output frequency is greater than 60Hz. As a result, only the speed ranges under CVM are tested. Testing frequencies include 80,120,160 and 200 Hz.

7.2 Experimental results

From Figure 7.3 and 7.4 when airgap=3mm, the thrust vs. velocity curve from the symmetric motor is very similar to the curve from the asymmetric motor when supplied frequency is 80,120 and 160Hz. There is very tiny improvement from the asymmetric motor when supplied frequency is 200Hz and LIM is spinning in the speed range. There is no much difference between the symmetric structure and the asymmetric structure when the airgap is very small.

When airgap increases to 5mm as shown in Figure 7.5 and Figure 7.6, there is some significant gain from the asymmetric motor when the motor line speed is more than 2.5 m/s. For instance the output thrust of the symmetric motor at 2.5m/s is less than 0.5 N, while the output thrust of the asymmetric motor can be nearly 0.6N, which is like 20% gain. In the case of f=200Hz, the output thrust curve from the asymmetric motor is always higher than the symmetric one in all speed range.

From figure 7.7 and 7.8 when the aigap=7mm, the asymmetric motor demonstrates much better performance than its symmetric counterpart for all frequencies in full speed range. For instance when supplied frequency is 80Hz, the output thrust increases from 1.65 N to 1.9 N at line speed 1 m/s, and the thrust at 1.5 m/s increases from 0.5 N to 0.6 N.

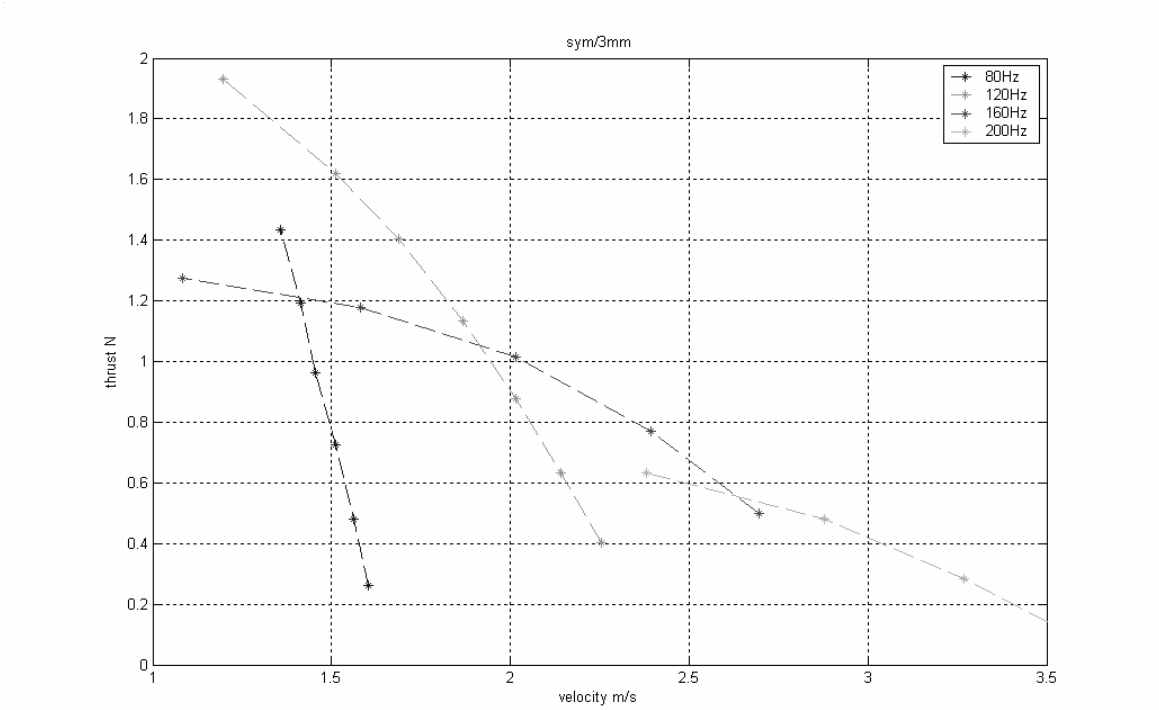

Figure 7.3 The thrust vs. velocity curve of the symmetric motor, airgap=3mm

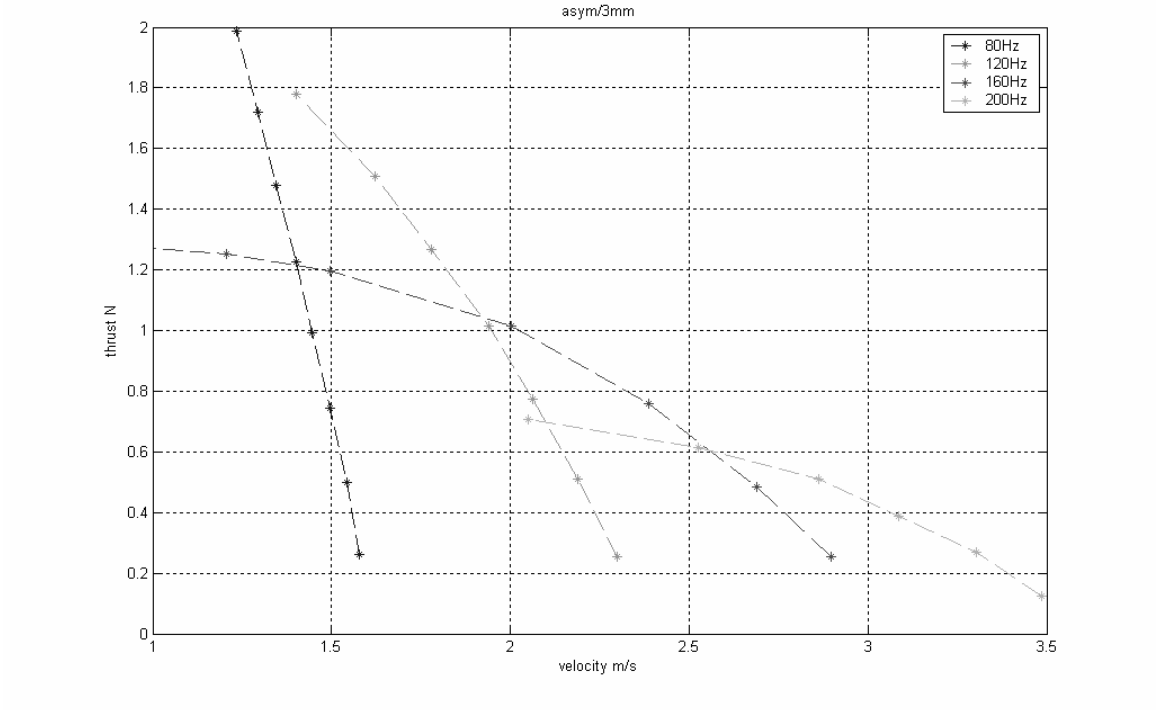

Figure 7.4 The thrust vs. velocity curve of the asymmetric motor, airgap=3mm

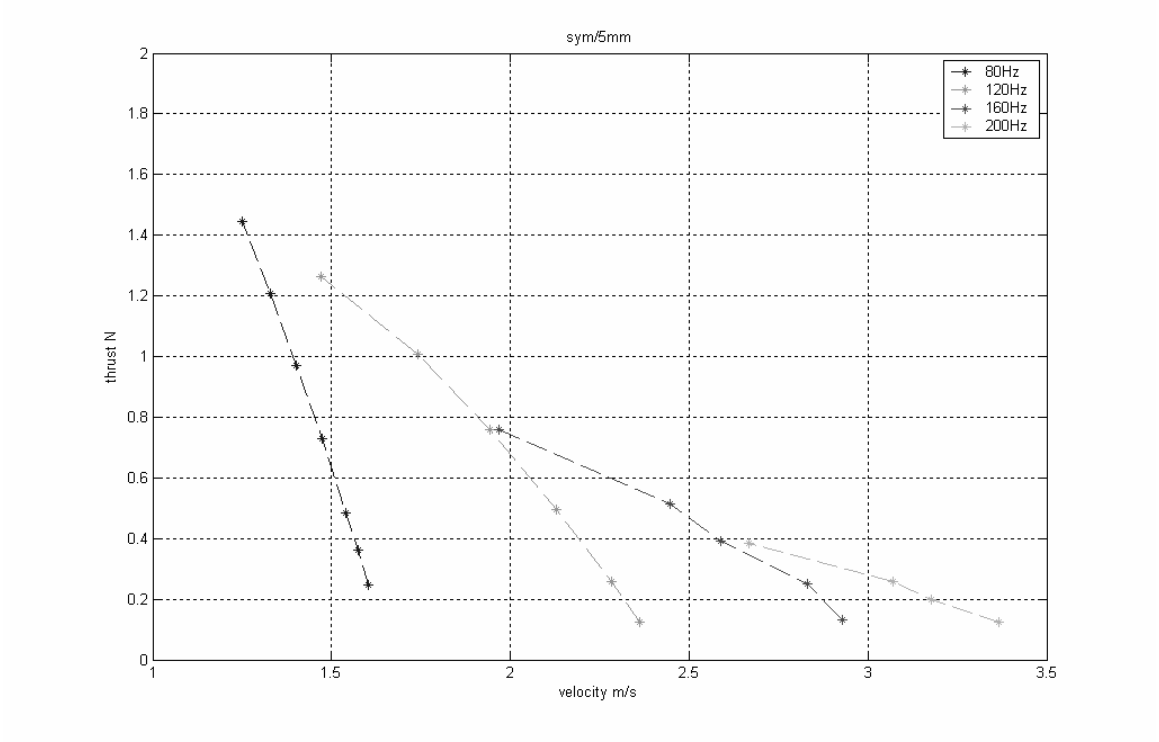

Figure 7.5 The thrust vs. velocity curve of the symmetric motor, airgap=5mm

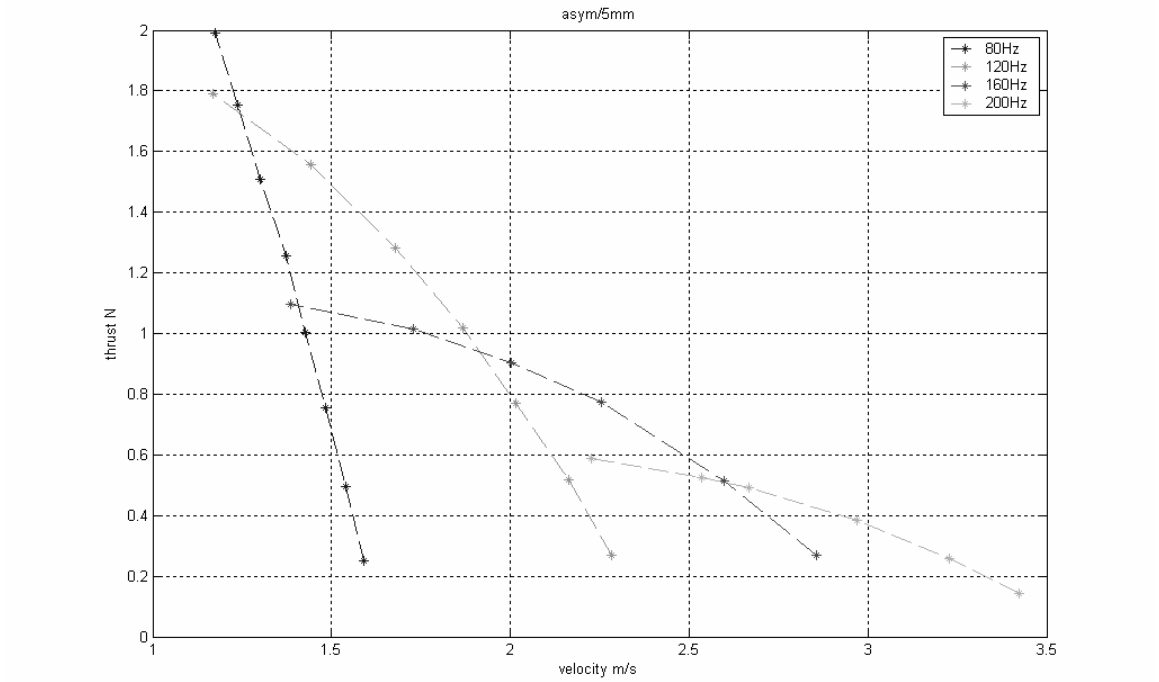

Figure 7.6 The thrust vs. velocity curve of the asymmetric motor, airgap=5mm

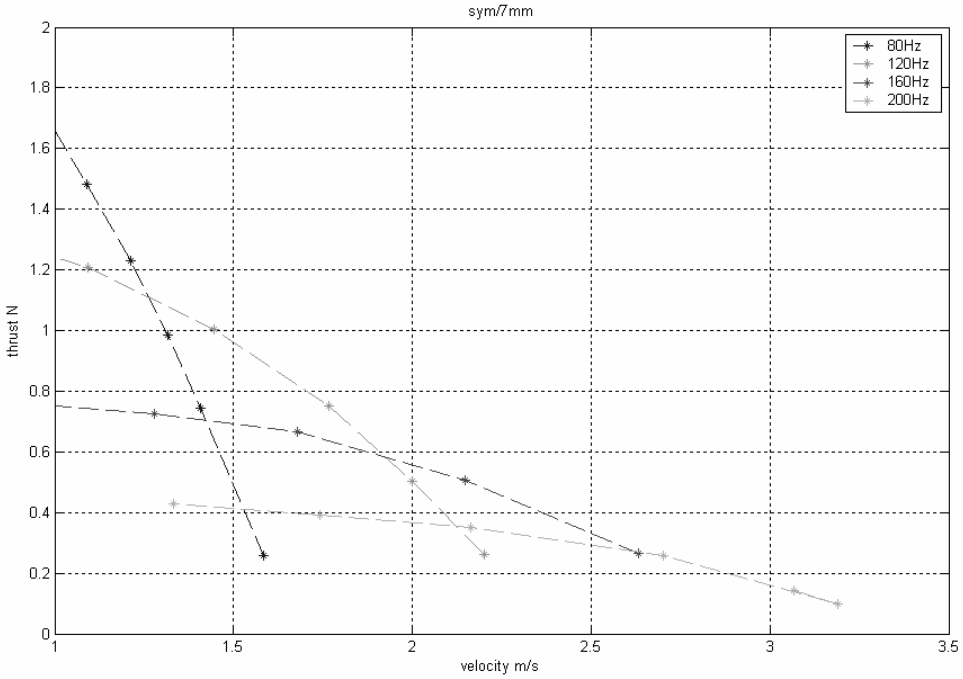

Figure 7.7 The thrust vs. velocity curve of the symmetric motor, airgap=7mm

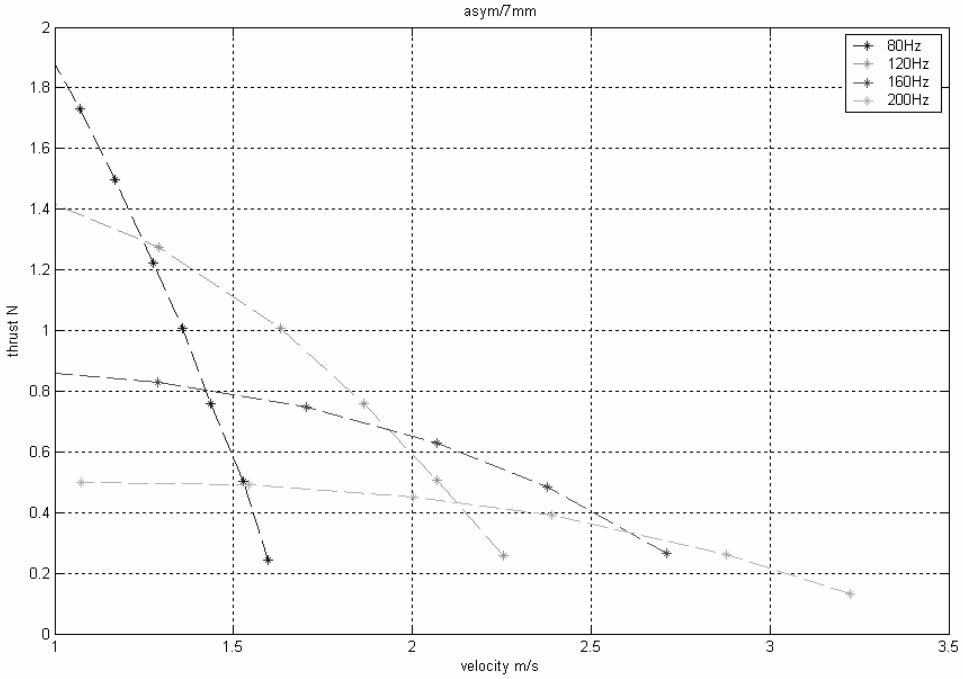

Figure 7.8 The thrust vs. velocity curve of the symmetric motor, airgap=7mm

7.3 Experimental Conclusion

The experiments verified the validity of the asymmetric structure. Through the comparison to the symmetric motor, the asymmetric structure demonstrates significant gains especially in high speed with large airgap, which is exactly the real situation of the high-speed transportation. By introducing the asymmetric structure, the flexibility of the LIM is doubled.

8 CHAPTER CONCLUSION

Two linear actuators are investigated in this research. Compared with the traditional hydraulic system, the SRM driven linear actuator offers a new solution for high thrust/short stroke application with less maintenance and higher reliability. Several methods are employed in the motor magnetic design to guarantee the high thrust requirement within the limited motor size. Sensorless control and fault tolerance ability are the additional contributions for this new linear actuator. The primary design is verified through both computer simulation and experimental tests. The simplicity of this design makes this SRM driven linear actuator an excellent replacement of the common hydraulic devices with little risk. Further improvements could include the acoustic noise study on the SRM and the control strategy on starting-up with full load.

This thesis also investigated alternative winding configurations to potentially enhance the performance characteristics of linear motors for transportation applications. The Linear induction motor (LIM) is an excellent cost-effective solution with linear motion. Instead of following the “even turn rule” which will result in too much redundancy in the design and significantly increase the motor weight and system cost, a novel asymmetric structure is proposed in this research. With the idea of asymmetric windings, the average number of turns per slot can be an integer instead of just the even number. The experiments verified possible improvements from the new asymmetric structure compared with the normal symmetric motor. The asymmetric structure provides a new opportunity for the LIM designer to find the trade-off between low-speed and high-speed performance.

BIBLIOGRAPHY

1. Miller, T.J.E, “Switched reluctance motors and their control”, Oxford press,1993

2. Zhen Zhong Ye; Martin, T.W.; Balda, J.C. “Maximation of starting torque of a 10/8 SRM with short flux path based on numerical analysis and calculation” , Industrial Electronics Society, 2000. IECON 2000. 26th Annual Confjerence of the IEEE Volume 1, 22-28 Oct. 2000 Page(s):362 - 368 vol.1

3. Tian-Hua Liu; Yih-Hua Chang; “Implementation of a microprocessor-based sensorless switched reluctance drive”, Industrial Electronics Society, 2000. IECON 2000. 26th Annual Confjerence of the IEEE Volume 1, 22-28 Oct. 2000 Page(s):375 - 380 vol.1

4. Gao, H.; Salmasi, F.R.; Ehsani, M.; “Sensorless control of SRM at standstill”, Applied Power Electronics Conference and Exposition, 2001. APEC 2001. Sixteenth Annual IEEE Volume 2, 4-8 March 2001 Page(s):850 - 856 vol.2

5. Jianrong Bu; Longya Xu;” Eliminating starting hesitation for reliable sensorless control of switched reluctance motors”, Industry Applications, IEEE Transactions on Volume 37, Issue 1, Jan.-Feb. 2001 Page(s):59 – 66

6. Longya Xu; Chuanyang Wang;” Accurate rotor position detection and sensorless control of SRM for super-high speed operation”, Power Electronics, IEEE Transactions on Volume 17, Issue 5, Sept. 2002 Page(s):757 – 763

7. Ehsani, M.; Fahimi, B.; “Elimination of position sensors in switched reluctance motor drives: state of the art and future trends” ,Industrial Electronics, IEEE Transactions on Volume 49, Issue 1, Feb. 2002 Page(s):40 – 47

8. Fahimi, B.; Suresh, G.; Ehsani, M.; “Review of sensorless control methods in switched reluctance motor drives”, Industry Applications Conference, 2000. Conference Record of the 2000 IEEE Volume 3, 8-12 Oct. 2000 Page(s):1850 - 1857 vol.3

9. Suresh, G.; Fahimi, B.; Ehsani, M.; “Improvement of the accuracy and speed range in sensorless control of switched reluctance motors” ,Applied Power Electronics Conference and Exposition, 1998. APEC '98. Conference Proceedings 1998., Thirteenth Annual Volume 2, 15-19 Feb. 1998 Page(s):771 - 777 vol.2

10. Hossain, S.A.; Husain, I.; Klode, H.; Lequesne, B.; Omekanda, A.M.; Gopalakrishnan, S.;” Four-quadrant and zero-speed sensorless control of a switched reluctance motor”, Industry Applications, IEEE Transactions on Volume 39, Issue 5, Sept.-Oct. 2003 Page(s):1343 – 1349

11. Krishnan, R.; “Sensorless operation of SRM drives: R & D status”, Industrial Electronics Society, 2001. IECON '01. The 27th Annual Conference of the IEEEVolume 2, 29 Nov.-2 Dec. 2001 Page(s):1498 - 1503 vol.2

12. Panda, D.; Ramanarayanan, V.; “Sensorless control of switched reluctance motor drive with self-measured flux-linkage characteristics”,Power Electronics Specialists Conference, 2000. PESC 00. 2000 IEEE 31st Annual Volume 3, 18-23 June 2000 Page(s):1569 - 1574 vol.3

13. Venkatesha, L.; Ramanarayanan, V.; “A comparative study of pre-computed current methods for torque ripple minimisation in switched reluctance motor” ,Industry Applications Conference, 2000. Conference Record of the 2000 IEEE Volume 1, 8-12 Oct. 2000 Page(s):119 - 125 vol.1

14. Akhter, H.E.; Sharma, V.K.; Chandra, A.; Al-Haddad, K.; “Starting performance of switched reluctance motor with fixed turn-off angle control scheme”, IECON 02 [Industrial Electronics Society, IEEE 2002 28th Annual Conference of the Volume 2, 5-8 Nov. 2002 Page(s):1020 - 1025 vol.2

15. Loop, B.P.; Sudhoff, S.D.;” Switched reluctance machine model using inverse inductance characterization” Industry Applications, IEEE Transactions on Volume 39, Issue 3, May-June 2003 Page(s):743 - 751

16. Texas Instruments, “A Variable-Speed Sensorless Drive System for Switched Reluctance Motors”, application report 1999

17. Visinka, R.;” Phase resistance estimation for sensorless control of switched reluctance motors” IECON 02 [Industrial Electronics Society, IEEE 2002 28th Annual Conference of the Volume 2, 5-8 Nov. 2002 Page(s):1044 - 1049 vol.2

18. Krishnan, R.; Staley, A.M.; Sitapati, K.;” A novel single-phase switched reluctance motor drive system”, Industrial Electronics Society, 2001. IECON '01. The 27th Annual Conference of the IEEE Volume 2, 29 Nov.-2 Dec. 2001 Page(s):1488 - 1493 vol.2

19. Fahimi, B.; Suresh, G.; Ehsani, M.;" Design considerations of switched reluctance motors: vibration and control issues", Industry Applications Conference, 1999. Thirty-Fourth IAS Annual Meeting. Conference Record of the 1999 IEEE Volume 4, 3-7 Oct. 1999 Page(s):2259 - 2266 vol.4

20. Gieras, J.F.;" Comparison of high-power high-speed machines: cage induction versus switched reluctance motors", AFRICON, 1999 IEEE Volume 2, 28 Sept.-1 Oct. 1999 Page(s):675 - 678 vol.2

21. Radun, A.V.;" Design considerations for the switched reluctance motor", Industry Applications, IEEE Transactions on Volume 31, Issue 5, Sept.-Oct. 1995 Page(s):1079 – 1087

22. Rahman, K.M.; Schulz, S.E.;" Design of high-efficiency and high-torque-density switched reluctance motor for vehicle propulsion", Industry Applications, IEEE Transactions on Volume 38, Issue 6, Nov.-Dec. 2002 Page(s):1500 – 1507

23. Husain, I, "Modern Trends in Automotive Motor Controls", presentation at Oregon State University 2002

24. Senol, I.; Gorgun, H.; Aydeniz, M.G.; "Comparison and determination the electrical motors which are used in electrical transportation systems", Electrotechnical Conference, 1998. MELECON 98., 9th Mediterranean Volume 2, 18-20 May 1998 Page(s):888 - 891 vol.2

25. Moghbelli, H.; Adams, G.E.; Hoft, R.G.; "Performance of a 10-Hp switched reluctance motor and comparison with induction motors", Industry Applications,

IEEE Transactions on Volume 27, Issue 3, May-June 1991 Page(s):531 – 538

26. Islam, M.S.; Anwar, M.N.; Husain, I.;" Design and control of switched reluctance motors for wide-speed-range operation", Electric Power Applications, IEE Proceedings- Volume 150, Issue 4, 8 July 2003 Page(s):425 – 430

27. Domijan, A., Jr.; Carkowski, D.; Johnson, J.H.;" Nonsinusoidal electrical measurement accuracy in adjustable-speed motors and drives",Industry Applications, IEEE Transactions on Volume 34, Issue 6, Nov.-Dec. 1998 Page(s):1225 – 1233

28. Matsui, N.; Kosaka, T.; Minoshima, N.; Ohdachi, Y.; "Development of SRM for spindle motor system", Industry Applications Conference, 1998. Thirty-Third IAS Annual Meeting.The 1998 IEEE Volume 1, 12-15 Oct. 1998 Page(s):580 - 585 vol.1

29. Clothier, A.C.; Mecrow, B.C.; "Inverter topologies and current sensing methods for short pitched and fully pitched winding SR motors", Applied Power Electronics Conference and Exposition, 1999. APEC '99. Fourteenth Annual Volume 1, 14-18 March 1999 Page(s):416 - 423 vol.1

30. Staton, D.A.; Deodhar, R.P.; Soong, W.L.; Miller, T.J.E.; "Torque prediction using the flux-MMF diagram in AC, DC, and reluctance motors", Industry Applications, IEEE Transactions on Volume 32, Issue 1, Jan.-Feb. 1996 Page(s):180 – 188

31. Alrifai, M.T.; Chow, J.H.; Torrey, D.A.;" Backstepping nonlinear speed controller for switched-reluctance motors", Electric Power Applications, IEE Proceedings- Volume 150, Issue 2, March 2003 Page(s):193 – 200

32. Sharma, V.K.; Murthy, S.S.; Singh, B.;" Analysis of switched reluctance motor drive under fault conditions" Industry Applications Conference, 1998. Thirty-Third IAS Annual Meeting. The 1998 IEEE Volume 1, 12-15 Oct. 1998 Page(s):553 - 562 vol.1

33. Stephens, C.M.;" Fault detection and management system for fault tolerant switched reluctance motor drives", Industry Applications Society Annual Meeting, 1989., Conference Record of the 1989 IEEE 1-5 Oct. 1989 Page(s):574 - 578 vol.1

34. Husain,I.;Radun,A. ;Nairus,J.;" Fault analysis and excitation requirements for switched reluctance-generators", Energy Conversion, IEEE Transactions on Volume 17, Issue 1, March 2002 Page(s):67 – 72

35. Husain, I.;" Minimization of torque ripple in SRM drives", Industrial Electronics, IEEE Transactions on Volume 49, Issue 1, Feb. 2002 Page(s):28 – 39

36. Husain,I.; Radun,A.; Nairus,J.; "Unbalanced force calculation in switched-reluctance machines", Magnetics, IEEE Transactions on Volume 36, Issue 1, Jan. 2000 Page(s):330 – 338

37. Russa, K.; Husain, I.; Elbuluk, M.E.;" A self-tuning controller for switched reluctance motors", Power Electronics, IEEE Transactions on Volume 15, Issue 3, May 2000 Page(s):545 – 552

38. Inderka, R.B.; De Doncker, R.W.; Krehenbrink, M. "On-line estimation of instantaneous torque in switched reluctance machine control"; Industrial Electronics, 2000. ISIE 2000. Proceedings of the 2000 IEEE International Symposium on Volume 2, 4-8 Dec. 2000 Page(s):385 - 389 vol.2

39. Motion control forum 2002, www.control.com/Papers/MotionForum2002_pdf

40. Gao Yuan, “Speed Control of Switched Reluctance Motors”, Mater thesis 2000, Hong Kong University of Science and Technology

41. Praveen Vijayraghavan, “Design of Switched Reluctance Motors and development of a universal controller for switched reluctance and permanent magnet brushless DC motor drives”, Ph.D dissertation 2001, Virginia Polytechnic Institute and State University

42. Russel, L; “Eddy Current and Wall Losses In Screened-Rotor Induction Motors”, the Institution of Electrical Engineers, April 1958

43. T.A. Nondahl, T.A. Lipo “Transent analysis of a linear induction machine using the d,q pole-by-pole model”, IEEE transactions on Power Apparatus and Systems, vol. PAS-98, No.4 July/Aug 1979 Page(s): 1366-1374

44. Bimal K. Bose, Thomas A. Lipo, “Control and simulation of a current-Fed linear inductor machine”, IEEE transaction on industry applications, vol.IA-15, No.6 November/December 1979, Page(s): 591-600

45. T.A. Lipo, T.A. Nondahl, “Pole-by-pole d-q model of a linear induction machine”, IEEE transaction on Power Apparatus and Systems, vol. PAS-98, No.2 March/April 1979, Page(s): 629-642

46. dos Santos, E.B.; Camacho, J.R.; de Paula, A.A.; Guimaraes, G.C.; “Efficiency of the linear induction motor (LIM) performance under constant voltage feeding-additional

finite elements considerations", Power Tech Proceedings, 2001 IEEE Porto Volume 4, 10-13 Sept. 2001 Page(s):5 pp. vol.4

47. Nozaki, Y.; Baba, J.; Shutoh, K.; Masada, E.; "Improvement of transverse flux linear induction motors performances with third order harmonics current injection" Applied Superconductivity, IEEE Transactions on Volume 14, Issue 2, June 2004 Page(s):1846 – 1849

48. da Silva, E.F.; dos Santos, C.C.; Nerys, J.W.L.;" Field oriented control of linear induction motor taking into account end-effects", Advanced Motion Control, 2004. AMC '04. The 8th IEEE International Workshop on 25-28 March 2004, Page(s):689 – 694

49. Stumberger, G.; Zarko, D.; Timur Aydemir, M.; Lipo, T.A.; "Design and comparison of linear synchronous motor and linear induction motor for electromagnetic aircraft launch system", Electric Machines and Drives Conference, 2003. IEMDC'03. IEEE International Volume 1, 1-4 June 2003 Page(s):494 - 500 vol.1

50. da Silva, E.F.; dos Santos, E.B.; Machado, P.C.M.; de Oliveria, M.A.A.;" Vector control for linear induction motor", Industrial Technology, 2003 IEEE International Conference on Volume 1, 10-12 Dec. 2003 Page(s):518 - 523 Vol.1

51. Yoshida, K.; Yoshida, T.; Noda, K.; "Influence of instantaneous end effects on attractive levitation force at standstill of combined-levitation-and-propulsion SLIM", Electrical Machines and Systems, 2003. ICEMS 2003. Sixth International Conference on Volume 1, 9-11 Nov. 2003 Page(s):187 - 190 vol.1

52. Hyung-Min Ryu; Jung-Ik Ha; Seung-Ki Sul; “A new sensorless thrust control of linear induction motor” Industry Applications Conference, 2000. Conference Record of the 2000 IEEE Volume 3, 8-12 Oct. 2000 Page(s):1655 - 1661 vol.3

53. Hofmann, R.; Binder, A.; Pfeiffer, R.; “Investigations on a linear induction machine for railway applications”, Electric Machines and Drives Conference, 2001. IEMDC 2001. IEEE International 2001 Page(s):20 – 26

54. Jacek F. Gieras, Linear Induction Drives, Clarendon Press, Oxford, 1994

55. S. A. Nasar, I. Boldea, Linear Electric Motors: Theory, Design, and Practical Applications, Prentice-Hall., Inc. Englewood Cliffs, N.J. 1987

APPENDICES

Appendix 1: SRM analytical design program

```
close all
clear all
%magnetic BH curve
Bin=[0.0 0.1 0.2 0.3 0.4 0.5 0.6 0.7 0.8 0.9 1.0 1.1
1.2 1.3 1.4 1.5 1.6...
1.7 1.8 1.9 2.0 2.1 2.2];
Hout=[0.0 14.7 29.4 44.1 58.7 73.4 86.2 95.3 116.1 154.0 185.9 227.0
278.5 362.9 517.1 909.8 1972.3 4171.2...
7394.8 11595.0 17737.0 27543.0 40000.0 ];
%testy=interp1(Bin,Hout,[0:0.01:1.65],'pchip');
%plot([0:0.01:1.65],testy);
%hold,plot(Bin,Hout,'or');

Ns=8;
Nr=6;
Pout=1.2; % output power (hp)
speed=1320;% rating speed (rpm)
Ipeak=12; %peak current (A)
Treq=Pout*746/(2*pi*speed/60);
beta_s=21;% stator angle(degree)
L=55;%shaft length (mm)
D=67.5;%the stator inner diameter(mm)
Bs=1.95;% the operating peak flux density (T)
As=D/2*L*beta_s*pi/180*1e-6; %stator pole area (m^2)
F_spole=Bs*As;          %stator pole flux density (wb)
F_syoke=F_spole/2; %stator yoke flux density (wb)
Ay=As;% (m^2)
```

```
C=Ay/L*1e6;%(mm)
D0=142;%frame diameter (mm)
hs=D0/2-C-D/2;%stator (mm)
g=0.25;%the airgap length (mm)
beta_r=23;%the rotor angle (degree)
Ar=(D/2-g)*L*beta_r*pi/180*1e-6;%rotor pole area(m^2)
Br=Bs*As/Ar;% the rotor pole flux density
Arc=As/1.6;%rotor core area    (m^2)
Dsh=12;%the shaft diameter (mm)
hr=(D/2-g-Dsh/2)-Arc/L*1e6;%height of the rotor pole (mm)
Ag=(D/2-g/2)*(beta_s/2+beta_r/2)*pi/180*L*1e-6; %airgap area (m^2)
Bg=As*Bs/Ag; %the flux density in the airgap
u0=4*pi*1e-7;
Hg=Bg/u0;
%----------a lookup table is used here
Brc=0.8*Bs;
By=.5*Bs;
Hr=interp1(Bin,Hout,Br,'pchip');
Hs=interp1(Bin,Hout,Bs,'pchip');
Hrc=interp1(Bin,Hout,Brc,'pchip');
Hy=interp1(Bin,Hout,By,'pchip');
%all the length (mm)
ls=hs+C/2;
lg=g;
lr=D/4-g/2+hr/2-Dsh/4;
lrc=pi*(D/4-g/2-hr/2+Dsh/4);
ly=pi*(D0/2-C/2);
```

```
mmf=(2*(Hs*ls+Hg*lg+Hr*lr)+Hrc*lrc/2+Hy*ly/2)*1e-3;%A
Tph=floor(mmf/Ipeak)-1
ipeak=mmf/Tph;
Laligned=Tph*F_spole/ipeak;

%winding design
hwedge=4;%(mm)
ts=(D/2+hwedge)*beta_s*pi/180; %stator pole arc length(mm)
lambda_s=pi*(D+2*hwedge)/Ns;%(mm)
Jmax=6;%(A/mm^2)
ac=ipeak/2/Jmax  %                                    ----------need
standardized

dw=sqrt(ac)+0.1;
%dw=sqrt(4*ac/pi)+0.1;
hw=hs-hwedge
ff=0.95;
Ntlayer=floor(hw*ff/dw);
Nlayer=floor(Tph/2/Ntlayer)+1;
Wt=dw*Nlayer/ff;%(mm)
Z=lambda_s-ts;%space between two stator(mm)
Cl=Z-2*Wt
%_____

%the minimum inductance
%tube 1
 A1s=beta_s/4*pi/180*D/2*L*1e-6; %(m^2)    2.55
```

```
theta2=beta_r/2*(D/3-g)/(D/2-g-hr);%(degree)
theta3=180/Nr-theta2; %(degree)
A1r=2*(D/2-g-hr)*theta3*pi/180*L*1e-6;%(m^2)
A1=(A1s+A1r)/2;
l1=(D/2-g-hr)*1e-3;    %(m)
R1=2*l1/u0/A1;%(m)

        B0s=Bs/2;
        step=Bs/4;
        target=mmf;
        cal_mmf=0;
while(abs(1-cal_mmf/target)>1e-3)
        B0rc=0.8*B0s;
        B0y=B0s/2;
        H0s=interp1(Bin,Hout,B0s,'pchip');
        H0rc=interp1(Bin,Hout,B0rc,'pchip');
        H0y=interp1(Bin,Hout,B0y,'pchip');
        cal_mmf=(2*H0s*ls+H0rc*lrc/2+H0y*ly/2)*1e-3+B0s*A1s*R1;
        if cal_mmf<target
              B0s=B0s+step;
        else B0s=B0s-step;
        end
        step=step/2;
end
Lu1=target*B0s*A1s/ipeak/ipeak;

%tube 2
```

```
A2s=beta_s/4*pi/180*D/2*L*1e-6;%m^2
A2r=hr/2*L*1e-6;%m^2
A2=(A2s+A2r)/2;
x1=D/2*sin(beta_s/4*pi/180)*1e-3;%m
y1=D/2*cos(beta_s/4*pi/180)*1e-3;%m
theta5=pi/Nr-beta_r/2*pi/180*(D/2-g)/(D/2-g-3/4*hr);%rad
x2=(D/2-g-3*hr/4)*sin(theta5)*1e-3;
y2=(D/2-g-3*hr/4)*cos(theta5)*1e-3;
l2=sqrt((x2-x1)^2+(y2-y1)^2)*pi/3;
l2rc=2/3*pi*(D/4-g/2-hr/2+Dsh/4)*1e-3;%m
l2r=hr/4;
R2=2*l2/u0/A2;

        B0s=Bs/2;
        step=Bs/4;
        target=mmf;
        cal_mmf=0;
while(abs(1-cal_mmf/target)>1e-3)
        B0r=B0s*A2s/A2r;
        B0rc=0.8*B0s;
        B0y=B0s/2;
        H0r=interp1(Bin,Hout,B0r,'pchip');
        H0s=interp1(Bin,Hout,B0s,'pchip');
        H0rc=interp1(Bin,Hout,B0rc,'pchip');
        H0y=interp1(Bin,Hout,B0y,'pchip');
        cal_mmf=2*H0s*ls*1e-3+2*H0r*l2r+H0rc*l2rc+H0y*ly*1e-3+B0s*A2s*R2;
        if cal_mmf<target
```

```
            B0s=B0s+step;
        else B0s=B0s-step;
        end
        step=step/2;
  end
  Lu2=target*B0s*A2s/ipeak/ipeak;

%tube3
A3s=3/4*beta_s/8*pi/180*D/2*L*1e-6;%m^2
A3r=hr/4*L*1e-6;%m^2
A3=(A3s+A3r)/2;%m^2
x1=D/2*sin(27/64*beta_s*pi/180);
y1=D/2*cos(27/64*beta_s*pi/180);
theta7=pi/Nr-beta_r/2*pi/180*(D/2-g)/(D/2-g-3/8*hr);
x2=(D/2-g-3/8*hr)*sin(theta7);
y2=(D/2-g-3/8*hr)*cos(theta7);
l3=pi/3*sqrt((x2-x1)^2+(y2-y1)^2)*1e-3;%m
l3r=5/8*hr*1e-3;%m
R3=2*l3/u0/A3;

        B0s=Bs/2;
        step=Bs/4;
        target=mmf;
        cal_mmf=0;
while(abs(1-cal_mmf/target)>1e-3)
        B0r=B0s*A3s/A3r;
        B0rc=0.8*B0s;
```

```
        B0y=B0s/2;
        H0r=interp1(Bin,Hout,B0r,'pchip');
        H0s=interp1(Bin,Hout,B0s,'pchip');
        H0rc=interp1(Bin,Hout,B0rc,'pchip');
        H0y=interp1(Bin,Hout,B0y,'pchip');
        cal_mmf=2*H0s*ls*1e-3+2*H0r*l3r+H0rc*l2rc+H0y*ly*1e-3+B0s*A3s*R3;%as page 31
        if cal_mmf<target
              B0s=B0s+step;
        else B0s=B0s-step;
        end
        step=step/2;
  end
  Lu3=target*B0s*A3s/ipeak/ipeak;

%tube4
A4s=(1/4*beta_s/8*pi/180*D/2*L+1/4*hs/4*L)*1e-6;%m^2
A4r=hr/4*L*1e-6;%m^2
A4=(A4s+A4r)/2;
x1=D/2*sin(1/2*beta_s*pi/180);
y1=D/2*cos(1/2*beta_s*pi/180);
theta9=pi/Nr-beta_r/2*pi/180*(D/2-g)/(D/2-g-1/8*hr);
x2=(D/2-g-3/8*hr)*sin(theta9);
y2=(D/2-g-3/8*hr)*cos(theta9);
l4=pi/3*sqrt((x2-x1)^2+(y2-y1)^2)*1e-3;%m
l4r=7*hr/8*1e-3;
R4=2*l4/u0/A4;
```

```
        B0s=Bs/2;
        step=Bs/4;
        target=mmf;
        cal_mmf=0;
while(abs(1-cal_mmf/target)>1e-3)
        B0r=B0s*A4s/A4r;
        B0rc=0.8*B0s;
        B0y=B0s/2;
        H0r=interp1(Bin,Hout,B0r,'pchip');
        H0s=interp1(Bin,Hout,B0s,'pchip');
        H0rc=interp1(Bin,Hout,B0rc,'pchip');
        H0y=interp1(Bin,Hout,B0y,'pchip');
        cal_mmf=2*H0s*ls*1e-3+2*H0r*l4r+H0rc*l2rc+H0y*ly*1e-3+B0s*A4s*R4;%as page 31
        if cal_mmf<target
              B0s=B0s+step;
        else B0s=B0s-step;
        end
        step=step/2;
  end
  Lu4=target*B0s*A4s/ipeak/ipeak;

%tube5
A5s=3/4*hs/4*L*1e-6;%m^2
A5r=beta_r/8*pi/180*L*(D/2-g)*1e-6;%m^2
A5=(A5s+A5r)/2;
x1=D/2*sin(1/2*beta_s*pi/180);
y1=D/2*cos(1/2*beta_s*pi/180)+5/32*hs;
```

```
theta1=atan(x1/(y1-(D/2-g-hr)));
theta2=pi/Nr-7/16*beta_r*pi/180;
x2=(D/2-g)*sin(theta2);
y2=(D/2-g)*cos(theta2)-(D/2-g-hr);
theta3=atan(y2/x2);
theta4=pi/2-theta1-theta3;
r1=x1/sin(theta1)*1e-3;%m
r2=sqrt(x2*x2+y2*y2)*1e-3;
l5=(r1+r2)/2*theta4;%m
l5r=hr*1e-3;
l5s=(hs+C/2-3/8*hs/4)*1e-3;
R5=2*l5/u0/A5;

    B0s=Bs/2;
   step=Bs/4;
   target=mmf;
   cal_mmf=0;
while(abs(1-cal_mmf/target)>1e-3)
   B0r=B0s*A4s/A4r;
   B0rc=0.8*B0s;
   B0y=B0s/2;
   H0r=interp1(Bin,Hout,B0r,'pchip');
   H0s=interp1(Bin,Hout,B0s,'pchip');
   H0rc=interp1(Bin,Hout,B0rc,'pchip');
   H0y=interp1(Bin,Hout,B0y,'pchip');
   cal_mmf=2*H0s*l5s+2*H0r*l5r+H0rc*l2rc+H0y*ly*1e-3+B0s*A5s*R5;%as page 31
   if cal_mmf<target
```

```
            B0s=B0s+step;
        else B0s=B0s-step;
        end
        step=step/2;
 end
 Lu5=target*B0s*A5s/ipeak/ipeak;

 %tube6
A6=hs/4*L*1e-6;%m^2l5s=(hs+C/2-3/8*hs/4)*1e-3;
x1=D/2*sin(1/2*beta_s*pi/180);
y1=D/2*cos(1/2*beta_s*pi/180)+3/8*hs;
theta1=atan(x1/y1);
theta2=2*pi/Ns-2*theta1;
r1=x1/sin(theta1)*1e-3;%m
l6=r1*theta2;%m
A6s=A6;
l6s=(5*hs/8+C/2)*1e-3;
l6y=pi/4*(D0/2-C/2)*1e-3;
R6=l6/u0/A6;

          B0s=Bs/2;
        step=Bs/4;
        target=3/8*mmf;    %2.141 page 39
        cal_mmf=0;
while(abs(1-cal_mmf/target)>1e-3)
        B0rc=0.8*B0s;
        B0y=B0s/2;
```

```
        H0s=interp1(Bin,Hout,B0s,'pchip');
        H0rc=interp1(Bin,Hout,B0rc,'pchip');
        H0y=interp1(Bin,Hout,B0y,'pchip');
        cal_mmf=2*H0s*l6s+H0y*l6y+B0s*A6s*R6;%as page 31
        if cal_mmf<target
              B0s=B0s+step;
        else B0s=B0s-step;
        end
        step=step/2;
  end
  Lu6=target*B0s*A6s/ipeak/ipeak;



  %tube7
A7=hs/2*L*1e-6;%m^2
l7=hs/4*pi/2*1e-3;%m
A7s=A7;
l7s=(hs/4+C/2)*1e-3;
l7y=hs/4*1e-3;
R7=l7/u0/A7;


        B0s=Bs/2;
        step=Bs/4;
        target=mmf/4;    %page 41
        cal_mmf=0;
while(abs(1-cal_mmf/target)>1e-3)
        B0y=B0s/2;
```

```
        H0s=interp1(Bin,Hout,B0s,'pchip');
        H0y=interp1(Bin,Hout,B0y,'pchip');
        cal_mmf=2*H0s*l7s+H0y*l7y+B0s*A7s*R7;%
        if cal_mmf<target
              B0s=B0s+step;
        else B0s=B0s-step;
        end
        step=step/2;
  end
  Lu7=target*B0s*A7s/ipeak/ipeak;
  Lu=Lu1+2*(Lu2+Lu3+Lu4+Lu5)+4*(Lu6+Lu7);



  %average torque
  K=30;
  Flux=zeros(30,1);
for k=1:K
          B0s=Bs/2;
        step=Bs/4;
        target=k/K*Tph*ipeak;
        cal_mmf=0;
    while(abs(1-cal_mmf/target)>1e-3)
        B0r=B0s*As/Ar;
        B0g=B0s*As/Ag;
        B0rc=0.8*B0s;
        B0y=B0s/2;
```

```
        H0r=interp1(Bin,Hout,B0r,'pchip');
        H0s=interp1(Bin,Hout,B0s,'pchip');
        H0g=B0g/u0;
        H0rc=interp1(Bin,Hout,B0rc,'pchip');
        H0y=interp1(Bin,Hout,B0y,'pchip');
        cal_mmf=(2*(H0s*ls+H0g*lg+H0r*lr)+H0rc*lrc/2+H0y*ly/2)*1e-3;%A
        if cal_mmf<target
            B0s=B0s+step;
        else B0s=B0s-step;
        end
        step=step/2;
    end
    Flux(k)=Tph*As*B0s;
end
plot([0:K]/K*ipeak,[0; Flux],'*--');
q1=linspace(0,ipeak,K+1);
q2=linspace(0,ipeak*Lu,K+1);
hold, plot(q1,q2);plot(q1(K+1),q2(K+1),'*'),grid
xlabel('phase current,A'),ylabel('flux linkage, web');

Waligned=sum(Flux)*ipeak/K-Flux(K)/2*ipeak/K;
Wunaligned=ipeak*ipeak*Lu/2;
Tav=(Waligned-Wunaligned)*Ns*Nr/4/pi
```

Appendix 2 Linear Induction Motor 1 design data:

	Design 1	Design 2	Design 3
Pole pitch (m)	0.318	0.318	0.318
Stack width m)	0.216	0.22	0.216
Secondary plate overhang (m)	0.05	0.05	0.05
Clearance (m)	0.011	0.009	0.011
Secondary plate depth (m)	0.0045	0.004	0.0045
Secondary plate in overhang (m)	0.0135	0.016	0.0135
Primary core depth (m)	0.037	0.037	0.037
Secondary core depth (m)	0.037	0.037	0.037
Series conductor/slot	16	12	14
Slot pitch (m)	0.0265	0.0265	0.0265
Depth of conductor in slot (m)	0.0415	0.0415	0.0415
Depth of non- conductor in slot (m)	0.0176	0.0176	0.0176
Slot width (m)	0.0169	0.0169	0.0169
Conductor cross section (m2)	0.0000342	0.0000456	0.0000390
Coil Pitch (m)	0.212	0.212	0.1855
Protrusion (m)	0.005	0.005	0.005
Overhang (m)	0.15	0.15	0.15
Primary resistivity (ohm-m)	0.172e-7	0.172e-7	0.172e-7
Secondary resistivity (ohm-m)	0.35e-7	0.35e-7	0.35e-7
Frequency (Hz)	5-25 (CCM) 25-60 (VCM)	5-25 (CCM) 25-60 (VCM)	5-25 (CCM) 25-60 (VCM)
Phase current limitation (Arms)	280	280	280
Line voltage limitation (V rms)	675	675	675
Pole pairs in Model	21	21	21
Pole pairs in Machine	4	4	4
Start harmonic	-12	-12	-12
End harmonic	36	36	36
Start point (m)	-0.9480	-0.9480	-0.9480
Interval (m)	0.04034	0.04034	0.04034

Appendix 3: LIM simulation program

% the main program

```
%currernt source
close all
clear all

STE =1 ;            %--- ENTER 0 FOR CONSTANT VOLTAGE
                    %---      OR 1 FOR CONSTANT CURRENT                    %1300C
IPOP =1 ;       %--- ENTER 0 TO OMIT FLUX MAP PRINTOUT
                    %---      OR 1 TO PRODUCE FLUX MAP PRINTOUT
                                                                           %1500C
STEDC =0 ;          %--- ENTER 0 FOR AC
                    %---      OR 1 FOR DC                                  %1700C

TP = .318;              %--- ENTER POLE PITCH (M)                          %2100C
W = .2160;              %--- ENTER STACK WIDTH (M)                         %2200C
OHANG = 0.05;           %--- ENTER SECONDARY PLATE OVERHANG                %2300C
G1 = .011;              %--- ENTER CLEARANCE(M)                            %2400C
G2 = .45e-2;        %--- ENTER SECONDARY PLATE DEPTH UNDER STACK(M)        %2500C
G3 =.0135 ;     %--- ENTER SECONDARY PLATE DEPTH IN OVERHANG(M)            %2600C

DC0 = .37e-1%--- ENTER PRIMARY CORE DEPTH BEHIND TEETH(M)                  %2900C
DC4 = .37e-1;           %--- ENTER SECONDARY CORE DEPTH (M):               %3000C
ZS =16 ;                %--- ENTER SERIES CONDUCTORS PER SLOT:             %3100C
SP = .265e-1;           %--- ENTER SLOT PITCH (M):                         %3200C
H1S = .415e-1    %--- ENTER DEPTH OF SLOT OCCUPIED BY CONDUCTOR:          %3300C
```

```
H2S = 1.76e-2;              %--- ENTER DEPTH OF SLOT FREE OF CONDUCTOR:%3400C

WS =.169e-1 ;               %--- ENTER SLOT WIDTH (M):                 %3700C
CSA = .342e-4 %--- ENTER CONDUCTOR CROSS SECTIONAL AREA (MxM);          %3800C
CP = .1855;                 %--- ENTER COIL PITCH (M):                  %3900C
YCOIL = .5e-2, %--- ENTER PRIMARY COIL SIDE PROTRUSION BEYOND STACK (M):
    %4000C
EOHANG = .15;          %--- ENTER PRIMARY COIL OVERHANG BEYOND PROTRUSION
(M):          %4100C
RHOCU = .172e-7;            %--- ENTER PRIMARY CONDUCTOR RESISTIVITY (OHM-M):
              %4200C

RHO1 = .35e-7;              %--- ENTER SECONDARY PLATE RESISTIVITY (OHM-M):
              %4500C
FREQ_all = [ 2.5:2.5:40];        %--- ENTER SUPPLY FREQUENCY (Hz):        %4600C
YPOSN=zeros(48,1);
YPOSN(1) = -0.948;
                    %--- ENTER START POINT FOR SPACE DISTRIBUTION (M):    %4700C
H = 0.4034e-1;      %--- ENTER INTERVAL FOR SPACE DISTRIBUTION (M):       %4800C
VIPH =280;                  %--- ENTER PHASE VOLTAGE OR CURRENT:          %4900C

PT =21 ;            %--- ENTER TOTAL NUMBER OF POLE-PAIR IN MODEL:        %5200C
PW = 4;             %--- ENTER TOTAL NUMBER OF POLE-PAIR IN MACHINE:      %5300C
NS =-12 ;                   %--- ENTER START HARMONIC NUMBER:             %5400C
NF = 36;            %--- ENTER END HARMONIC NUMBER:                       %5500C

SLIP =[0:-0.005:-1.0];           %--- ENTER SLIP
```

```
%%%%%%%%%%%%%%%%%%%%%%%%%%%%%%%%%%%%%%%%%%%%%%%%%
%%%%%%%%%%%%%%%%%%%%%%%%%%%%%
CR = 5;                                         %7600C
LP = 6;                                         %7700C

figure(2),
subplot(2,1,1),hold
xlabel('VELOCITY M/S'),ylabel('EXIT CORRECTED THRUST N'),title('2'),grid;

subplot(2,1,2),,hold
xlabel('VELOCITY M/S'),ylabel('VOLTAGE'),title('3'),grid;



figure(3),
subplot(3,1,1),hold
xlabel('VELOCITY M/S'),ylabel('OUTPUT POWER W'),title('2'),grid;
subplot(3,1,2),,hold
xlabel('VELOCITY M/S'),ylabel('PRIMARY LOSSES'),grid;
subplot(3,1,3),,hold
xlabel('VELOCITY M/S'),ylabel('SECONDARY    LOSSES'),grid;

figure(4),
subplot(3,1,1),hold
xlabel('VELOCITY M/S'),ylabel('L1 H'),title('2'),grid;
subplot(3,1,2),hold
xlabel('VELOCITY M/S'),ylabel('L2 H'),title('3'),grid;
subplot(3,1,3),,hold
```

```
xlabel('VELOCITY M/S'),ylabel('Lm H'),title('4'),grid;

figure(5),
subplot(2,1,1),hold
xlabel('VELOCITY M/S'),ylabel('R1 ohm'),title('4'),grid;
subplot(2,1,2),hold
xlabel('VELOCITY M/S'),ylabel('R2 ohm'),title('4'),grid;

figure(6),
subplot(3,1,1),hold
xlabel('VELOCITY M/S'),ylabel('EFF %'),grid;
subplot(3,1,2),hold
xlabel('VELOCITY M/S'),ylabel('PF'),grid;
subplot(3,1,3),hold
xlabel('VELOCITY M/S'),ylabel('PFEFF'),grid;

FREQ_LOOP=length(FREQ_all);
%**********************************
%find the maximium
Max_thrust=zeros(FREQ_LOOP,1);
Max_supply=zeros(FREQ_LOOP,1);
Max_velocity=zeros(FREQ_LOOP,1);
Max_ploss=zeros(FREQ_LOOP,1);
Max_sloss=zeros(FREQ_LOOP,1);
Max_outputpower=zeros(FREQ_LOOP,1);

Max_l2=zeros(FREQ_LOOP,1);
```

```
Max_r2=zeros(FREQ_LOOP,1);


Max_eff=zeros(FREQ_LOOP,1);
Max_pf=zeros(FREQ_LOOP,1);
Max_pfeff=zeros(FREQ_LOOP,1);
%************************************
%OUT_matrix=zeros(FREQ_LOOP,9);
for KK=1:FREQ_LOOP
      FREQ=FREQ_all(KK);
      LIMSIMcomp_FINAL;
%       OUT_matrix(KK,:)=OUTPUT1(:,2:10);


%-------------------------------------------------------------------------------
%OUTPUT GRAPHS
%X AXIS IS FREQUENCY. SLIP=1,
%-------------------------------------------------------------------------------


figure(2),
subplot(2,1,1),
plot(OUTPUT1(:,2),OUTPUT1(:,5),'-*'),


subplot(2,1,2),
plot(OUTPUT1(:,2),OUTPUT1(:,3),'-*'),


[a,b]=min(OUTPUT1(:,5)); %a is the thrust value and b is the index
Max_thrust(KK)=a;
Max_supply(KK)=OUTPUT1(b,3);
```

```
Max_velocity(KK)=OUTPUT1(b,2);

%----------------------------------------
figure(3),
subplot(3,1,1),
plot(OUTPUT1(:,2),OUTPUT2(:,2),'-*'),
subplot(3,1,2),
plot(OUTPUT1(:,2),OUTPUT2(:,3),'-*'),
subplot(3,1,3),
plot(OUTPUT1(:,2),OUTPUT2(:,4),'-*'),
Max_ploss(KK)=OUTPUT2(b,3);
Max_sloss(KK)=OUTPUT2(b,4);
Max_outputpower(KK)=OUTPUT2(b,2);



figure(4),
subplot(3,1,1),
plot(OUTPUT1(:,2),OUTPUT2(:,7)/2/pi/FREQ,'-*'),
subplot(3,1,2),
plot(OUTPUT1(:,2),OUTPUT2(:,10)/2/pi/FREQ,'-*'),
subplot(3,1,3),
plot(OUTPUT1(:,2),OUTPUT2(:,8)/2/pi/FREQ,'-*'),
Max_l2(KK)=OUTPUT2(b,10)/2/pi/FREQ;


figure(5)
```

```
subplot(2,1,1),
plot(OUTPUT1(:,2),OUTPUT2(:,6),'-*'),
subplot(2,1,2),
plot(OUTPUT1(:,2),OUTPUT2(:,9),'-*'),
Max_r2(KK)=OUTPUT2(b,9);

figure(6),
subplot(3,1,1),
plot(OUTPUT1(:,2),OUTPUT1(:,8)./OUTPUT1(:,4),'-*'),
subplot(3,1,2),
plot(OUTPUT1(:,2),OUTPUT1(:,4),'-*'),
subplot(3,1,3),
plot(OUTPUT1(:,2),OUTPUT1(:,8),'-*'),
Max_eff(KK)=OUTPUT1(b,8)/OUTPUT1(b,4);
Max_pf(KK)=OUTPUT1(b,4);
Max_pfeff(KK)=OUTPUT1(b,8);
%figure(3),
%plot(FREQ_all,OUT_matrix(:,2),'-*'),grid,
%xlabel('FREQUENCY'),ylabel('PHASE VOLTAGE V'),title('3');

%figure(4),
%plot(FREQ_all,OUT_matrix(:,3),'-*'),grid,
%xlabel('FREQUENCY'),ylabel('POWER FACTOR'),title('4');

%figure(5),
%plot(FREQ_all,OUT_matrix(:,4),'-*'),grid,
%xlabel('FREQUENCY'),ylabel('EXIT CORRECTED THRUST N'),title('5');
```

```
%figure(6),
%plot(FREQ_all,OUT_matrix(:,5),'-*'),grid,
%xlabel('FREQUENCY'),ylabel('LIFT FORCE N'),title('6');

%figure(7),
%plot(FREQ_all,OUT_matrix(:,6),'-*'),grid,
%xlabel('FREQUENCY'),ylabel('EXIT CORRECTED EFF'),title('7');

%figure(8),
%plot(FREQ_all,OUT_matrix(:,7),'-*'),grid,
%xlabel('FREQUENCY'),ylabel('POWER FACTOR * EFF'),title(8');

%figure(9),
%plot(FREQ_all,OUT_matrix(:,8),'-*'),grid,
%xlabel('FREQUENCY'),ylabel('TOTAL INPUT POWER W'),title('9');

%figure(10),
%plot(FREQ_all,OUT_matrix(:,9),'-*'),grid,
%xlabel('FREQUENCY'),ylabel('TOTAL INPUT VARS VAR'),title('10');

end

figure(2)
subplot(2,1,1);
plot(Max_velocity,Max_thrust,'r');
```

```
subplot(2,1,2);
plot(Max_velocity,Max_supply,'r');

figure(3)
subplot(3,1,1);
plot(Max_velocity,Max_outputpower,'r');

subplot(3,1,3);
plot(Max_velocity,Max_sloss,'r');

figure(4)
subplot(3,1,2)
plot(Max_velocity,Max_l2,'r');

figure(5)
subplot(2,1,2)
plot(Max_velocity,Max_r2,'r');

figure(6)
subplot(3,1,1);
plot(Max_velocity,Max_eff,'r');
subplot(3,1,2);
plot(Max_velocity,Max_pf,'r');
subplot(3,1,3);
plot(Max_velocity,Max_pfeff,'r');

%figure(4),subplot(3,1,2),axis([-10 20 0 6e-3]);
```

```
%figure(5),subplot(2,1,1),axis([-10 20 0.17 0.18])
%figure(6),subplot(3,1,1),axis([-10 20 40 80])
```

% the subroutine %LIMSIMcomp_FINAL.m

```
% DEFINE CONSTANTS
OMEG = 2*pi*FREQ;                                                    %15800C
MU0= pi*4.0E-07;                                                     %15900C
Q = TP/(3*SP);                                                       %16000C
ALPHA = pi/(3*Q);                                                    %16100C
KD = sin(.5*Q*ALPHA)/(Q*sin(.5*ALPHA));                              %16200C
YC = .5*CP;                                                          %16300C
KP = sin(pi*YC/TP);                                                  %16400C

%%%%%%%%%%%%%%%%%%%%%%%%%%%%%%%%%%%%%%%%%%%%%%%%%%%%%%%%%%%%%%%%%%%%%%%
%%%%%%%%%%%%%%%%%%%%%%%%%%%%%%%%%%%%%%%%%%%%%%%%%%%%%%%%%%%%%%%%%%%%%%%
% SET ISET FOR CURRENT OR VOLTAGE SOURCE                             %16600C
if STE==0
    ISET = 100;
    VPH = VIPH;
else
    ISET = VIPH;
end
JS = ZS*KD*ISET/(SP*2);                    %NOTE JS IS PER LAYER     %17600C

%%%%%%%%%%%%%%%%%%%%%%%%%%%%%%%%%%%%%%%%%%%%%%%%%%%%%%%%%%%%%%%%%%%%%%%
%%%%%%%%%%%%%%%%%%%%%%%%%%%%%%%%%%%%%%%%%%%%%%%%%%%%%%%%%%%%%%%%%%%%%%%
% CALCULATE PRIMARY RESISTANCE & LEAKAGE REACTANCE                   %17700C
LMT = sqrt(YC*YC + EOHANG*EOHANG);
LMT = 2*W + 4*YCOIL + 4*LMT + 1.6*pi*H1S;
```

```
%LMT = LMT + 1.6*pi*H1S;                                    %MOVED TO LINE ABOVE

NC = .5*ZS;

AP = 2*PW;

R1 = RHOCU*LMT*NC*Q*AP/CSA;                                                 %18900C


%%%%%%%%%%%%%%%%%%%%%%%%%%%%%%%%%%%%%%%%%%%%%%%%%%%%%%%%%%%%%%%%%%%%%%%%%%%%
%%%%%%%%%%%%%%%%%%%%%%%%%%%%%%%%%%%%%%%%%%%%%%%%%%%%%%%%%%%%%%%%%%%%%%%%%%%%
% X1 CALCULATION                                                            %18700C

KXCO = (9*CP/TP + 7)/16;

KXT = (3*CP/TP + 1)/4;

LAMS = (H1S*KXCO/(3*WS)) + (H2S*KXT/WS);

KW1 = KD*KP;

LAMEW = 1.2*KW1*KW1*Q*(YCOIL + .5*EOHANG)/W;

X1 = OMEG*(1.6E-06*pi*NC*NC*Q*AP*W*(LAMS + LAMEW));

%X1 = X1*OMEG;                          %MOVED TO LINE ABOVE               %19800C


%%%%%%%%%%%%%%%%%%%%%%%%%%%%%%%%%%%%%%%%%%%%%%%%%%%%%%%%%%%%%%%%%%%%%%%%%%%%
%%%%%%%%%%%%%%%%%%%%%%%%%%%%%%%%%%%%%%%%%%%%%%%%%%%%%%%%%%%%%%%%%%%%%%%%%%%%
% MOTOR DESIGN CALCULATIONS

LCU = LMT*NC*Q*AP;                          %LENGTH COPPER/PHASE           %20200C

WCU = 3*LCU*CSA*8890;                       %TOTAL WEIGHT COPPER           %20500C

SLOTS = ((2*PW+(2/3))*TP/SP)-1;             %NUMBER OF SLOTS               %20700C

NSLOTS = SLOTS + .5;

LENGTH = (NSLOTS*SP)+(SP-WS);               %MOTOR LENGTH                  %21000C

HEIGHT = DC0 + H1S + H2S;                   %MOTOR HEIGHT                  %21200C

WIDTH = W+2*(YCOIL + EOHANG);               %MOTOR TOTAL WIDTH             %21400C

SVOL = NSLOTS*WS*(H1S+H2S)*W;               %SLOT VOLUME                   %21600C
```

```
WFE = ((LENGTH*HEIGHT*W)-SVOL)*7870;        %TOTAL MASS IRON              %21800C
WTOT = WCU+WFE;                             %TOTAL WEIGHT                 %22000C
OUTPUT1=zeros(length(SLIP),10);
OUTPUT2=zeros(length(SLIP),10);
%%%%%%%%%%%%%%%%%%%%%%%%%%%%%%%%%%%%%%%%%%%%%%%%%%%%%%%%%%%%%%%%%%%%%%%%%%%%%%%%%%%
%%%%%%%%%%%%%%%%%%%%%%%%%%%%%%%%%%%%%%%%%%%%%%%%%%%%%%%%%%%%%%%%%%%%%%
%%%%%%%%%%%%%%%%%%%%%%%%%%%%%%%%%%%%%%%%%%%%%%%%%%%%%%%%%%%%---------------------------------
--------------------------
                                                                 %no    line 229- 248
for I=2:48                                                              %249-254
    YPOSN(I,1)=YPOSN(1,1)+(I-1)*H;
end;
YEXT=PW*TP-YC;
YEXT1=PW*TP+YC;
NOUT=1;
ITEST=0;
while (ITEST~=111)                                                          %255
   for I=1:48
       if (abs(YPOSN(I))-YEXT1<1.0e-7)
           JD(I)=JS;
       else
           JD(I)=0;
       end
       if (abs(YPOSN(I))-YEXT<1.0e-7)
           JD(I)=(JD(I)+JS)*KP;;
       else
           JD(I)=JD(I);
```

```
    end
end
PIN=0.0;                                                    %270
PL=0.0;
VAR=0.0;
FT=0.0;
BEND=0.0;
BD1=zeros(48,1);
BD2=zeros(48,1);
BD3=zeros(48,1);
BD4=zeros(48,1);
BD5=zeros(48,1);
STRESS=zeros(48,1);
%
%*******START OF MAIN HARMONIC LOOP                           %282
NR=NF-NS+1;
for N=1:NR
    R=NS+N-1;
    if (R~=0)
        KR=R*pi/(PT*TP);
        SR=1.0-(1.0-SLIP(NOUT))*R/PT;
        if (STEDC==1)
            SR=-(1.0-SLIP(NOUT))*R/PT;
        end
         %RUSSELL AND NORWORTHY CALCULATION                  %292
         EPSR=0.5*KR*W;
         PHIR=KR*OHANG;
```

```
DENOMR=G3*tanh(EPSR)*tanh(PHIR)/G2;
DENOMR=EPSR*(1.0+DENOMR);
AKER=DENOMR/(DENOMR-tanh(EPSR));
RHO=RHO1*AKER;                                          %THIS IS OU
%                                                       %302
GAMR=KR*KR+OMEG*MU0*SR/RHO*i;
GAMR=sqrt(GAMR);
ZO1R=OMEG*MU0/KR*i;                                     %OU
ZO2R=OMEG*MU0*i;
ZO2R=ZO2R/GAMR;
ZA1R=ZO1R*tanh(0.5*KR*G1);
ZB1R=ZO1R/(0.5*(exp(KR*G1)-exp(-KR*G1)));
A1=GAMR*G2;
ZB2R=ZO2R/(0.5*(exp(A1)-exp(-A1)));
A1=0.5*A1;
ZA2R=ZO2R*(exp(A1)-exp(-A1))/(exp(A1)+exp(-A1));
ZSR=ZA1R+ZA2R+ZB2R;
ZPR=ZB1R*ZSR/(ZB1R+ZSR);
ZR=ZA1R+ZPR;
%
%******* HARMONIC CURRENT CALCULATIONS                    %317
P2=sin(KR*YC);
if (R==PT)
    JR=2.0*JS*PW/PT;
    JR=JR*P2;
else
    JR=2.0*JS*sin((R-PT)*pi*PW/PT)/(pi*(R-PT));
```

```
    JR=JR*P2;
end
AREA=2.0*PT*TP*W;                                          %327
PINR=JR*JR*real(ZR)*AREA;
PIN=PIN+PINR;
PLR=SR*PINR;
PL=PL+PLR;
VARR=JR*JR*imag(ZR)*AREA;
VAR=VAR+VARR;
FTR=PINR*R/(2.0*FREQ*TP*PT);
FT=FT+FTR;
%                                                          %337
E1R=-ZR*JR;
H1R=-JR;
H2R=H1R*(1+ZA1R/ZB1R)-E1R/ZB1R;
E3R=H2R*ZB2R;
E2R=E3R+H2R*ZA2R;
BR=-KR/OMEG;
B1R=BR*E1R;
B2R=BR*E2R;
B3R=BR*E3R;
ARG3=i/(DC0*KR);
ARG4=i/(DC4*KR);
%                                                          %348
for K=1:48
ARG1=-KR*YPOSN(K)*i;
BD1(K)=BD1(K)+B1R*exp(ARG1);
```

```
                BD2(K)=BD2(K)+B2R*exp(ARG1);
                BD3(K)=BD3(K)+B3R*exp(ARG1);
                BD4(K)=BD4(K)+ARG3*B1R*exp(ARG1);
                BD5(K)=BD5(K)+ARG4*B3R*exp(ARG1);
                end
                ARG2=-KR*YEXT1*i;
                BEND=BEND+B2R*exp(ARG2);
        end
    end                                                          %358 end

R2=PIN/(3.0*ISET*ISET);
X2=VAR/(3.0*ISET*ISET);
Z2=R2+X2*i;
XM=12.0*TP*W*MU0*FREQ*PW/(pi*(G1+G2));
XM=XM*(ZS*Q*KD*KP)*(ZS*Q*KD*KP);
ZM=XM*i;
Z22=Z2*ZM/(ZM-Z2);
%
V=ISET*sqrt((R1+R2)*(R1+R2)+(X1+X2)*(X1+X2));                    %366
if (STE==0)
    SF=VPH/V;
else
    SF=1.0;
    VPH=V;
end
IPH=SF*ISET;
P1=3.0*IPH*IPH*R1;
```

```
AJCOND=IPH/CSA;
%
for K1=1:48                                                    %375
B1=abs(BD1(K1))*SF;
B2=abs(BD2(K1))*SF;
B3=abs(BD3(K1))*SF;
B4=abs(BD4(K1))*SF;
B5=abs(BD5(K1))*SF;
BD1(K1)=B1;
BD2(K1)=B2;
BD3(K1)=B3;
BD4(K1)=B4;
BD5(K1)=B5;
JD(K1)=JD(K1)*SF;
STRESS(K1)=0.5*MU0*(JD(K1)*JD(K1)-(B1/MU0)*(B1/MU0));
end

%
%**********EXIT EDGE CALCULATION                               %389
BEX=abs(BEND)*SF;
GI=G1+G2;
FRET=TP/pi-GI;
FRET=FRET*(1.0-SLIP(NOUT));
if STEDC==1
      FRET=-FRET*SLIP(NOUT);
end
FRET=FRET*BEX*BEX*W/(2.0*MU0);
```

```
%
%                                                                    %398
PIN=PIN*SF*SF+IPH*IPH*R1*3.0;
VAR=VAR*SF*SF+IPH*IPH*X1*3.0;
VA=sqrt(PIN*PIN+VAR*VAR);
FT=FT*SF*SF;
FCOR=FT-FRET;
PL=PL*SF*SF;
POUT=2.0*TP*FREQ*FT*(1.0-SLIP(NOUT));
POUTC=2.0*TP*FREQ*FCOR*(1.0-SLIP(NOUT));
EFF=POUT*100.0/PIN;
EFFEC=POUTC*100.0/PIN;
PF=PIN/VA;
FL=0.0;
for K2=1:48
    FL=FL+STRESS(K2)*H*W;
end

VEL=2*TP*FREQ*(1.0-SLIP(NOUT));
PFEFF=PF*EFF;
%
if STE==0                                                            %415
    SOURCE=IPH;
else
    SOURCE=VPH;
end
```

```
OUTPUT1(NOUT,1)=SLIP(NOUT);       %USING THE COLUMN FOR EACH VARIABLE
OUTPUT1(NOUT,2)=VEL;
OUTPUT1(NOUT,3)=SOURCE;
OUTPUT1(NOUT,4)=PF;
OUTPUT1(NOUT,5)=FCOR;
OUTPUT1(NOUT,6)=FL;
OUTPUT1(NOUT,7)=EFFEC;
OUTPUT1(NOUT,8)=PFEFF;
OUTPUT1(NOUT,9)=PIN;
OUTPUT1(NOUT,10)=VAR;
%%%%%%%%%%%%%%%%%%%%%%%%419,420
%MOVE LINE 421 TO RENEW NOUT IN THE END
%ASSIGN REMAINING OUTPUT VARIABLES TO PUTPUT ARRAY
OUTPUT2(NOUT,1)=SLIP(NOUT);              %USING THE COLUMN FOR EACH VARIABLE
OUTPUT2(NOUT,2)=POUT;
OUTPUT2(NOUT,3)=P1;
OUTPUT2(NOUT,4)=PL;
OUTPUT2(NOUT,5)=AJCOND;
OUTPUT2(NOUT,6)=R1;
OUTPUT2(NOUT,7)=X1;
DV=imag(ZM);
DW=imag(Z22);
DX=real(Z22);
OUTPUT2(NOUT,8)=DV;
OUTPUT2(NOUT,9)=DX;
OUTPUT2(NOUT,10)=DW;
```

```
NOUT=NOUT+1;                                                    %421
if NOUT>=size(SLIP)+1                                           %stop the loop
    ITEST=111;
end
end%                                                            %as 459
```